Processing of sky compass cues and wide-field motion in the central complex of the desert locust (*Schistocerca gregaria*)

Verarbeitung von Himmelskompasssignalen und Großfeldbewegung im Zentralkomplex der Wüstenheuschrecke (*Schistocerca gregaria*)

DISSERTATION

zur Erlangung des Doktorgrades der
Naturwissenschaften (Dr. rer. nat.)

---

dem Fachbereich Biologie
der Philipps-Universität Marburg
vorgelegt von

Uta Pegel
aus Haltern am See

Marburg/Lahn, Juni 2018

Vom Fachbereich Biologie der Philipps-Universität

Marburg als Dissertation am 11.06.2018 angenommen.

Erstgutachter: Prof. Dr. Uwe Homberg

Zweitgutachter: Prof. Dr. Joachim Schachtner

Tag der mündlichen Prüfung am: 04.09.2018

Contents

Erklärung: Eigene Beiträge und veröffentlichte Teile der Arbeit

Entsprechend §9 (1) der Promotionsordnung der Philipps-Universität Marburg (Fassung vom 15.07.2009) werden im Folgenden die eigenen Anteile an den einzelnen Kapiteln detailliert erläutert.

Kapitel 1: Integration of celestial compass cues in the central complex of the locust brain

- Durchführung aller 87 Experimente
- Konzeption und Interpretation der Auswertung und statistischen Analyse in Kooperation mit Prof. Dr. Uwe Homberg und Prof. Dr. Keram Pfeiffer
- Durchführung der Auswertung und statistischen Analyse aller physiologischen Daten, ausschließlich mittels selbstständig verfasster MATLAB-kodierung
- Histologische Aufarbeitung aller fluoreszenzmarkierten Präparate und Auswertung mittels konfokaler Mikroskopie
- 2-dimensionale Rekonstruktion von 11 der 13 Neurone (84%), die in den Abbildungen gezeigt sind
- Anfertigung aller Abbildungen
- Anfertigung des Manuskriptes in Zusammenarbeit (Korrektur) mit Prof. Dr. Uwe Homberg
- Dieses Kapitel wurde in der hier vorliegenden Form (von kleinen sprachlichen Änderungen abgesehen) beim *Journal of Experimental Biology* veröffentlicht: Pegel U, Pfeiffer K, Homberg U (2018) Integration of celestial compass cues in the central complex of the locust brain. J Exp Biol 221: 10.1242/jeb.171207.

Kapitel 2: Two compasses in the central complex of the locust brain

- Konzeption und Durchführung aller 79 Experimente
- Konzeption der Auswertung und statistischen Analyse aller physiologischen Daten
- Durchführung der Auswertung und statistischen Analyse aller physiologischen Daten, ausschließlich mittels selbstständig verfasster MATLAB-Kodierung, mit Ausnahme einer Funktion zur zirkulär-linearen Korrelation (verfasst von Christine Scholtyssek), sowie einer Funktion zur Darstellung eines zirkulären Histogramms (verfasst von Frederick Zittrell)
- Interpretation der Auswertung und statistischen Analyse in Kooperation mit Prof. Dr. Uwe Homberg

- Histologische Aufarbeitung aller fluoreszenzmarkierten Präparate und Auswertung mittels konfokaler Mikroskopie
- Anfertigung aller Abbildungen
- Anfertigung des Manuskriptes in Zusammenarbeit (Korrektur) mit Prof. Dr. Uwe Homberg
- Dieses Kapitel wurde in der hier vorliegenden Form (von geringfügigen Änderungen abgesehen) am 13.04.2018 beim *Journal of Neuroscience* eingereicht

Kapitel 3: Influence of wide-field motion on the signalling of sky compass cues in the locust central complex

- Konzeption der Durchführung der kombinierten Reizgebung
- Durchführung von 14 aus 15 (93%) Experimenten
- Konzeption und Interpretation der Auswertung und statistischen Analyse aller physiologischer Daten
- Durchführung der Auswertung und statistischen Analyse aller physiologischen Daten, ausschließlich mittels selbstständig verfasster MATLAB-kodierung
- Histologische Aufarbeitung von 14 der 15 (93%) fluoreszenzmarkierten Präparate und Auswertung mittels konfokaler Mikroskopie
- Dreidimensionale Darstellung des CL2 Neurons und dreidimensionale Rekonstruktion der Neuropile des Zentralkomplexes
- Anfertigung aller Abbildungen, wobei die Teilabbildung 1B in ihrer Grundform aus einer Teilabbildung eines anderen Manuskriptes hervorging
- Anfertigung des Manuskriptes in Zusammenarbeit (Korrektur) mit Prof. Dr. Uwe Homberg
- Dieses Kapitel soll in der hier vorliegenden Form bei dem Fachjournal *Scientific Reports* eingereicht werden, sobald Kapitel 2 für die Veröffentlichung akzeptiert ist

Introduction

Spatial orientation

Spatial orientation is a crucial task for most animal species. It is needed for the most basic things of life: finding shelter or home, finding food, a place for reproduction and conspecifics (e.g. mates or offspring). A variety of cues can be used for spatial orientation. Often animals are able to exploit more than one cue, in order to improve orientation accuracy and to avoid getting lost if one cue is temporally not available. For instance, a long distance homing bird like the pigeon uses a sun compass for orientation, but when the Sun is obscured by clouds it is able to find home by instead using the Earth's magnetic field (Bookman, 1977; Wiltschko et al., 1981). Nocturnal predators like owls or bats mainly rely on auditory signals either coming from the environment itself or the prey it is hunting (Knudsen and Konishi, 1978) or by echolocation to catch their prey (Simmons et al., 1979). Spatial orientation based on olfaction is highly debated especially for birds (Wiltschko, 2017), as most olfactory cues are available only locally. Yet, for a short distance, orientation based on olfaction might be well suited, as for a plume tracking moth, trying to find a mate. There are many other possible cues depending on the animal's habitat, like air or water currents, any type of gradient (e.g. temperature) or any cues of the sky like the pattern of stars. However, the most reliable cues for many long-distance migrants, like birds (e.g. robins), mammals (e.g. caribous), or insects (e.g. monarch butterflies) critically involve vision, as eyes may perceive not only multiple types of visual cues, but also geomagnetic cues (Clites and Pierce, 2017).

Spatial orientation can be achieved either by using a compass, landmarks, or navigational mechanisms. Compass orientation is a kind of menotactic behavior. Menotaxis means that the animal is able to hold a constant course relative to a light source (e.g. the Sun). For instance, dung beetles need to roll their dung ball as far away as possible from any competitors. To do so they use (among other cues) the position of the Sun to maintain a straight direction (Dacke et al., 2014). Sun compass orientation is known from many insect species, like ants (Wehner and Müller, 2006), butterflies (Mouritsen and Frost, 2002) and bees (Brines and Gould, 1979), but also from vertebrates like the pigeon (Schmidt-Koenig, 1960). When landmarks are used for spatial orientation, their relation to each other and to the nest has to be learned in some animals, as demonstrated for bees (Menzel et al., 2006). As vertebrates most likely store landmarks in a cognitive map (Bennett, 1996), insects are suggested to use image-matching to identify familiar views of the panorama (Zeil, 2012). In many animals compass cues and landmarks are used to complement navigational abilities, resulting in complex strategies. The more simple form of navigation is based on a vector. Vector navigating animals have information about direction and distance towards their goal. The vector defining the travel route can be innate as shown for migratory birds, such as the European warbler or the starling (Perdeck, 1958; Berthold and Querner, 1981). Central place foragers like bees and ants that need to find their way back to a nest or hive (homing) calculate the home vector bringing them straight back, a phenomenon termed path integration (Collett and Collett, 2000; Wehner, 2003). Animals using this strategy update their internal position estimate relative to a nest or hive, based on distance and direction information of all performed movements (Collett and Collett, 2000), using celestial

compass cues (Evangelista et al., 2014). However, when they are displaced before starting homing they are not able to find their way back, as the home vector leads them to a wrong position (Müller and Wehner, 1988). In this situation landmarks can augment homing performance (Menzel et al., 2005). The more sophisticated navigational strategy is "true navigation", which can be observed in some animals homing across large distances. True navigators like the homing pigeon have the ability to find home from an unfamiliar location, thus relying neither on information of the outbound trip to the release site nor on landmarks (Gould and Gould, 2012). Instead they may be able to determine their exact geographical position and find home by using a geomagnetic and sun compass (Wiltschko, 2017).

In insects true navigation has not, to date been demonstrated. However, despite their tiny brains they show remarkable strategies, like the above mentioned path integration. The desert locust studied here might use a compass system for spatial orientation (Mappes and Homberg, 2004)). In their gregarious phase (Fig. 1*A*), these animals can build large swarms in which they travel long distances across the desert of Africa and the Middle East (Uvarov, 1977). Their migrations are seasonal (Fig. 1*B*) and highly directed, and serve to find new feeding and breeding grounds. Although it has been suggested that locusts simply fly downwind, there is evidence that these animals actively steer a steady course by using compass cues of the diurnal sky (Merlin et al., 2012; Homberg, 2015).

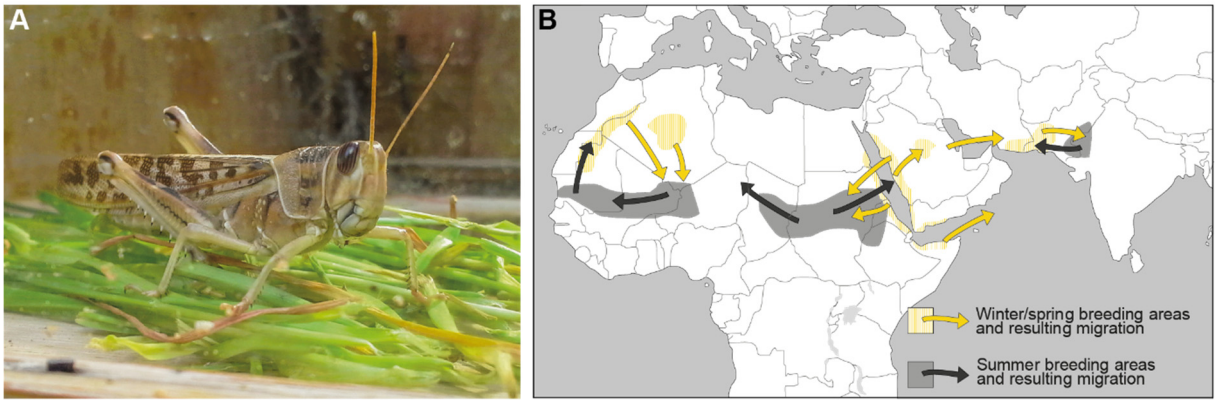

Fig. 1. Morphology and seasonal migration of the desert locust *Schistocerca gregaria*. *A,* Female desert locust of the gregarious phase, raised together with other individuals in the summer, partly in a greenhouse, partly under the open sky. ***B,*** Migration routes of desert locust swarms in the autumn (black arrows) and in spring (yellow arrows). Modified from Symmons and Cressman (2001).

Diurnal sky compass signals and their relevance for insect navigation

The most prominent cue in the diurnal sky is the Sun. Its position in the sky has a horizontal component (azimuth) and a vertical component (elevation). Over the course of the day both change in a predictable way, making the solar azimuth (the horizontal position of the Sun) a highly reliable navigational cue. Several animals use direct sunlight to keep their straight heading relative to the solar azimuth. These animals include bees (Brines and Gould, 1979), ants (Wehner and Müller, 2006) and dung beetles (Dacke et al., 2014). However, the Sun is not always visible, e.g. if it is obscured by clouds, so that users of a sun compass must rely on additional signals providing reference for solar position. The polarization pattern of the sky that arises from scattering of direct sunlight in the Earth's atmosphere provides such an additional signal. It is not visible to the human eye, but is visible to many insects, including the locust. Light as an electromagnetic wave has two components:

The magnetic field vector and the electric field vector (*E*-vector). Direct sunlight is unpolarized, meaning that the *E*-vector oscillates in all possible planes perpendicular to the propagation of light. However, after passing a polarization filter the *E*-vector oscillates in only one remaining plane. In the Earth's atmosphere unpolarized light is scattered by air molecules, inducing linear polarization. Depending on the viewing angle of an observer the degree (i.e. the percentage) of polarization varies (Fig. 2*A*). In the sky Rayleigh scattering results in a pattern of polarized light with dominant *E*-vectors tangentially aligned along concentric circles around the Sun (Fig. 2*B*; Strutt 1871a, 1871b). The degree of polarization is low in proximity of the Sun and increases to a maximum of 75% at an angle 90° away from the Sun (Coulson, 1988). From there, the degree of polarization decreases again toward the anti-solar point (i.e. 180° away from the Sun). As the polarization pattern is linked to solar position, it changes orientation in a similar way as the Sun over the course of a day. However, the pattern is mirrored at a circle at 90° distance to the Sun (see Fig. 2B), therefore, ambiguously referencing the position of the Sun and of the anti-solar point.

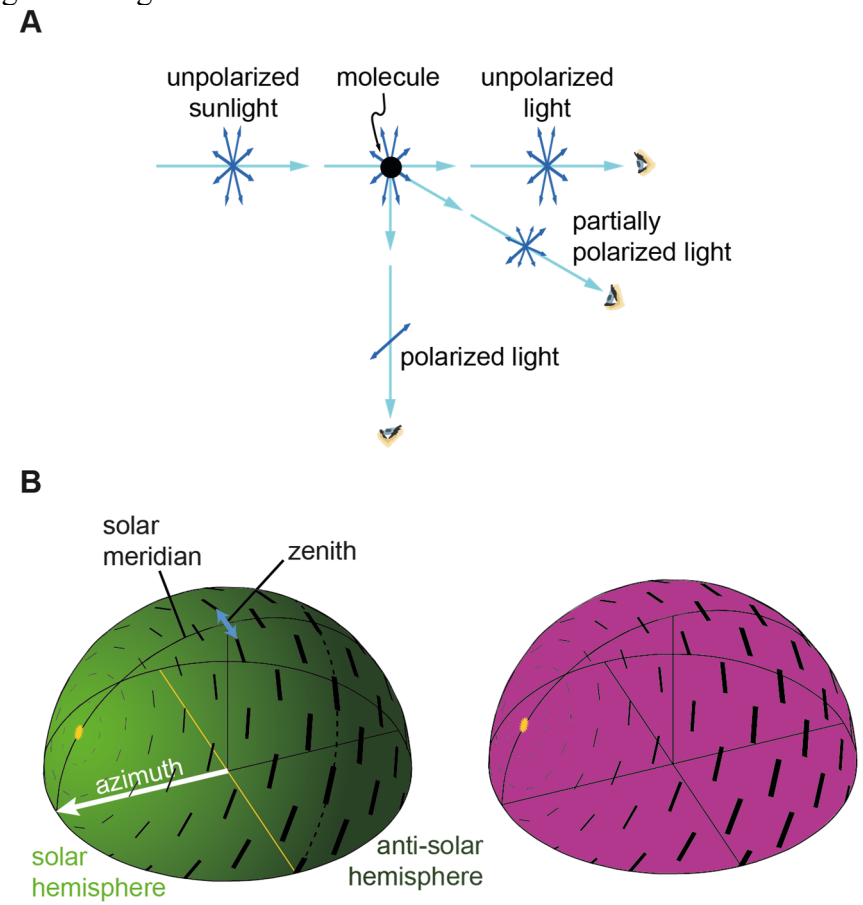

Fig. 2. Polarized and unpolarized sky compass cues. ***A,*** Polarization of sunlight. In unpolarized sunlight the electric field vector (dark blue) oscillates in all possible planes perpendicular to the propagation of light (light blue). Unpolarized sunlight gets scattered by air molecules (black dot) in the atmosphere. The degree of polarization depends on the viewing angle. At 0° viewing angle (direct sunlight) the degree of polarization is 0% (unpolarized light). With increasing viewing angle the degree of polarization increases (partially polarized light), and is maximal at an angle of 90° (polarized light). Template for illustration taken from https://opentextbc.ca/physicstestbook2/wp-content/uploads/sites/211/2017/10/Figure_28_08_11a.jpg. ***B,*** Schematic illustration of the polarization pattern and the chromatic gradient in the sky. The *E*-vectors of polarized light (black bars) are aligned along concentric circles around

the Sun. Across the sky, light is only partially polarized. The degree of polarization (i.e. the percentage of polarization) is indicated by the thickness of the bars and increases from solar position (0%; yellow dot indicates the Sun) toward a circle at 90° distance to the Sun (75%; black dotted line). From this 90° distance the polarization degree decreases again towards the non-visible anti-solar point (solar position plus 180°). The polarization pattern provides reference for solar azimuth (white arrow). The light blue double arrow shows the orientation of the zenithal *E*-vector, being always perpendicular to the solar azimuth, as the Sun changes position along the solar meridian. While the intensity of long-wavelength green light decreases from the solar hemisphere (to the left of the yellow line) towards the anti-solar hemisphere (to the right of the yellow line; left panel), short-wavelength UV light is uniformly distributed across both hemispheres (right panel).

Many insect species are known to use polarized light for spatial orientation. Experiments on monarch butterflies (Reppert, 2004; but also see Stalleicken et al., 2005), crickets (Brunner and Labhart, 1987), flies (von Philipsborn and Labhart, 1990; Warren et al., 2018), bees (von Frisch, 1949; Evangelista et al., 2014), ants (Wehner, 1984), dung beetles (Dacke et al., 2003) and locusts (Mappes and Homberg, 2004) showed alignment of their body orientation relative to the *E*-vector of polarized light presented from dorsal direction during locomotion. This behavior is known as polarotaxis and allows the animal to steer a steady course. However, when changing direction (e.g. when beginning homing after foraging) additional signals might be necessary to distinguish between solar and anti-solar hemisphere.

A clear reference for the solar and anti-solar hemisphere (for illustration see Fig. 2B) is provided by the light intensity gradient and the chromatic gradient. Rayleigh scattering causes an irregular distribution of long wavelength light (green range) in the sky with a maximum light intensity at the position of the Sun (Fig. 2*B*; Coemans, 1994). From this position, the intensity decreases constantly towards the anti-solar hemisphere. The resulting green light intensity gradient alone might be sufficient to distinguish between the solar and the anti-solar hemisphere. That such a simple light intensity gradient can be sufficient for spatial orientation has been shown in ball-rolling dung beetles (el Jundi et al., 2014b). However, the chromatic gradient of the sky might be more useful. In contrast to long wavelength light, short wavelength light (UV range) is uniformly distributed across the visible parts of the solar and anti-solar hemispheres (Fig. 2*B*; Coemans, 1994). Even though the intensity of green light is comparatively higher throughout the entire sky, the ratio between green and UV light is higher close to the Sun than in the anti-solar hemisphere. By comparing the intensities of green and UV light, animals might obtain a more reliable reference for solar position than by using a simple brightness gradient.

Spatial orientation using the chromatic gradient has been demonstrated in bees (Brines and Gould, 1979; Rossel and Wehner, 1984), ants (Wehner, 1997) and dung beetles (el Jundi et al., 2015a). The detection of the two colors (green and UV) constituting the chromatic gradient is achieved by photoreceptors of the compound eye with spectral sensitivity in the green and UV range of light (Daumer, 1956). However, these photoreceptors are not optimized for the perception of polarized light.

Polarized light perception

Many animals are able to detect polarized light, either arising from reflection on shiny surfaces, such as the water surface, or from the scattering of sunlight in the atmosphere. Polarized light originating from reflection is used by cuttlefish for communication (Mäthger et al., 2009), by fiddler crabs for object detection (How et al., 2015), by butterflies and dragonflies for finding oviposition sites (Wildermuth, 1998; Kelber, 1999), and by bumblebees for recognizing flowers as a food source (Foster et al., 2014). However, as mentioned above a broad taxonomic range of insects is able to use the polarization of light for orientation (Horváth, 2014). These insects have a specialized region at the dorsal tip if the eye in common, termed the dorsal rim area (DRA; Fig. 3; Labhart and Meyer, 1999; Stalleicken et al., 2006; Weir et al., 2016).

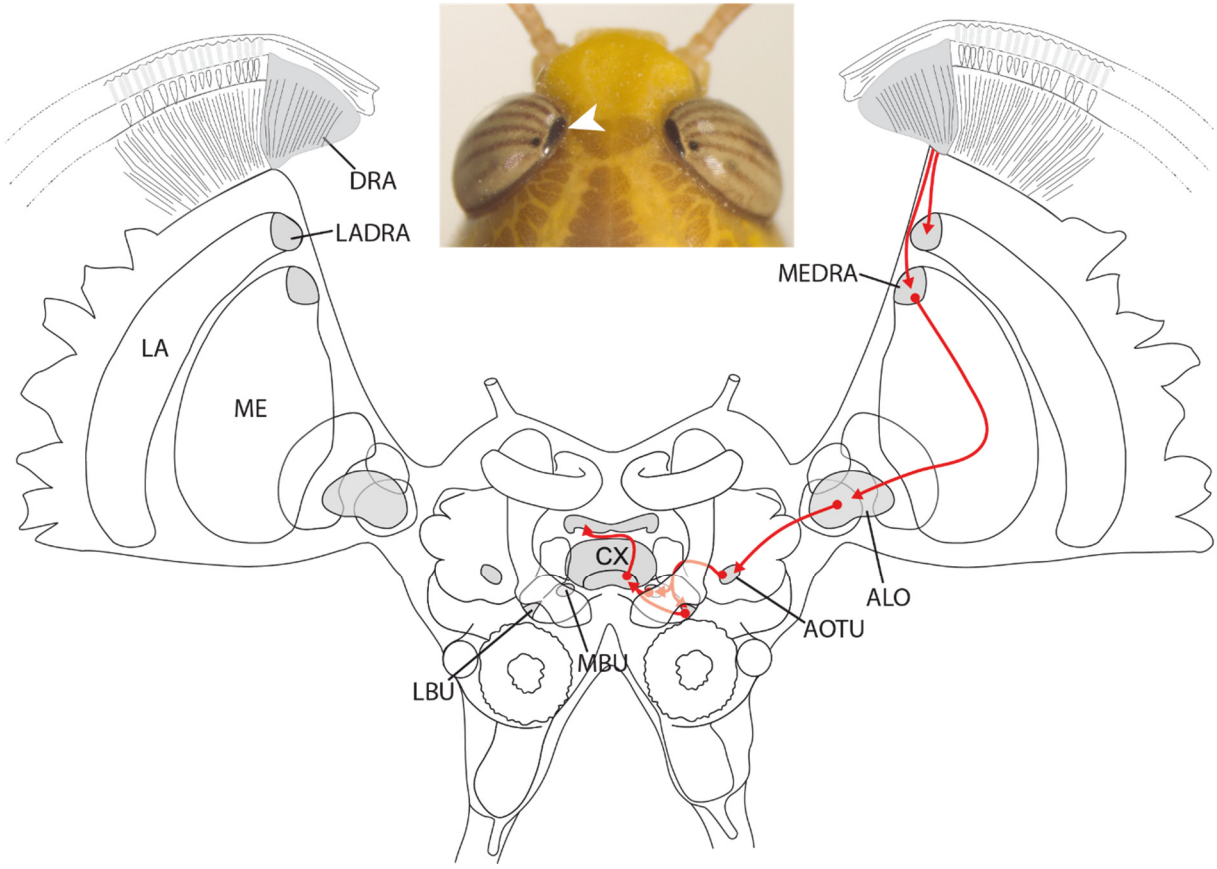

Fig. 3. The polarization vision pathway in the locust brain. Image showing dorsal view of the head of the locust including the dorsal rim areas of the compound eyes. White arrowhead points to the left dorsal rim area (DRA). The dark dot right next to the DRA is the pseudopupil. Schematic frontal view of the locust brain with its major neuropils, including those involved in polarization vision (grey). The polarization vision pathway is marked by red lines with presynapses indicated by arrowheads, and postsynapses indicated by filled circles. ALO, anterior lobula; AOTU, anterior optic tubercle; CX, central complex; DRA; dorsal rim area; LA, lamina; LADRA, dorsal rim of the lamina; LBU, lateral bulb; MBU, medial bulb; ME, medulla; MEDRA, dorsal rim of the medulla. Drawing of the brain envelope and neuropils adapted from Heinze (2009).

The DRA is optimized for polarization vision. Its morphology has been studied in several insect species. Photoreceptors of the DRA are homochromatic (i.e. they have similar spectral sensitivity), and are thus not suited for color vision (Labhart and Meyer, 1999). Within each rhabdomere of a photoreceptor (i. e. the light absorbing part of the photoreceptor), the microvilli are strictly aligned. As in the main retina, several photoreceptors cluster together building one ommatidium. In the DRA of the locust and some other insects, two subsets of photorecptors exist. Within an ommatidium a subset of photoreceptors typically shares the same orientation of microvilli alignment, while in the other subset microvilli orientation is perpendicular. Therefore, photoreceptors can act as *E*-vector analyzers, as each subset will maximally absorb light if the incoming *E*-vector is parallel to the long axis of the microvilli (Hardie, 1985). Owing to the lack of screening pigment and the presence of scattering structures (Homberg and Peach, 2002), DRA photoreceptors can have large receptive fields for polarized light, as demonstrated for the locust (Schmeling et al., 2015).

Some insects like the backswimmer (Schwind et al., 1984; Schwind, 1983), and the dragonfly (Armett-Kibel and Meinertzhagen, 1983) additionally have a ventral rim area, enabling them to detect polarization coming from below, like reflections of light on a water surface. Independent of whether polarized light is perceived by the dorsal or ventral rim area, the signal needs to be processed in distinct brain areas in order to produce a behavioral output.

The polarization vision pathway

At least two pathways are known, that process polarized light signals within the desert locust brain. I will focus here on the so called "anterior polarization vision pathway" leading from the eyes to the central complex. This pathway includes several neuropils and, thus, processing stages. Axons of DRA photoreceptors project to distinct dorsal parts of the lamina and the medulla (Fig. 3; Homberg and Paech, 2002). Transmedulla neurons connect the dorsal medulla and the 4th layer of the medulla with the anterior lobula and the lower unit of the anterior optic tubercle (AOTU; Homberg et al., 2003; el Jundi et al., 2011). They are suggested to integrate polarization signals coming from the DRA photoreceptors and unpolarized chromatic light information coming from intrinsic medulla neurons (el Jundi et al., 2011). Two types of polarization sensitive neurons project from the lower unit of the AOTU to the lateral bulb (TULAL1a) or the lateral and the medial bulbs (TULAL1b). Polarization sensitivity has been reported for both types of neurons (Pfeiffer et al., 2005). In the bulbs the TULAL neurons make direct contact to types of tangential neurons (TL2 and TL3) via microglomerular synaptic complexes (Fig. 4*A*; Träger et al., 2008), transferring the signal to the central complex (CX).

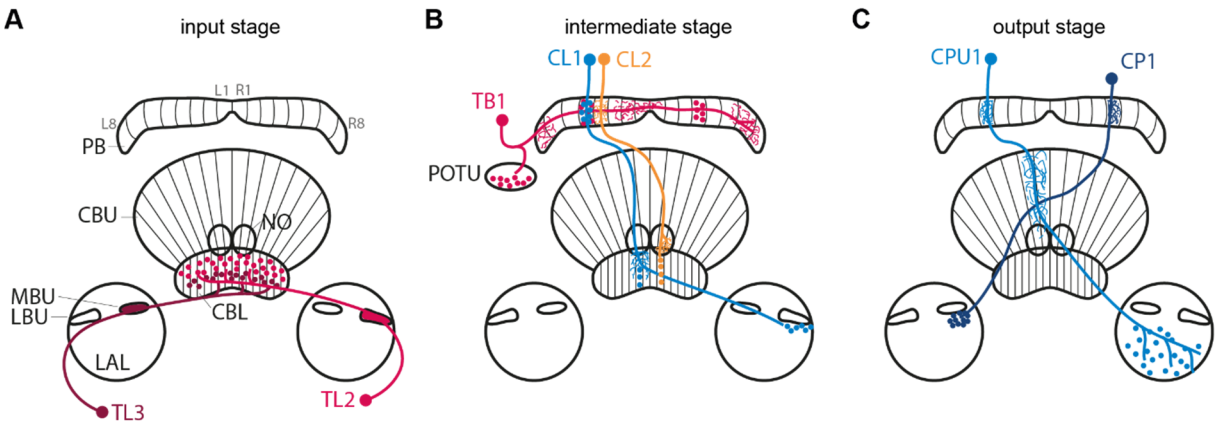

Fig. 4. Neuropils and most prominent neurons of the locust central complex. ***A,*** Neurons of the input processing stage of the polarization vision network. Tangential neurons of the lower division of the central body (CBL), TL2 and TL3 neurons, transfer the signal from the lateral and medial bulbs (LBU, MBU) to distinct horizontal layers of the CBL. Filled neuropils indicate microglomerular complexes, dots indicate varicose arborizations. The protocerebral bridge (PB), the upper division of the central body (CBU) and the CBL are structured into 16 vertical slices (thin black lines), 8 in the left brain hemisphere (L1-L8) and 8 in the right brain hemisphere (R1-R8). LAL, lateral accessory lobe; NO, noduli. ***B,*** Neurons of the intermediate processing stage. Columnar neurons of the CBL (CL1, CL2) transfer the signal between slices of the CBL and slices of the PB. Tangential neurons of the PB (TB1) connect different slices of the PB with the posterior optic tubercle (POTU). ***C*** Neurons of the output processing stage. Neurons of the PB (CP1) and of the CBU (CPU1) transfer the pre-motor output signal from the PB to the LAL.

The central complex

The CX is a group of midline-spanning neuropils in the brain of many insects. In the locust, it consists of the upper (CBU) and lower division (CBL) of the central body (CB), the protocerebral bridge (PB), and the paired noduli (NO; Fig. 4*A*). The CBU is structured in three and the CBL in 6 horizontal layers (Müller et al., 1997; Heinze and Homberg, 2008). The noduli can be divided into an upper division with three horizontal layers, and a lower division without layers (Heinze and Homberg, 2008). The layered structure arises from distinct innervation by different types of tangential neurons. Apart from the noduli, columnar neurons structure the CX into 16 vertical slices (Williams et al., 1975).

In the locust, a variety of cell types arborizing in the CX belongs to the polarization vision network (Vitzthum et al., 2002; Heinze et al., 2009; Heinze and Homberg, 2009). Four types of tangential neurons (TL1-4) are suggested to provide input to the different layers of the CBL. Polarization sensitivity has been reported for TL1-3 neurons (Vizthum et al., 2002). In the CBL columnar neurons (CL1) likely receive the signal from TL neurons and transfer it to the PB (Fig. 4*B*), showing robust polarization sensitivity (Heinze et al., 2009; Bockhorst and Homberg, 2015a). CL2 neurons connect distinct slices of the PB with the contralateral nodulus and slices of the CBL (Fig. 4*B*). In the PB polarization sensitive TB1 neurons (Fig. 4B) likely receive input from CL1 neurons, and connect distinct slices of the PB with the posterior optic tubercle (POTU; Heinze and Homberg, 2007). Columnar neurons with fine arborizations in the PB and the CBU and widespread varicosities in the lateral accessory lobe (LAL) likely transfer the pre-motor output signal of the CX to descending neurons arborizing in the LAL (Williams, 1975). Out of five existing types of CPU neurons only two (CPU1, CPU2) have been reported to belong to the polarization signaling network (Heinze et al., 2009). Along with two other types of polarization sensitive columnar

neurons (CP1 and CP2) they complement the final processing stage of polarization vision in the CX (Fig. 4*C*; Heinze et al., 2009).

Polarization sensitivity in neurons of the CX has been demonstrated not only in locusts, but also in dung beetles (el Jundi et al., 2015b), crickets (Sakura et al., 2008), monarch butterflies (Heinze and Reppert, 2011) and sweat bees (Stone et al., 2017). Besides polarization a multitude of other sensory stimuli, related to navigational tasks, are processed in this brain area, like the azimuth of a salient bright landmark in flies (Seelig and Jayaraman, 2013), dung beetles (el Jundi et al., 2015) and monarch butterflies (Heinze and Reppert, 2011), optic flow in flies (Weir and Dickinson, 2015), cockroaches (Kathman et al., 2014) and sweat bees (Stone et al., 2017), and small moving objects and looming stimuli in the locust (Bockhorst and Homberg, 2015b; Rosner and Homberg, 2013). Furthermore, the coding for azimuth information in the locust was shown in recordings of three CX neurons (el Jundi et al., 2014a).

In addition to these visual cues, internal motion information, derived from passive or active movement of the animal, is also processed in the CX (Varga and Ritzmann, 2016; Seelig and Jayaraman, 2015). CX neurons are reported to respond to mechanosensory cues in locusts (Homberg, 1994) and cockroaches (Ritzmann et al., 2008), and to olfactory cues in bees (Homberg, 1985). Besides sensory processing the CX is involved in locomotor control, as lesion studies showed in flies (Strauss, 2002), crickets (Huber, 1960) and cockroaches (Harley and Ritzmann, 2010; Ritzmann et al., 2012). Extracellular recordings in cockroaches showed that the activity of CX neurons is correlated with the animal's walking speed and stepping frequency (Bender et al., 2010; Martin et al., 2010). In the same studies a current injection through recording electrodes in this brain area induced walking in stationary animals, and increased walking speed in moving animals (Bender et al., 2010; Martin et al., 2015). Additionally, a prediction of movement in CX neurons is shown in locusts and cockroaches (Homberg, 1994, Bender et al., 2010). Furthermore, the *Drosophila* CX is involved in visual and spatial memory (Liu et al., 2006; Ofstad et al., 2011), and in controlling states of arousal and sleep (Ueno et al., 2012; Donlea et al., 2014). Taken together these findings suggest that the CX is a center integrating navigational signals with behavioral states, and planning a goal-directed locomotor output (Varga et al., 2017).

The map inside the brain

As discussed above, neurons of the desert locust CX respond to the plane of polarized light presented from dorsal direction. The activity of these neurons is sinusoidally modulated during a 360° rotation of the polarizer (Fig. 5*A*), revealing a preferred *E*-vector orientation with highest firing rate (Φ_{max}; Fig. 5*A'*). Therefore, these neurons encode the animals head direction with respect to the orientation of the zenithal *E*-vector. In the fruit fly the animal's representation of head direction relative to a salient landmark is shifted across the slices of the CX as the animal turns in a certain direction (Seelig and Jayaraman, 2015). In the PB a total range of 2×360° horizontal directions are represented (Turner-Evans et al., 2017; Green et al., 2017). A similar representation of heading directions was found in the locust CX as well. Here the relative orientation toward an *E*-vector presented from dorsal direction is topographically represented in two cell types of the PB (Heinze and Homberg, 2007). TB1 and CPU1 neurons both represent 360° of

horizontal directions across all PB slices (Fig. 5*B*). The locust CX, therefore, likely acts as an internal sky compass. Because the Sun changes its position in the sky over the course of a day, a day-time compensation of this internal compass is crucial for long distance flights, as performed by the locust. Such a compensation remains to be shown, but it has been suggested that neurons connecting the accessory medulla (the likely site of the locust internal clock) with the POTU deliver day-time information to the compass neurons (TB1; el Jundi and Homberg, 2010).

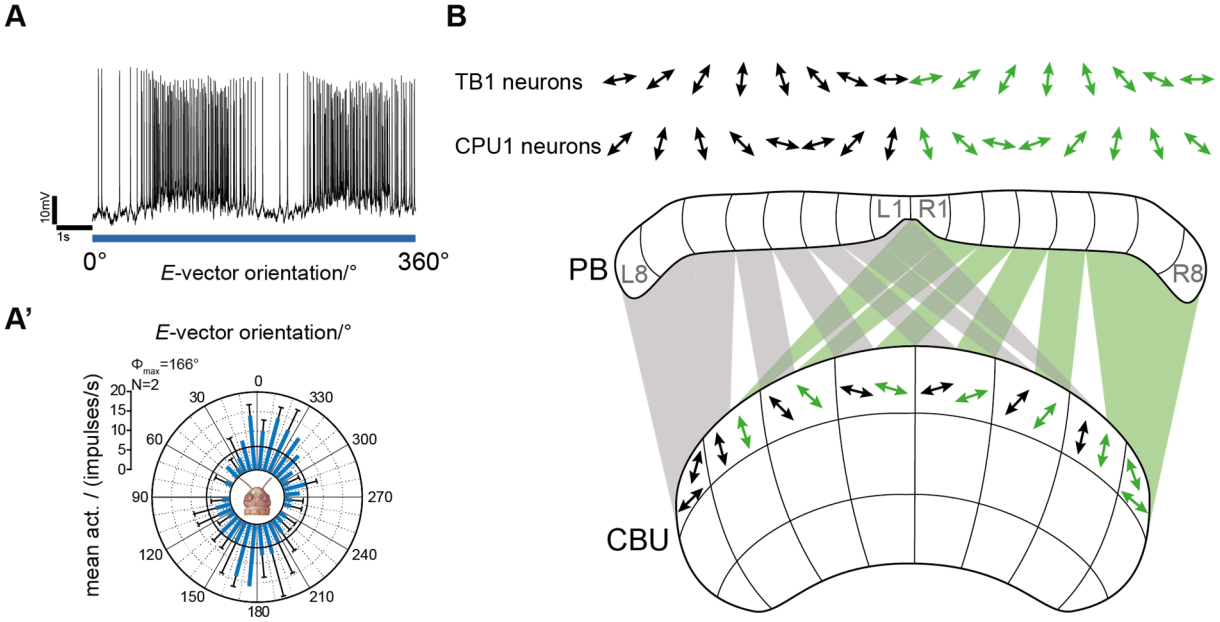

Fig. 5. Topographic representation of *E*-vectors. ***A,*** Spike train of a polarization sensitive central-complex neuron showing its response to a 360° rotation of the polarizer. ***A',*** Tuning of the same neuron to the *E*-vector. One clockwise and one counterclockwise rotation were binned in 10° bins. Resulting stimulus response curves were averaged. Firing rate is highest at the cell's preferred head direction relative to the *E*-vector (Φ_{max}). Error bars indicate standard deviation. Black circle shows background activity. N, number of trials. Image of locust head taken by Keram Pfeiffer. ***B,*** TB1 and CPU1 neurons topographically represent the zenithal *E*-vector (double arrows) in the protocerebral bridge (PB). This topographic map roughly covers 360° across the left brain hemisphere (black, L1-L8) and the right brain hemisphere (green, R1-R8) in both cell types. CPU1 neurons arborize additionally in the first horizontal layer of the upper division of the central body (CBU). Here they represent 280° of horizontal directions. Modified from Pfeiffer and Homberg (2014).

References

Armett-Kibel C, Meinertzhagen IA (1983) Structural organization of the ommatidium in the ventral compound eye of the dragonfly *Sympetrum*. J Comp Physiol A 151:285-295.

Bender JA, Pollack AJ, Ritzmann RE (2010) Neural activity in the central complex of the insect brain is linked to locomotor changes. Curr Biol 10:921-26.

Bennett AT (1996) Do animals have cognitive map? J Exp Biol 199:219-224.

Berthold P, Querner U (1981) Genetic basis of migratory behavior in European warblers. Science 212:77-79.

Bockhorst T, Homberg U (2015a) Amplitude and dynamics of polarization-plane signaling in the central complex of the locust brain. J Neurophysiol 113:3291-3311.

Bockhorst T, Homberg U (2015b) Compass cells in the brain of an insect are sensitive to novel events in the visual world. PLos One 10:10.1371/journal.pone.0144501.

Bookman MA (1977) Sensitivity of the homing pigeon to an Earth-strength magnetic field. Nature 267:340-342.

Brines ML, Gould JL (1979) Bees have rules. Science 206:571-573.

Brunner D, Labhart T (1987) Behavioural evidence for polarization vision in crickets. Physiol Entomol 12:1-10.

Clites BL, Pierce JT (2017) Identifying cellular and molecular mechanisms for magnetosensation. Ann Rev Neurosci 40:231-250.

Coemans MA, Vos HJJ, Nuboer JF (1994) The relation between celestial color gradients and the position of the sun with regard to the sun compass. Vision Res 34:1461-1470.

Collett TS, Collett M (2000) Path integration in insects. Curr Opin Neurobiol 10:757-762.

Coulson KL (1988) Polarization and intensity of light in the atmosphere. Deepak, Hampton, VA.

Dacke M, Nordström P, Scholtz CH (2003) Twilight orientation to polarized light in the crepuscular dung beetle *Scarabaeus zambesianus*. J Exp Biol 206:1535-1543.

Dacke M, el Jundi B, Smolka J, Byrne M, Baird E (2014) The role of the sun in the celestial compass of dung beetles. Philos Trans R Soc B 369: 10.1098/rstb.2013.0036.

Daumer K (1956) Reizmetrische Untersuchungen des Farbensehens der Bienen. Z Vergl Physiol 38:413-478.

Donlea JM, Pimentel D, Miesenböck G (2014) Neuronal machinery of sleep homeostasis in *Drosophila*. Neuron 81:860-872.

el Jundi B, Homberg U (2010) Evidence for the possible existence of a second polarization-vision pathway in the locust brain. J Insect Phyiol 56:971-979.

el Jundi B, Pfeiffer K, Homberg U (2011) A distinct layer of the medulla integrates sky compass signals in the brain of an insect. PLoS One 6:10.1371/journal.pone.0027855.

el Jundi B, Pfeiffer K, Heinze S, Homberg U (2014a) Integration of polarization and chromatic cues in the insect sky compass. J Comp Physiol A 200:575-589.

el Jundi B, Smolka J, Baird E, Byrne MJ, Dacke M (2014b) Diurnal dung beetles use the intensity gradient and the polarization pattern of the sky for orientation. J Exp Biol 217:2422-2429.

el Jundi B, Foster JJ, Byrne MJ, Baird E, Dacke M (2015a) Spectral information as an orientation cue in dung beetles. Biol Lett 11: 10.1098/rsbl.2015.0656.

el Jundi B, Warrant EJ, Byrne MJ, Khaldy L, Baird E, Smolka J, Dacke M (2015b) Neural coding underlying cue preference for celestial orientation. Proc Natl Acad Sci U S A 112:11395-11400.

Evangelista C, Kraft P, Dacke M, Labhart T, Srinivasan MV (2014) Honeybee navigation: Critically examining the role of the polarization compass. Philos Trans R Soc Lond B Biol Sci 369: 10.1098/rstb.2013.0037.

Foster JJ, Sharkey CR, Gaworska AVA, Roberts NW, Whitney HM, Partridge JC (2014) Bumblebees learn polarization patterns. Curr Biol 24:1415-1420.

Gould JL, Gould CG (2012) Nature's compass: The mystery of animal navigation. Princeton University Press, Princeton.

Green J, Adachi A, Shah KK, Hirokawa JD, Magani PS, Maimon G (2017) A neural circuit architecture for angular integration in *Drosophila*. Nature 546:101-106.

Hardie RC (1985) Functional organization of the fly retina. In: Autrum H, Ottoson D, Perl ER, Schmidt RF, Shimazu H, Willis WD (eds) Progress in Sensory Physiology. (vol. 5) Springer, Berlin, Heidelberg.

Harley CM, and Ritzmann RE (2010). Electrolytic lesions within central complex neuropils of the cockroach brain affect negotiation of barriers. J Exp Biol 213:2851-2864.

Heinze S, Gotthardt S, Homberg U (2009) Transformation of polarized light information in the central complex of the locust. J Neurosci 29:11783-11793.

Heinze S, Homberg U (2007) Maplike representation of celestial *E*-vector orientations in the brain of an insect. Science 315:995-997.

Heinze S, Homberg U (2008) Neuroarchitecture of the central complex of the desert locust: intrinsic and columnar neurons. J Comp Neurol 511:454-478.

Heinze S (2009) Characterization of polarization sensitive neurons of the central complex in the brain of the desert locust (*Schistocerca gregaria*). Doctoral thesis, University of Marburg.

Heinze S, Homberg U (2009) Linking the input to the output: New sets of neurons complement the polarization network in the locust central complex. J Neurosci 29:4911-4921.

Heinze S, Reppert SM (2011) Sun compass integration of skylight cues in migratory monarch butterflies. Neuron 69:345-358.

Homberg U (1985) Interneurones of the central complex in the bee brain (*Apis mellifera, L*). J Insect Physiol 31:251-264.

Homberg U (1994) Flight-correlated activity changes in neurons of the lateral accessory lobes in the brain of the locust *Schistocerca gregaria*. J Comp Physiol A 175:597-610.

Homberg U (2015) Sky compass orientation in desert locusts – Evidence from field and laboratory studies. Front Behav Neurosci 9: 10.3389/fnbeh.2015.00346.

Homberg U, Paech A (2002) Ultrastructure and orientation of ommatidia in the dorsal rim area of the locust compound eye. Arthropod Struct Dev 30:271-280.

Homberg U, Reischig T, Stengl M (2003) Neural organization of the circadian system of the cockroach *Leucophaea maderae*. Chronobiol Int 20:577-590.

Horváth, G D (2014) Polarized light and polarization vision in animal science. Springer Berlin.

How MJ, Christy JH, Temple SE, Hemmi JM, Marshall NJ, Roberts NW (2015) Target detection is enhanced by polarization vision in a fiddler crab. Curr Biol 25:3060-3073.

Huber F (1960) Untersuchungen über die Funktion des Zentralnervensystems und insbesondere des Gehirnes bei der Fortbewegung und der Lauterzeugung der Grillen. Z Vgl Physiol 44:60-132.

Kathman ND, Kesavan M, Ritzmann RE. (2014) Encoding wide-field motion and direction in the central complex of the cockroach *Blaberus discoidalis*. J Exp Biol 217:4079-4090.

Kelber A (1999) Why 'false' colours are seen by butterflies. Nature 402:251.

Knudsen EL, Konishi M (1978) A neural map of auditory space in the owl. Science 200:795-797.

Labhart T, Meyer EP (1999) Detectors for polarized skylight insects: a survey of ommatidial specializations in the dorsal rim area of the compound eye. Microsc Res Tech 47:368-379.

Liu G, Seiler H, Wen A, Zars T, Ito K, Wolf R, Heisenberg M, Liu L (2006) Distinct memory traces for two visual features in the *Drosophila* brain. Nature 439:551-556.

Mappes M, Homberg U (2004) Behavioral analysis of polarization vision in tethered flying locusts. J Comp Physiol A 190:61-68.

Martin JP, Guo P, Mu L, Harley CM, Ritzmann RE (2015) Central-complex control of movement in the freely walking cockroach. Curr Biol 25:2795-2803.

Mäthger LM, Shashar N, Hanlon RT (2009) Do cephalopods communicate using polarized light reflections from their skin? J Exp Biol 212:2133-2140.

Menzel R, De Marco RJ, Greggers U (2006) Spatial memory, navigation and dance behavior in *Apis mellifera*. J Comp Physiol A 192:889-903.

Menzel R, Greggers U, Smith A, Berger S, Brandt R, Brunke S, Bundrock G, Hülse S, Plümpe T, Schaupp F, Schüttler E, Stach S, Stindt J, Stollhoff N, Watzl S (2005) Honey bees navigate according to a map-like spatial memory. Proc Natl Acad Sci U S A 102:3040-3045.

Merlin C, Heinze S, Reppert SM (2012) Unraveling navigational strategies in migratory insects. Curr Opin Neurobiol 22:353-361.

Menzel R, Greggers U, Smith A, Berger S, Brandt R, Brunke S, Bundrock G, Hülse S, Plümpe T, Schaupp F, Schüttler E, Stach S, Stindt J, Stollhoff N, Watzl S (2005) Honey bees navigate according to a map-like spatial memory. Proc Natl Acad Sci U S A 102:3040-3045.

Mouritsen H, Frost BJ (2002) Virtual migration in tethered flying monarch butterflies reveals their orientation mechanisms. Proc Natl Acad Sci U SA 99:10162-10166.

Müller M, Homberg U, Kühn A (1997) Neuroarchitecture of the lower division of the central body in the brain of the locust (*Schistocerca gregaria*). Cell Tissue Res 288:159-176.

Müller M, Wehner R (1988) Path integration in desert ants, *Cataglyphis fortis*. Proc Natl Acad Sci U S A 85:5287-5290.

Ofstad, TA, Zuker CS, Reiser MB (2011) Visual place learning in *Drosophila melanogaster*. Nature 474:204-207.

Perdeck AC (1958) Two types of orientation in migrating starlings, Sturnus yulgaris L., and Chaffinches, Fringilla coelebs L., as revealed by displacement experiments. Ardea 56 1-37, in Schöne H (1980) Orientierung im Raum. Wissenschaftliche Verlagsgesellschaft, Stuttgart.

Pfeiffer K, Kinoshita M, Homberg U (2005) Polarization-sensitive and light-sensitive neurons in two parallel pathways passing through the anterior optic tubercle in the locust brain. J Neurophysiol 94:3903-3915.

Reppert SM, Zhu H, White RH (2004) Polarized light helps monarch butterflies navigate. Curr Biol 14:155-158.

Ritzmann RE, Harley CM, Daltorio KA, Tietz BR, Pollack AJ, Bender JA, Guo P, Horomanski AL, Kathman ND, Nieuwoudt C, Brown AE, Quinn RD (2012) Deciding which way to go: how do insects alter movements to negotiate barriers? Front Neurosci 6:10.3389/fnins.2012.00097.

Ritzmann RE, Ridgel AL, Pollack AJ (2008) Multi-unit recording of antennal mechano-sensitive units in the central complex of the cockroach *Blaberus discoidalis*. J Comp Physiol A 194:341-360.

Rosner R, Homberg U (2013) Widespread sensitivity to looming stimuli and small moving objects in the central complex of an insect brain. J Neurosci 33:8122-8133.

Rossel S, Wehner R (1984) Celestial orientation in bees: the use of spectral cues. J Comp Physiol A 155:605-613.

Sakura M, Lambrinos D, Labhart T (2008) Polarized skylight navigation in insects: model and electrophysiology of e-vector coding by neurons in the central complex. J Neurophysiol 99:667-682.

Schmeling F, Tegtmeier J, Kinoshita M, Homberg U (2015) Photoreceptor projections and receptive fields in the dorsal rim area and main retina of the locust eye. J Comp Physiol A 201:427-440.

Schmidt-Koenig K (1960) The sun azimuth compass: One factor in the orientation of homing pigeons. Science 131:826-828.

Schwind R (1983) Zonation of the optical environment and zonation in the rhabdom structure within the eye of the backswimmer, Notonecta glauca. Cell Tissue Res 232:53-63.

Schwind R, Schlecht P, Langer H (1984) Microspectrophotometric characterization and localization of three viual pigments in the compound eye of *Notonecta glauca* L. (Heteroptera). J Comp Physiol A 154:341-346.

Seelig JD, Jayaraman V (2013) Feature detection and orientation tuning in the *Drosophila* central complex. Nature 503:262-266.

Seelig JD, Jayaraman V (2015) Neural dynamics for landmark orientation and angular path integration. Nature 521:168-191.

Simmons JA, Fenton MB, O'Farrell MJ (1979) Echolocation and pursuit of prey by bats. Science 203:16-21.

Stalleicken J, Labhart T, Mouritsen H (2006) Physiological characterization of the compound eye in monarch butterflies with focus on the dorsal rim area. J Comp Physiol A 192:321-331.

Stalleicken J, Mukhida M, Labhart T, Wehner R, Frost B, Mouritsen H (2005) Do monarch butterflies use polarized skylight for migratory orientation? J Exp Biol 208:2399-2408.

Stone T, Webb B, Adden A, Weddig NB, Honkanen A, Templin R, Wcislo W, Scimeca L, Warrant E, Heinze S (2017) An anatomically constrained model for path integration in the bee brain. Curr Biol 27:3069-3085.

Strauss R (2002) The central complex and the genetic dissection of locomotor behavior. Curr Opin Neurobiol 12:633-638.

Strutt JW (1871a) On the light from the sky, its polarization and color. Philos Mag 41:107-120.

Strutt JW (1871b) On the scattering of light by small particles. Philos Mag 41:447-454.

Symmons PM, Cressman K (2001) Desert locust guidelines 1. Biology and behavior. FAO, Rome.

Träger U, Wagner R, Bausenwein B, Homberg U (2008) A novel type of microglomerular synaptic complex in the polarization vision pathway of the locust brain. J Comp Neurol 506:299-300.

Turner-Evans D, Wegener S, Rouault H, Franconville R, Wolff T, Seelig JD, Druckmann S, Jayaraman V (2017). Angular velocity integration in a fly heading circuit. Elife 6:10.7554/eLife.23496.

Ueno T, Tomita J, Tanimoto H, Endo K, Ito K, Kume S, Kume K (2012) Identification of a dopamine pathway that regulates sleep and arousal in *Drosophila*. Nat Neurosci 15:1516-1523.

Uvarov B (1977) Grasshoppers and locusts. A handbook of general acridology. (vol. 2) London: Centre for Overseas Pest Research.

Varga AG, Kathman ND, Martin JP, Guo P, Ritzmann RE (2017) Spatial navigation and the central complex: Sensory acquisition, orientation, and motor control. Front Behav Neurosci 11: 10.3389/fnbeh.2017.00004.

Varga AG, Ritzmann RE (2016). Cellular basis of head direction and contextual cues in the insect brain. Curr Biol 26:1816-1828.

Vitzthum H, Müller M, Homberg U (2002) Neurons of the central complex of the locust *Schistocerca gregaria* are sensitive to polarized light. J Neurosci 22:1114-1125.

von Frisch K (1949) Die Polarisation des Himmelslichtes als orientierender Faktor bei den Tänzen der Bienen. Experientia 5:142-148.

Von Philipsborn A, Labhart T (1990) A behavioural study of polarization vision in the fly, *Musca domestica*. J Comp Physiol A 167:737-743.

Warren TL, Weir PT, Dickinson MH (2018) Flying *Drosophila melanogaster* maintain arbitrary but stable headings relative to the angle of polarized light. J Exp Biol 221: 10.1242/jeb.177550.

Wehner R (1984) Astronavigation in insects. Annu Rev Entomol 29:277-298.

Wehner R (1997) The ant's celestial compass system: spectral and polarization channels. In: Lehrer M (eds) Orientation and Communication in Arthropods. EXS (vol. 84) Birkhäuser, Basel.

Wehner R (2003) Desert ant navigation: how miniature brains solve complex tasks. J Comp Physiol A 189:579-588.

Wehner R, Müller M (2006) The significance of direct sunlight and polarized skylight in the ant's celestial system of navigation. Proc Natl Acad Sci U S A 103:12575-12579.

Weir PT, Dickinson MH (2015). Functional divisions for visual processing in the central brain of flying *Drosophila*. Proc Natl Acad Sci U S A 112:5523-5532.

Weir PT, Henze MJ, Bleul C, Baumann-Klausener F, Labhart T, Dickinson MH (2016) Anatomical reconstruction and functional imaging reveal an ordered array of skylight polarization detectors in *Drosophila*. J Neurosci 36:5397-5404.

Wildermuth H (1998) Dragonflies recognize the water of rendezvous and oviposition sites by horizontally polarized light: A behavioural field test. Naturwissenschaften 85:297-302.

Williams JLD (1975) Anatomical studies of the insect central nervous system: A ground-plan of the midbrain and an introduction to the central complex in the locust, *Schistocerca gregaria* (Orthoptera). J Zool Lond 176:67-86.

Wiltschko R (2017) Navigation. J Comp Physiol A 203:455-463.

Wiltschko R, Nohr D, Wiltschko W (1981) Pigeons with a deficient sun compass use the magnetic compass. Science 214:343-345.

Zeil J (2012) Visual homing: an insect perspective. Curr Opin Biol 22:285-293.

Zusammenfassung

Allgemeine Fragestellung

Um verlässlich zu navigieren, nutzen Tiere meist mehrere richtungsweisende Signale. Da die Verarbeitung von polarisiertem Licht im Zentralkomplex der Wüstenheuschrecke bereits in mehreren Studien untersucht wurde, widmet sich die vorliegende Arbeit der Bedeutung von unpolarisierten Signalen, die eine Kompassfunktion im Polarisations-netzwerk unterstützen könnten. Dabei handelt es sich zum einen um die Rolle des Farbgradienten des Himmels als zusätzliches Signal für die Repräsentation der Kopfrichtung anhand eines Kompasses. Zum anderen soll der Einfluss von Bewegungsinformation, die als eine Art visueller Kontext dienen könnte, auf die genannte interne Repräsentation untersucht werden.

Kapitel1

Integration of celestial compass cues in the central complex of the locust brain

Wie in der Einleitung bereits erwähnt, sind eine Reihe von Zelltypen des Zentralkomplexes polarisationssensititv (Heinze et al., 2009). Das bedeutet, dass sie bei einer bestimmten Orientierung des *E*-Vektors eine gesteigerte Aktivität zeigen. Dieser *E*-Vektor wird als Φmax, der bevorzugte Winkel bezeichnet. Der *E*-Vektor 90° versetzt zu Φ_{max} löst eine verhältnismäßig geringere Aktivität aus und wird daher auch als anti-bevorzugter *E*-Vektor oder Φ_{min} bezeichnet. Dabei kann es zu einer Gegenpol-Antwort kommen. Diese zeichnet sich dadurch aus, dass das Neuron bei Φ_{max} erregt wird (d.h. die Aktivität liegt oberhalb der Hintergrundaktivität) und bei Φ_{min} inhibiert wird (d.h. die Aktivität liegt unterhalb der Hintergrundaktivität). Da nun Zellen des Zentralkomplexes den zenitalen *E*-Vektor kodieren, stellt sich die Frage, ob die Neurone zusätzlich auch auf chromatische Signale in einer Art antworten, die eine Unterstützung des internen Polarisations-kompasses erlauben würde.

Um dies herauszufinden, habe ich die Tiere aus dorsaler Richtung mit polarisiertem Licht stimuliert. Eine blaue Leuchtdiode (LED) wurde hinter einem Polarisator platziert. Dieser wurde um 360° im Uhrzeigersinn und gegen den Uhrzeigersinn gedreht (Abb. 1A). Während der Stimulation wurde die Aktivität eines Zentralkomplex-neurons mittels intrazellulärer Ableitung aufgezeichnet. Neurone, die aufgrund ihrer Aktionspotenzial-Charakteristika dem Zentralkomplex zugeordnet werden konnten, oder die sich polarisationssensitiv zeigten, wurden zusätzlich mit einer grünen und ultravioletten LED stimuliert. Vor den LEDs wurden Streuscheiben platziert, sodass diese als helle unpolariserte Lichtpunkte erschienen. Diese Lichtpunkte wurden in einer Elevation von 45° ebenfalls um 360° mit und gegen den Uhrzeigersinn um den Kopf des Tieres bewegt (Abb. 1A).

Die Neurone des Himmelskompass-Netzwerkes im Zentralkomplex antworteten auf polarisiertes Licht, wie es bereits bekannt ist (vgl. dazu Beispielantwort aus Introduction Fig. 5A,B). Zusätzlich antworteten alle bekannten Typen des Polarisationsnetzwerkes zusätzlich auf den grünen oder den UV-Lichtpunkt in einer Azimut-abhängigen Weise. Das bedeutet, dass an einem für jedes

Neuron individuellen Azimut des Lichtpunktes das Neuron eine verstärkte Aktivität zeigte (Abb. 1B,B'). Befand sich der Lichtpunkt an einem anderen Azimut, war die Aktivität vergleichsweise reduziert. Einige Neurone zeigten dabei eine Gegenraum-Antwort, mit Erregung bei Φ_{max} und Inhibition bei Φ_{min}. Diese Azimut-abhängigen Antworten deuten darauf hin, dass die Zentralkomplex-Neurone den Azimut der Sonne kodieren. Experimente in *Drosophila* zeigten in Zentralkomplex-Neuronen eine ähnliche Physiologie (Seelig und Jayaraman, 2015). Allerdings wurde in diesen Versuchen nicht mit einem Lichtpunkt sondern einem hellen unpolarisierten Lichtbalken stimuliert, sodass diese Antworten als Kodierung von Kopfrichtungen relativ zu einer Landmarke interpretiert wurden (Seelig und Jayaraman, 2015). Allerdings sind Landmarken in der Regel dunkler als ihre Umgebung und nicht heller wie die Sonne, die am Himmel der hellste Punkt ist. Die Kodierung der Kopfrichtung relativ zum Sonnenazimut ist daher wahrscheinlich, jedoch lassen die hier durchgeführten Experimente nicht ausschließen, dass der unpolarisierte Lichtpunkt vom Tier als lokale Landmarke interpretiert wird. Interessanterweise gab es in beinahe allen Neuronen nur geringfügige Unterschiede zwischen dem bevorzugten Azimut des grünen und dem des UV-Lichtpunktes (Abb. 1C). Diese Insensitivität der Neurone gegenüber der Wellenlänge der Lichtquelle spricht dafür, dass die Wüstenheuschrecke nicht den chromatischen Gradienten des Himmels zur räumlichen Orientierung nutzt, sondern entweder wie bereits beschrieben den bloßen Sonnenazimut in Form von direktem Sonnenlicht, oder den Intensitätsgradienten des grünen Lichtes.

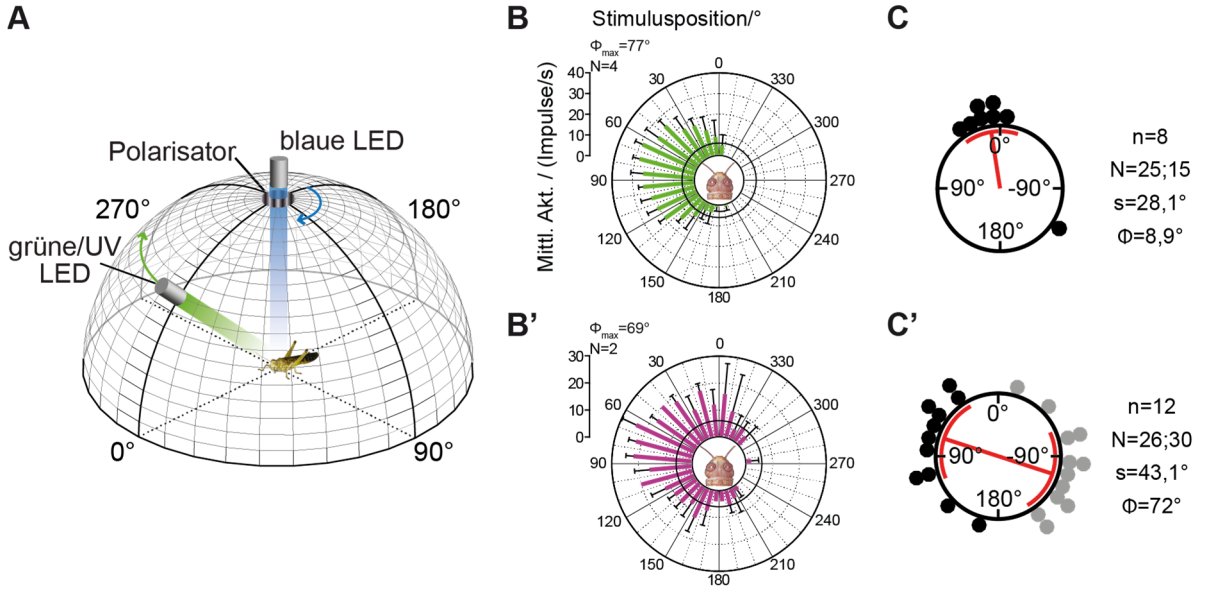

Abb. 1. Visuelle Reizgebung und neuronale Antworten. ***A,*** Visuelle Reizgebung. Das Licht einer blauen LED passierte einen sich drehenden Polarisator, der sich dorsal zum Tier befand. Eine grüne (oder UV) LED bewegte sich auf einer zirkulären Bahn um den Kopf des Tieres (Elevation 45°). ***B,*** Zirkuläres Histogramm der gemittelten Antworten auf den grünen Lichtpunkt eines TL2 Neurons. Fehlerbalken zeigen die Standardabweichung, der schwarze Kreis die Hintergrundaktivität des Neurons. Φ_{max}, bevorzugter Winkel; N, Anzahl der Tests. ***B',*** Histogramm der Antworten desselben Neurons auf unpolarisiertes UV Licht. ***C,*** Relative Winkeldifferenzen der CPU1 Neurone zwischen den bevorzugten Winkeln des grünen und des UV Lichtpunktes. Ein Rayleightest zeigte eine gerichtete Verteilung der Winkeldifferenzen (α = 0,05). Der rote Balken gibt den mittleren Winkel (Φ) an, die roten Halbkreise die zirkuläre Standardabweichung. n, Anzahl der Neurone; N, Anzahl der Tests (Drehrichtungen im Uhrzeigersinn; Drehrichtungen gegen den Uhrzeigersinn); s, zirkuläre Standardabweichung; Φ, mittlerer Differenzwinkel. ***C',*** Positive relative Winkeldifferenzen (schwarze Punkte) und negative relative Winkeldistanzen (graue Punkte) der CPU1 Neurone zwischen den bevorzugten Winkeln des *E*-vektors und des grünen Lichtpunktes. Ein Rayleightest zeigte die gerichtete Verteilung (α = 0,05). Abkürzungen wie in ***C***. Die Fotografien der Heuschrecke in ***A***, ***B*** und ***B'*** stammen von Keram Pfeiffer.

Der *E*-Vektor im Zenit ist unabhängig von der Sonnenposition immer orthogonal zum Sonnenazimut ausgerichtet (vgl. *Introduction* Fig. 2*B*). Daher sollte für eine optimale Unterstützung des internen Polarisations-kompasses durch unpolarisiertes Himmelslicht der bevorzugte *E*-Vektor eines Neurons einen 90° Winkelabstand zum bevorzugten Azimut des unpolarisierten grünen Lichtpunktes haben. Dies konnte ich für die erste Verarbeitungsstufe, die TL2 und TL3 Neurone zeigen, nicht jedoch für alle nachgeschalteten Neurone (vgl. CPU1 Neurone in Abb. 1*C*'). In der letzten Verarbeitungsstufe (CPU1) waren die relativen Winkelabstände gerichtet kleiner als 90°. Daher könnte es sein, dass die rezeptiven Felder dieser Neurone für polarisiertes Licht nicht Zenit-zentriert sind (d.h., dass die Antwort auf polarisiertes Licht nicht im Zenit am stärksten wäre, sondern seitlich vom Tier bei geringerer Elevation). Dies würde jedoch zuvor publizierten Daten widersprechen. Heinze et al. (2009) beschrieben rezeptive Felder für polarisiertes Licht der CPU1 Neurone als Zenit-zentriert, jedoch wurden dort Mittelwerte aus nur drei völlig unterschiedlichen rezeptiven Feldern gebildet. Daher wäre eine detaillierte Analyse der rezeptiven Felder notwendig, um die hier gezeigten Daten in diesem Zusammenhang zu interpretieren. Eine weitere mögliche Erklärung wäre eine unabhängige Nutzung von Polarisations- und Azimut-Signalen, je nachdem welches Signal für das Tier am besten zugänglich ist. Bei klarem Himmel würde direktes Sonnenlicht den Sonnenazimut eindeutig signalisieren. Zögen dagegen Wolken auf, könnte das Polarisationsmuster das verlässlichste Signal sein. Eine unabhängige Nutzung eines Polarisations- und Sonnen-Kompasses wurde bereits in einer Verhaltensstudie über das Heimfinde-vermögen von Wüstenameisen spekuliert (Wehner und Müller, 2006).

Um die bevorzugten Winkel der Einzelantworten auf polarisiertes Licht und die unpolarisierten Lichtpunkte genauer zu analysieren, wurden diese für Rotation im Uhrzeigersinn und Rotation gegen den Uhrzeigersinn verglichen. Wie zuvor schon für *E*-Vektor Antworten von Zentralkomplex-neuronen gezeigt werden konnte (Bockhorst und Homberg, 2015), wurde hier ein antizipationsartiges Antwortverhalten in allen Zelltypen und für alle Stimuli beobachtet. Bei einer Antizipation sind die bevorzugten Winkel für Rotation im Uhrzeigersinn kleiner, als die für Rotation gegen den Uhrzeigersinn und geben damit einen Aufschluss auf Stimuluswinkel der nahen Zukunft. Dieses Phänomen findet sich auch in den Kopfrichtungszellen der Ratte (Taube und Muller, 1998). Jedoch wird für diese Tiere angenommen, dass Antizipation aus dem vestibulären Signal entsteht, also der Eigenbewegung. Dies kann für die Heuschrecke nicht zutreffen, da diese im Versuch fixiert war. Die hier gezeigte Antizipation könnte daher ausschließlich aus der Wahrnehmung der vergangenen Stimuluswinkel und der Rotations-geschwindigkeit des Stimulus entstehen.

Neben den bevorzugten Winkeln der *E*-Vektor- und Azimut-Antworten wurden auch noch andere Parameter der Tuningkurven bestimmt, die die Antworten charakterisierten. Dazu gehörten die Korrelation zwischen Stimulus-Winkel und Aktivität des Neurons, die Amplitude und die Breite der Tuningkurve, sowie das Ausmaß von Erregung und Inhibition beim bevorzugten, respektive anti-bevorzugtem Winkel. Größtenteils konnten Charakteristika der *E*-Vektor-Antworten aus früheren Studien (Bockhorst und Homberg, 2015) bestätigt werden. Der Vergleich der Charakteristika für *E*-Vektor- und Azimut-Tunings ergab jedoch Unterschiede auf der Eingangsebene (TL Neurone), wohingegen die Charakteristika in

Neuronen der Ausgangsebene (CPU Neurone) sich ähnelten. Dies könnte auf zwei unterschiedliche Eingänge für polarisierte und unpolarisierte Signale über TL2 und TL3 Neurone hindeuten.

Zusammengenommen konnte ich in so gut wie allen bisher bekannten Neuronen des Polarisationsnetzwerkes eine Sensitivität für den Azimut eines hellen unpolarisierten Lichtpunktes zeigen. Unsere Resultate liefern einen starken Hinweis, dass in diesem Netzwerk mehrere Kompasssignale integriert sind und dass von der Heuschrecke neben dem Polarisationssignal auch ein Azimutsignal aus direktem Sonnenlicht zur räumlichen Orientierung verwendet wird.

Kapitel2

Two compasses in the central complex of the locust brain

In der Arbeit von Heinze und Homberg (2007) wurde eine topographische Repräsentation des zenitalen *E*-Vektors in verschiedenen Zelltypen der Protozerebralbrücke (PB) gefunden. Diese Polarotopie lässt eine Art von internem Himmels- oder Polarisationskompass annehmen. Wie im ersten Kapitel dargelegt, kodieren Neurone, die den internen Polarisationskompass darstellen, ebenfalls den Azimut eines hellen unpolarisierten Lichtpunktes. Daraus ergibt sich die Frage, ob neben dem zenitalen *E*-vektor auch der Azimut eines unpolarisierten grünen Lichtpunktes in der Protozerebralbrücke topographisch repräsentiert ist. Um dies zu beantworten untersuchte ich verschiedene Zelltypen der Protozerebralbrücke, einschließlich aller Neurone, die schon in früheren Studien in diesem Hinblick analysiert wurden (CL1, TB1, CPU1, CP1, CP2), sowie CPU2 Neurone, die bisher noch nicht in dieser Hinsicht analysiert wurden. Ich leitete Neurone aus verschiedenen Scheiben der PB ab, und testete diese sowohl auf polarisiertes Licht (*E*-Vektor Kodierung) und einen unpolarisierten grünen Lichtpunkt, der sich in einer Kreisbahn um das Tier bewegte (Azimut-Kodierung).

Die hier gezeigten *E*-Vektor Repräsentationen passen zu denen, die zuvor schon gefunden wurden. CL1 Neurone zeigen keine Topographie für polarisiertes Licht (Abb. 2*A*; Heinze und Homberg, 2009). Dagegen decken TB1 Neurone, sowie CPU1 und CP1/CP2 Neurone grob einen Winkelbereich von 360° über die gesamte Protozerebralbrücke ab (vgl. Abb.2*B*; Heinze und Homberg, 2007). Aufgrund der geringen Anzahl von Ableitungen von CPU2, CP1 und CP2 Neuronen wurden diese hier als ein Datensatz behandelt, passten jedoch äußerst gut zusammen. Zusätzlich konnte ich für alle der hier untersuchten Zelltypen eine topographische Repräsentation des Azimuts des unpolarisierten Lichtpunktes in der Protozerebralbrücke feststellen. Diese Repräsentation deckte in CL1 und TB1 Neuronen etwa 2×360° ab (Abb. 2*A*',*A*''), in CPU1 und CP1/CP2/CPU2 Neuronen jedoch nur 360° (Abb. 2*B*',*B*''). Die Repräsentation in CL1 Neuronen in der PB passt etwa zu der, die schon für die equivalenten Neurone bei der Fliege *Drosophila* gezeigt wurde (Turner-Evans et al., 2017). Die übrigen hier präsentierten Zelltypen wurden in *Drosophila* und auch in keinem anderen Insekt in diesem Hinblick analysiert. Die Transformation von 2×360° in CL1 Neuronen zu 1×360° in den kolumnären Ausgangsneuronen könnte insofern sinnvoll sein, dass die Kopfrichtungsinformation relativ zum Sonnenazimut oder zu einer Landmarke

konsequent zu Neuronen der einen oder anderen Gehirnhemisphäre geleitet wird (d.h. Ausgang im rechten oder linken LAL), sodass eine mögliche gerichtete Bewegung stattfinden kann.

Die Orientierung des *E*-Vektors und die des Azimut Kompasses sind jedoch entgegengesetzt (vgl. Abb. 2*B*,*B*'). Würde also das Tier während des Fluges den Kurs nach rechts ändern, so würden nach dem *E*-Vektor-Kompass Neurone in Scheiben der PB weiter rechts zu der ursprünglich aktiven Scheibe aktiv werden (vgl. Abb. 2B''). Nach dem Azimut-Kompass dagegen wären es bei einer Rechtsdrehung des Tieres die Scheiben weiter links. Die beiden Kompasse könnten also entweder auf komplexe Art miteinander in Verbindung stehen, oder sie sind unabhängig voneinander. Um dies zu testen, präsentierte ich den zenitalen *E*-vektor gemeinsam mit dem unpolarisierten Lichtpunkt. Die Winkel der Stimuli waren dabei um 90° zueinander versetzt, so wie es für das Tier am Himmel zu sehen ist. Einige Neurone bevorzugten eindeutig entweder den einen oder anderen Reiz, d.h. sie zeigten eine reine Azimut-abhängige Antwort oder eine reine *E*-vektor abhängige Antwort. Andere Neurone zeigten verschiedene Varianten von gemischten Antworten mit mehr oder weniger dominierendem *E*-Vektor- oder Azimut Tuning. Dies könnte darauf hindeuten, dass die beiden internen Kompasse auf komplexe Art miteinander verbunden und voneinander abhängig sind.

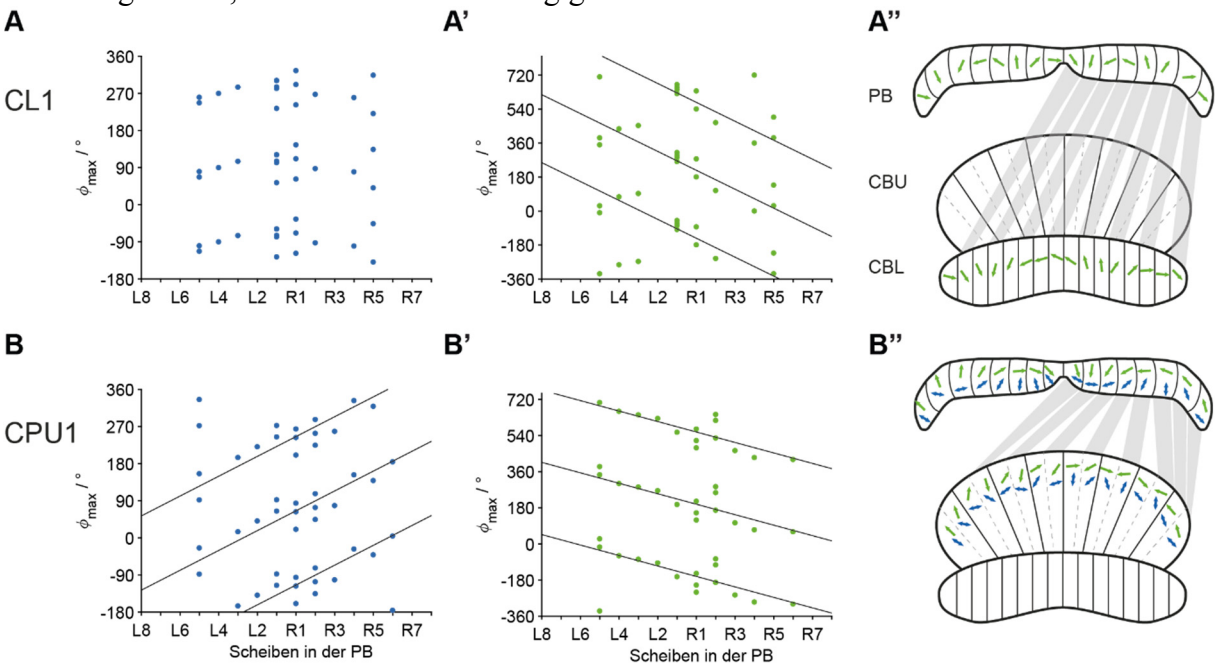

Abb. 2. Topographische Repräsentation von *E*-Vektor- und Azimutwinkeln. ***A, B,*** Bevorzugte *E*-Vektor-Orientierungen von CL1 Neuronen (***A***) und von CPU1 Neuronen (***B***), aufgetragen gegen ihre Verzweigungsdomäne in der Protozerebralbrücke. ***A,*** Eine zirkulär-lineare Korrelationsanalyse ergab keine Korrelation (α = 0,05). ***B,*** Eine zirkulär-lineare Korrelationsanalyse ergab eine Korrelation. ρ = 0,33; y = 24x – 126. ***A', B',*** Bevorzugte Azimutwinkel des grünen Lichtpunktes von CL1 Neuronen (***A'***) und von CPU1 Neuronen (***B'***), aufgetragen gegen ihre Verzweigungsdomänen in der PB. ***A',*** Eine zirkulär-lineare Korrelationsanalyse ergab eine Korrelation. ρ = -0,71; y = -50x + 616. ***B',*** Eine zirkulär-lineare Korrelationsanalyse ergab eine Korrelation. ρ = -0,54; y = -26x + 46. ***A'',*** Mittlere Winkel aus dem Regressionsmodell in ***A'*** dargestellt als Pfeile (Azimut). Pfeile in der PB wurden gemäß dem Verzweigungsschema der CL1 Neurone (Heinze und Homberg, 2008) in die CBL transferiert (graue Schattierungen). In der PB wird ein Winkelbereich von 750° abgedeckt, in der CBL ein Bereich von 391°. ***B'',*** Mittlere Winkel aus dem Regressionsmodell in ***B*** und ***B'*** dargestellt als Pfeile (Azimut). Pfeile in der PB wurden gemäß dem Verzweigungsschema der CPU1 Neurone (Heinze und Homberg, 2008) in die CBU transferiert (graue Schraffierungen). In der PB und der CBU deckt der Polarisationskompass einen Winkelbereich von 360° ab. Der Azimutkompass deckt in der PB einen Bereich von 390° ab, in der CBU ist keine Topographie zu erkennen, da je zwei Zellen einer Doppelkolumne der CBU entgegengesetztes Tuning zeigen.

Neben den internen Kompassen in der PB ist in diesem Kapitel eine grobe Richtungskodierung in zwei Zelltypen der tangentialen Eingangsneurone des Netzwerkes gezeigt. Zwei TL2 Subtypen verzweigen in verschiedenen Bereichen der CBL, sowie des lateralen Bulbus. TL2a Neurone verzweigten in der dorsalen dritten und zweiten Schicht der CBL und im ventro-lateralen Bereich des lateralen Bulbus. TL2b Neurone verzweigten in der weiter ventral liegenden Schicht 4 der CBL und im dorso-medialen Bereich des lateralen Bulbus. TL2a Neurone bevorzugten den Azimut eines unpolarisierten grünen Lichtpunktes auf kontralateraler Seite des Tieres, wohingegen TL2b Neuronen den Lichtpunkt auf ipsilateraler Seite präferierten. Diese Ergebnisse passen zu denen aus früheren Studien an den tangentialen Ringneuronen (äquivalent zu TL) des Ellipsoidkörpers (äquivalent zu CBL) in *Drosophila* (Seelig und Jayaraman, 2013). Dort sind in den Mikroglomeruli der Ringneurone im lateralen Bulbus Azimut als auch Elevation eines hellen Lichtbalkens topographisch repräsentiert. Neurone, die im linken Bulbus verzweigen, wurden bei der Fliege durch den Balken auf der linken Seite aktiviert, Neurone, die auf der rechten Seite verzweigen durch den Balken auf der rechten.

Wie zuvor schon erwähnt, ändern sich Azimut als auch Elevation kontinuierlich im Verlauf des Tages. Würden die Zentralkomplex-Neurone die Sonnen-position kodieren und nicht nur den Azimut, so wären die Azimutkodierungen abhängig von der Elevation des Stimulus. Ich testete daher CL1, TB1 und CPU1 Neurone auf Azimutkodierung in verschiedenen Eleva-tionen (20° bis 60°). Unabhängig von wenigen Einzelfällen konnte kein gerichteter Einfluss der Elevation auf das Azimut-Tuning festgestellt werden. Würden die Zellen, ähnlich der *Drosophila* Ringneurone für eine bestimmte Elevation kodieren (Seelig and Jayaraman, 2013), so würden die Neurone nur bei einer bestimmten Stimuluselevation eine Azimutantwort zeigen. Dies war nur in einem Neuron der Fall. TL Neurone konnten zum besseren Vergleich mit den *Drosophila* Ringneuronen nicht getestet werden. Dahingegen wurden in allen Studien, die Neurone der Protozerebralbrücke in *Drosophila* untersuchten, keine verschiedenen Stimulus-Elevationen mehr getestet. Daher kann schlussendlich nicht festgestellt werden ob sich *Drosophila* und die Wüstenheuschrecke hinsichtlich der Kodierung der Elevation des Lichtstimulus im Zentralkomplex grundsätzlich unterscheiden, oder ob in beiden Tieren die Elevation gleichermaßen nur in der Eingangsebene des Zentralkomplexes repräsentiert ist.

Kapitel3

Influence of wide-field motion on the signalling of sky compass cues in the locust central complex

Das dritte Kapitel behandelt den Zusammen-hang zwischen dem internen Polarisations- sowie Azimut-Kompass und der Verarbeitung von Großfeldbewegung. Während des Laufens und Fliegens, d.h. immer wenn das Tier in Bewegung ist, wird es, je nach Struktur der visuellen Umwelt, optischen Fluss, ausgelöst durch Eigenbewegung, wahrnehmen. Optischer Fluss kann daher dem Tier eine Information über die Eigenbewegung im Raum geben. Es wurde bereits an der Fruchtfliege (Weir und Dickinson, 2015), der

Schabe (Kathman et al., 2014) und Bienen (Stone et al., 2017) gezeigt, dass Neurone des Zentralkomplexes optischen Fluss verarbeiten. Ich testete daher Neurone der Protozerebralbrücke (CL1 und TB1) auf progressiven optischen Fluss bzw. . Dazu wurde mit Hilfe von zwei LCD Monitoren, die sich lateral neben dem Tier befanden, ein bewegtes sinusförmiges Streifenmuster präsentiert. Dieses bewegte sich von vorn nach hinten, und simulierte damit dem Tier einen progressiven optischen Fluss, d.h. eine nach vorn gerichtete Bewegung. Nicht alle Neurone antworteten auf den Stimulus. Diejenigen, die antworteten zeigten meist jedoch eine den gesamten Stimulus andauernde Erregung. Keines der Neurone antwortete mit Inhibition.

Um nun die Interaktion zwischen der Verarbeitung von optischem Fluss und polarisiertem Licht zu untersuchen, wurde vor der Reizung mit Großfeldbewegung ein stationärer *E*-vektor eingestellt, einmal bei Φ_{max}, einmal bei Φ_{min}. Die Neurone des Polarisationsnetzwerkes im Zentralkomplex antworten auf einen stationären *E*-Vektor, wie er vom Tier, das sich auf stetem Kurs befindet, wahrgenommen würde, meist mit rascher Adaptation (Bockhorst und Homberg, 2015). So ist in den ersten Sekunden des stationären *E*-Vektors die Antwort (Erregung bei Φ_{max}, Inhibition bei Φ_{min}) noch vorhanden. Diese verschwindet allerdings innerhalb von 7-10 Sekunden (Bockhorst und Homberg, 2015). Aus der Reizgebung ergaben sich so drei Stimuluskonditionen: 1) Stimulation mit Großfeldbewegung ohne gleichzeitige Präsentation von polarisiertem Licht; 2) Stimulation mit Großfeldbewegung mit gleichzeitiger Präsentation des bevorzugten *E*-Vektors; 3) Stimulation mit Großfeld-bewegung mit gleichzeitiger Präsentation des anti-bevorzugten *E*-Vektors. Die Verteilung der Stärke der Antworten für Kondition 1 und 2 sowie 1 und 3 war über alle getesteten Zellen gleich. Dagegen waren die Antworten unter Kondition 2 stärker als die unter Kondition 3. Dies deutet darauf hin, dass der Anstieg der neuronalen Aktivität ausgelöst durch optischen Fluss von der gegenwärtigen Modulation durch den *E*-vektor beeinflusst wird. Daher habe ich jedes Neuron auf einen Zusammenhang zwischen *E*-Vektor-induzierter Feuerrate und Bewegungs-induzierter Feuerrate untersucht. Tatsächlich zeigte sich eine Korrelationen zwischen diesen beiden Variablen in 8 von 12 Neuronen. Eine Regressionsanalyse ergab einen positiven Zusammenhang in 9 von 12 Neuronen. Die Antworten aller Neurone für Kondition 2 zeigten Disadaptation, d.h. die Zelle wurde durch den Bewegungsreiz erregt. Dies wurde durch eine weitere Korrelation zwischen den *E*-Vektor induzierten Feuerraten und den Bewegungs-induzierten Feuerraten über alle Neurone, nur für die Stimulationen unter Kondition 2, bestätigt. Die Antworten für Kondition 3 dagegen waren nur in drei Neuron disadaptierend, d.h. die Neurone wurden inhibiert. Alle anderen Neurone zeigten hier entweder keine Antwort oder wurden leicht erregt. Folglich wurde bei Vergleich zwischen den Feuerraten aller Neurone unter Kondition 3 keine Korrelation festgestellt. Zusammengefasst antworteten die Neurone bei der Stimulation bei Φ_{max} mit Disadaptation, bei Φ_{min} wurde dagegen der Reiz weitestgehend ignoriert. Dies könnte dem Tier dabei helfen, seinen Kurs zu halten, während es in Bewegung ist, da die interne Repräsentation der Kopfrichtung relativ zum zenitalen *E*-Vektor in den Neuronen der PB durch Disadaptation verstärkt werden könnte. Disadaptation wurde bereits in kombinatorischer Reizung von polarisiertem Licht und einem bewegten Kleinfeldreiz beobachtet (Bockhorst und Homberg, 2017). Allerdings trat diese dort bei Φ_{max} als auch Φ_{min} auf. Zudem waren die Antworten auf den bewegten Kleinfeldreiz sehr kurzlebig, d.h. nach spätestens einer Sekunde adaptierten die

Neurone wieder. Diese Antworten deuten also eher auf eine kurzfristig erhöhte Aufmerksamkeit ausgelöst durch den Bewegungsstimulus hin. In der hier vorliegenden Studie dagegen waren die Antworten auf den Bewegungsreiz meist andauernd, manchmal länger als der Stimulus selbst, sodass es sich hierbei eher um eine langfristige Modulation handeln könnte, die nicht durch erhöhte Aufmerksamkeit ausgelöst wird.

Da die Heuschrecke während eines Fluges theoretisch auch von ihrem Kurs abkommen könnte, stellt sich die Frage, wie Zentralkomplex-Neurone auf ein bewegtes Streifenmuster reagieren, das eine Drehung des Tieres um die Hochachse simuliert. Ein TB1 Neuron und zwei CL2 Neurone wurden auf diesen Reiz getestet. CL2 Neurone innervieren stets eine Scheibe der ipsilateralen Hemisphere der PB und die untere Einheit des kontralateralen Nodulus, sowie eine Scheibe der CBL in der ipsi- oder kontralateralen Hemisphere (Heinze und Homberg, 2008). Die CL2 Neurone antworteten mit Erregung und Inhibition in Abhängigkeit von der Drehrichtung und von der Lage des innervierten Nodulus. Das CL2 Neuron, das im linken Nodulus verzweigte und damit in der rechten Hemisphäre der PB, antwortete auf eine simulierte Drehung des Tieres im Uhrzeigersinn mit starker Erregung (Abb. 3*A*), und auf eine simulierte Drehung des Tieres gegen den Uhrzeigersinn mit starker Inhibition (Abb. 3*A*'). Das CL2 Neuron, welches im rechten Nodulus verzweigte, zeigte entgegengesetzte Antworten (Abb. 3*B*,*B*'). Diese Antworten sind denen der P-EN-Neurone aus *Drosophila* (äquivalent zu CL2 in der Wüstenheuschrecke) ähnlich. Diese kodieren sowohl die Drehrichtung als auch die Drehgeschwindigkeit der laufenden (Turner-Evans et al., 2017) oder fliegenden (Green et al., 2017) Fliege bei gleichzeitiger Sichtbarkeit einer Landmarke. Sie sind geeignet, die Repräsentation der Kopfrichtung relativ zu einer Landmarke in E-PG-Neuronen (äquivalent zu CL1a Neuronen der Heuschrecke) über die Scheiben der PB zu verschieben, wenn sich das Tier nach rechts oder links dreht (Kakaria und de Bivort, 2017). Das Antwortverhalten der hier präsentierten CL2 Neurone lässt auf eine ähnliche Funktion schließen. Sie wären durch ihre feinen Verzweigungen in den Noduli geeignet, von dort Signale aus Drehbewegungen aufzunehmen. CL1 Neurone verzweigen fein und varikös in der CBL und klauenartig in der PB, wohingegen CL2 Neurone in der PB glatte und in der CBL variköse Verzweigungen aufweisen. Es wäre daher möglich, dass in der PB und der CBL zwischen CL1 und CL2 Neuronen ein gerichteter Signalaustausch vorliegt. Unter der Annahme, dass CL1 und CL2 Neurone die gleiche topographische Azimut-Repräsentation in der PB aufweisen, könnten CL2 Neurone die Aktivität der CL1 Neurone über die Scheiben der PB verschieben, wenn das Tier sich dreht (Abb. 3*C*-*C*''). Sie könnten so bei Bewegung des Tieres für ein sicheres „Update" der internen Repräsentation der Kopfrichtung sorgen.

Die Antworten des TB1 Neurons ähnelten dem des CL2 Neurons aus der gleichen Hirnhemisphäre. Sie lassen darauf schließen, dass CL2 Neurone das Drehrichtungssignal vermutlich über CL1 Neurone an weitere Zellen stromabwärts im Netzwerk weitergeben.

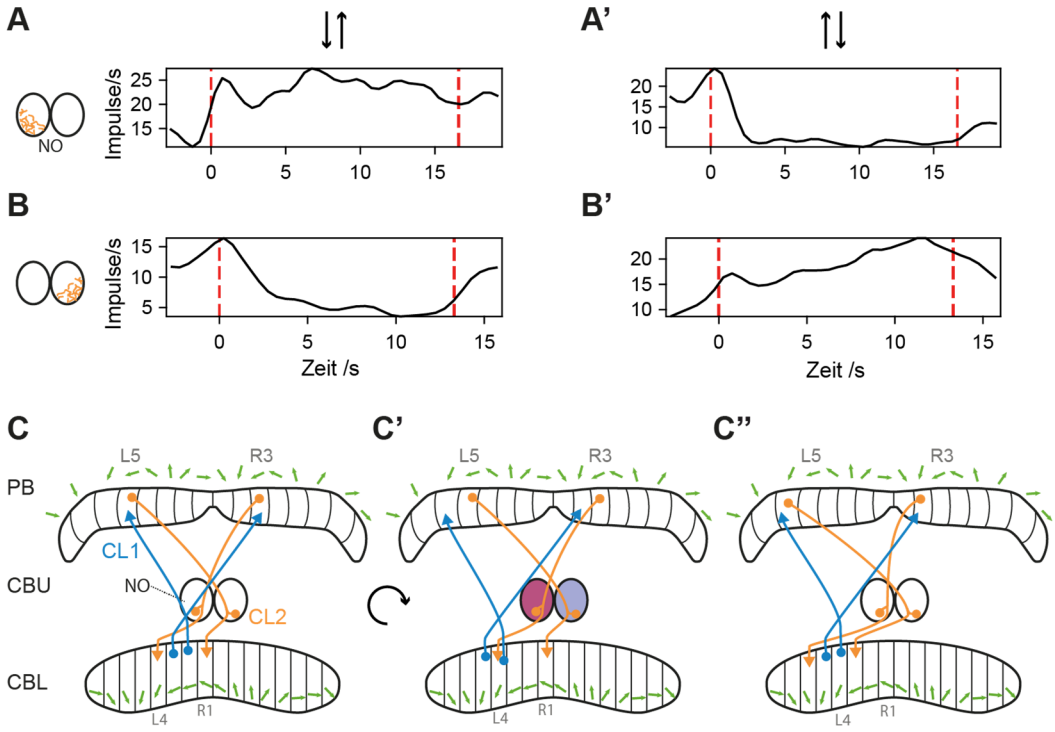

Abb. 3. Antworten auf simulierte Drehbewegung und resultierendes hypothetisches Modell. ***A, A',*** Geglättete und gemittelte Antworten eines CL2 Neurons, mit Verzweigungen im linken Nodulus (orange), auf simulierte Drehbewegung um die Hochachse der Heuschrecke. ***B, B',*** Geglättete und gemittelte Antworten eines CL2 Neurons, mit Verzweigungen im rechten Nodulus (orange), auf simulierte Drehbewegung um die Hochachse. ***A, B,*** Antworten der beiden CL2 Neurone auf eine simulierte Rechtsdrehung. Das Streifenmuster auf dem linken Monitor bewegte sich dazu von vorn nach hinten, das auf dem rechten Monitor von hinten nach vorn (Pfeile). ***A', B',*** Antworten der beiden CL2 Neurone auf eine simulierte Linksdrehung. Das Streifenmuster auf dem linken Monitor bewegte sich dazu von unten nach oben, das auf dem rechten Monitor von oben nach unten (Pfeile). Rote gestrichelte Linien geben in allen Graphen das Einsetzen und die Beendigung des Bewegungsreizes an. ***C-C'',*** Hypothetisches aus den obigen Antworten abgeleitetes Modell. Schematische Darstellung des Zentralkomplexes inklusive der vertikalen Scheiben. Grüne Pfeile zeigen die Topographie des Azimuts des grünen Lichtpunktes in CL1 Neuronen (siehe Kapitel 2). CBL, untere Einheit des Zentralkörpers; CBU, obere Einheit des Zentralkörpers; NO, Noduli; PB, Protozerebralbrücke. ***C,*** Es wird angenommen, dass CL2 (orange) Neurone die gleiche topographische Azimutrepräsentation in der PB aufweisen wie CL1 Neurone (hellblau). Punkte bedeuten mögliche postsynaptische Endigungen, Pfeile dagegen mögliche Präsynapsen. Gemäß ihrer Verzweigungsschemata (Heinze und Homberg, 2008) würden CL1 Neurone mit gleichem Vorzugswinkel in der PB in zwei benachbarten Scheiben in der CBL verzweigen. Die CL2 Neurone mit demselben Vorzugswinkel wie diese beiden CL1 Neurone würden in denselben Scheiben in der PB verzweigen, in der CBL jedoch in den Scheiben links und rechts von denen der CL1 Neurone. ***C',*** Dreht sich das Tier nach rechts (runder Pfeil) so würden durch den dadurch entstehenden optischen Fluss die CL2 Neurone, die im linken Nodulus verzweigen erregt (rot), und die die im rechten Nodulus verzweigen inhibiert (dunkelblau). Das CL2 Neuron aus R1 der CBL würde durch seine nun verringerte Aktivität verhindern, dass CL1 Neurone, die in derselben Scheibe verzweigen dort erregt würde. Das CL2 Neuron aus L4 der CBL würde durch seine nun erhöhte Aktivität das dortige CL1 Neuron erregen. Eine gleichzeitige Erregung des CL1 Neurons aus L5 der CBL wird dadurch allerdings nicht erklärt. ***C'',*** Durch die in der CBL nach links verschobene erhöhte Aktivität würden diese in der PB die dort in den gleichen Scheiben (L6, R2) verzweigenden CL2 Neurone erregen. Damit wäre die interne Repräsentation der Kopfrichtung relativ zu einem Kompasssignal im Zentralkomplex nach einer Rechtsdrehung des Tieres aktualisiert, da die Scheiben weiter links im Zentralkomplex eine Kopfrichtung des Tieres relativ weiter rechts zu einem Kompasssignal codieren.

Fazit

Wie an Wirbeltieren (Blair and Sharp, 1996), aber auch an Insekten (Varga und Ritzmann, 2016) gezeigt werden konnte, wird die Kodierung der Kopfrichtung im Gehirn von mehreren Signalen generiert und aufrechterhalten bzw. aktualisiert. Dazu gehören Informationen über die Eigenbewegung (z.B. Beinbewegung beim Laufen, optischer Fluss) sowie externe Signale aus der Umwelt (z.B. eine Landmarke). Während ersteres am Zentralkomplex der Wüstenheuschrecke bisher nicht untersucht ist, wurde eine Bedeutung von visuellen externen Signalen, insbesondere die des polarisierten Himmelslichtes für eine interne Repräsentation der Kopfrichtung bereits festgestellt (Heinze und Homberg, 2007). Die hier vorliegenden Daten zeigen umfangreich, dass neben dem polarisierten Licht auch die reinen Azimutsignale eine wichtige Bedeutung für die Repräsentation der Kopfrichtung des Tieres im Zentralkomplex haben. Daher ist es wahrscheinlich, dass für migratorische Insekten wie die Wüstenheuschrecke sowohl Polarisation als auch direktes Sonnenlicht zur zielgerichteten Lokomotion nach einem Himmelskompass beitragen. Mit den hier präsentierten neuronalen Antworten auf die Großfeldbewegungen ist zum ersten Mal gezeigt, dass im Zentralkomplex der Wüstenheuschrecke visuelle Informationen über die Eigenbewegung des Tieres (in Form von optischem Fluss) verarbeitet werden. Der Einfluss einer tatsächlichen passiven oder aktiven Bewegung des Tieres auf die Verarbeitung von Kompasssignalen im Zentralkomplex wurde hier nicht untersucht. Allerdings gibt diese Arbeit einen Hinweis darauf, dass schon die Simulation einer solchen, einen verstärkenden Einfluss auf das interne Kompasssignal haben könnte. Der Einfluss der (in diesem Falle simulierten) Drehbewegung auf die Aktualisierung des internen Kompasssignals bestätigt Resultate vorheriger Studien an *Drosophila* (Turner Evans et al., 2017) und verdeutlicht, dass neben den Himmelskompasssignalen optischer Fluss ein wichtiges Signal für die korrekte Repräsentation der aktuellen Kopfrichtung im Zentralkomplex ist.

Referenzen

Blair HT, Sharp PE (1996) Visual and vestibular influences on head-direction cells in the anterior thalamus of the rat. Behav Neurosci 110:643-660.

Bockhorst T, Homberg, U (2015) Amplitude and dynamics of polarization-plane signaling in the central complex of the locust brain. J Neurophysiol 113:3291-3311.

Bockhorst T, Homberg U (2017) Interaction of compass-sensing and object-motion detection in the locust central complex. J Neurophysiol 113:3291-3311.

Green J, Adachi A, Shah KK, Hirokawa JD, Magani PS, Maimon G (2017) A neural circuit architecture for angular integration in *Drosophila*. Nature 546:101-106.

Heinze S, Gotthardt S, Homberg U (2009) Transformation of polarized light information in the central complex of the locust. J Neurosci 29:11783-11793.

Heinze S, Homberg U (2007) Maplike representation of celestial *E*-vector orientations in the brain of an insect. Science 315:995-997.

Heinze S, Homberg U (2008) Neuroarchitecture of the central complex of the desert locust: intrinsic and columnar neurons. J Comp Neurol 511:454-478.

Heinze S, Homberg U (2009) Linking the input to the output: New sets of neurons complement the polarization network in the locust central complex. J Neurosci 29:4911-4921.

Kakaria KS, de Bivort BL (2017) Ring attractor dynamics emerge from a spiking model of the entire protocerebral bridge. Front Behav Neurosci 11: 10.3389/fnbeh.2017.00008.

Kathman ND, Kesavan M, Ritzmann RE (2014) Encoding wide-field motion and direction in the central complex of the cockroach *Blaberus discoidalis*. J Exp Biol 217:4097-4090.

Pfeiffer K, Homberg U (2007) Coding of azimuthal directions via time-compensated combination of celestial compass cues. Curr Biol 17:960-965.

Seelig JD, Jayaraman V (2013) Feature detection and orientation tuning in the *Drosophila* central complex. Nature 503:262-266.

Seelig JD, Jayaraman V (2015) Neural dynamics for landmark orientation and angular path integration. Nature 521:168-191.

Stone T, Webb B, Adden A, Weddig NB, Honkanen A, Templin R, Wcislo W, Scimeca L, Warrant E, Heinze S (2017) An anatomically constrained model for path integration in the bee brain. Curr Biol 27:3069-3085.

Taube JS, Muller RU (1998) Comparisons of head direction cell activity in the postsubiculum and anterior thalamus of freely moving rats. Hippocampus 8:87-108.

Turner-Evans D (2017) Angular velocity integration in a fly heading circuit. Elife 6:10.7554/eLife.23496.

Wehner R, Müller M (2006) The significance of direct sunlight and polarized skylight in the ant's celestial system of navigation. Proc Natl Acad Sci U S A 103:12575-12579.

Weir PT, Dickinson MH (2015) Functional divisions for visual processing in the central brain of flying *Drosophila*. Proc Natl Acad Sci U S A 112:10.1073/pnas.1514415112.

Chapter 1

Integration of celestial compass cues in the central complex of the locust brain

Integration of celestial compass cues in the central complex of the locust brain

Uta Pegel, Keram Pfeiffer, Uwe Homberg

Many insects rely on celestial compass cues such as the polarization pattern of the sky for spatial orientation. In the desert locust, the central complex (CX) houses multiple sets of neurons, sensitive to the oscillation plane of polarized light and, thus, likely acts as an internal polarization compass. We investigated whether other sky compass cues like direct sunlight or the chromatic gradient of the sky might contribute to this compass. We recorded from polarization-sensitive CX neurons while an unpolarized green or UV light spot was moved around the head of the animal. All types of neuron that were sensitive to the plane of polarization (*E*-vector) above the animal also responded to the unpolarized light spots in an azimuth-dependent way. The tuning to the unpolarized light spots was independent of wavelength, suggesting that the neurons encode solar azimuth based on direct sunlight and not on the sky chromatic gradient. Two cell types represented the natural 90°-relationship between solar azimuth and zenithal *E*-vector orientation, providing evidence to suggest that solar azimuth information supports the internal polarization compass. Most neurons showed advances in their tuning to the *E*-vector and the unpolarized light spots dependent on rotation direction, consistent with anticipatory signaling. The amplitude of responses and its variability were dependent on the level of background firing, possibly indicating different internal states. The integration of polarization and solar azimuth information strongly suggests that besides the polarization pattern of the sky, direct sunlight might be an important cue for sky compass navigation in the locust.

Summary statement

Polarization-sensitive neurons of the locust central complex show azimuth-dependent responses to unpolarized light spots. This suggests that direct sunlight supports the sky polarization compass in this brain area.

Introduction

For navigation, defined as the ability to reach a desired goal, many animals rely on visual cues, such as landmarks and sky compass signals. Whereas the presence of landmarks depends on the structure of the habitat, sky compass signals are available almost everywhere, and thus represent highly reliable navigational cues (Gould, 1998; Frost and Mouritsen, 2006). Features of the sky providing navigational information include its polarization pattern, its chromatic gradient, and the position of the sun. By scattering at air molecules unpolarized sunlight becomes partly linearly polarized (Rossel, 1993; Wehner, 2001). The electric field vectors (*E*-vectors) in the sky are arranged tangentially along concentric circles around the sun (Fig. 1), and thus reference solar/antisolar position (Rossel et al., 1978; Rossel, 1993). The percentage of polarization increases from the solar and antisolar position to a maximum at an angle 90° from the sun (Fig. 1A). In contrast, the chromatic gradient arises from an intensity gradient of long wavelength light and a uniform distribution of short wavelength light across the sky (Fig. 1A). The resulting color contrast is high at the solar position and low at the antisolar point (Coemans et al., 1994). It allows for distinction between the solar and the antisolar hemisphere, especially at low solar elevations, when the polarization pattern is ambiguous.

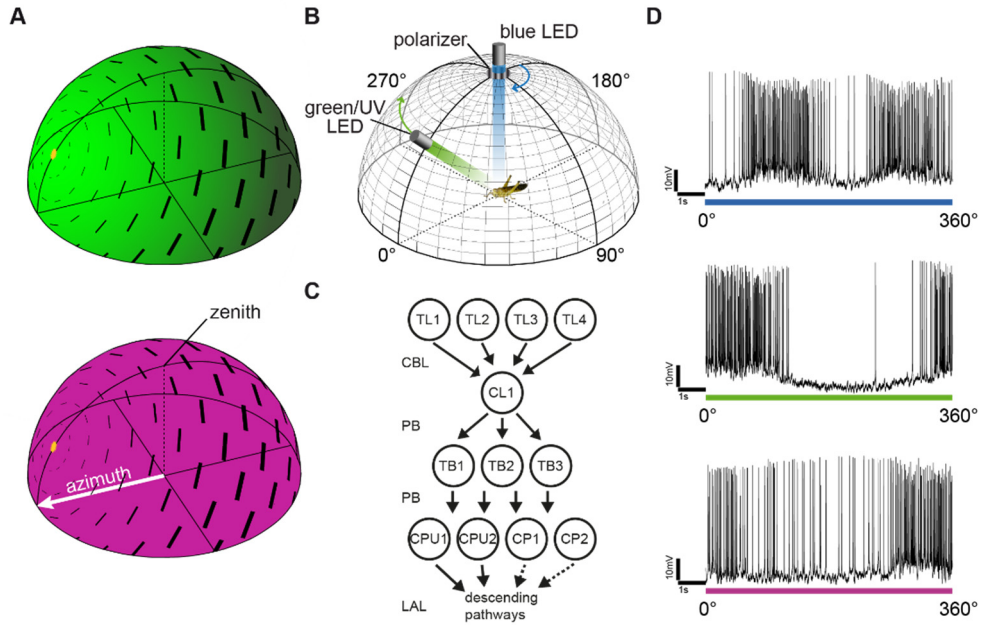

Fig. 1. Compass cues of the sky and visual stimulation. (A) Schematic illustration of the polarization pattern and the spectral gradient in the sky. Electric field vectors (black bars) are arranged tangentially along concentric circles around the sun. The degree of polarization, indicated by the thickness of bars, increases from the sun toward a 90° angle and decreases again toward the antisolar point. The chromatic gradient is the product of a long-wavelength light intensity gradient (green) and a uniform distribution of short-wavelength light (purple), resulting in a high color contrast near the sun and a lower color contrast near the antisolar point. The solar azimuth, indicating the horizontal direction of the sun, and the zenith, the point in the sky vertically above the observer, are labelled. (B) Visual stimulation. The light of a blue LED passed a rotating polarizer in the zenith. A green (or UV) LED rotated at an elevation of 45° around the head of the animal to produce an unpolarized light stimulus. (C) Schematic illustration of information flow in the CX. Circles represent neuron types. Arrows indicate the suggested direction of connectivity between neurons. Because varicose arborizations of CP1 and CP2 neurons are confined to small areas in the lateral accessory lobe (LAL) their contacts to descending neurons are hypothetical and shown as dotted lines. (D) Spike train from TL2 neuron shown in Fig. 2B during a 360° clockwise rotation of the zenithal polarizer (left panel), the green light spot (middle panel) and the UV light spot (right panel). CBL, central body lower division; CL1, columnar neuron of the CBL type 1; CP1/2, columnar neuron of the PB type 1/2; CPU1/2, columnar neuron of the PB and central body upper unit type 1/2; PB, protocerebral bridge. TB1/2/3, tangential neuron of the PB type 1/2/3; TL1/2/3/4, tangential neuron of the CBL type 1/2/3/4.

Sky compass navigation has been demonstrated in several insect species, including bees (Brines and Gould, 1979; von Frisch, 1949), ants (Wehner and Müller, 2006), locusts (Kennedy, 1951), monarch butterflies (Reppert et al., 2004; Stalleicken et al., 2005), dung beetles (Dacke et al., 2003; el Jundi et al., 2014b), and fruit flies (Weir and Dickinson, 2012). All of these animals possess a region of the compound eye containing specialized homochromatic photoreceptors, the dorsal rim area (DRA), which serves as a polarization detector (Labhart and Meyer, 1999). In contrast, chromatic signals are perceived by photoreceptors in the main retina with different spectral sensitivities enabling color vision (Wernet et al., 2015). In the locust, intracellular recordings showed that polarization-sensitive neurons of the medulla and anterior optic tubercle (AOTU) integrate polarized and chromatic light information by responding to unpolarized chromatic stimuli in an azimuth-dependent way (Kinoshita et al., 2007; Pfeiffer and Homberg, 2007; el Jundi et al., 2011). Neurons of the AOTU are connected to neurons of the central complex (CX), a group of neuropils spanning the midline of the brain. In fruit flies several studies revealed the importance of the CX for navigational tasks (Neuser et al., 2008; Ofstad et al., 2011; Seelig and Jayaraman, 2015; Weir and Dickinson, 2015). A prominent role of the CX in sky compass signaling has been demonstrated in monarch butterflies (Heinze and Reppert, 2011), dung beetles (el Jundi et al., 2015), crickets (Sakura et al., 2008), and desert locusts (Homberg et al., 2011). In monarchs and dung beetles, CX neurons are sensitive to plane polarized light and the azimuth of unpolarized chromatic cues. The processing of polarized light signals has been studied most extensively in neurons of the locust CX (Heinze and Homberg, 2007; Bech et al., 2014; Bockhorst and Homberg, 2015), but only little is known about their coding of other sky compass cues (el Jundi et al., 2014a). In order to uncover the role of direct sunlight and chromatic information in sky compass signaling in the locust, we studied the processing of chromatic cues in comparison to the processing of polarized light signals, using intracellular recordings from a variety of CX neurons.

Materials and methods

Animals and Preparation

Desert locusts (*Schistocerca gregaria*) were reared under crowded conditions either in the laboratory at 28°C under a 12:12-h light-dark cycle or during summer in a greenhouse. Experiments were performed on sexually mature animals at least one week after final moult. Animals were mounted onto a metal holder using dental wax. Wings and legs were cut off, and the mouthparts were immobilized by wax. The head capsule was opened anteriorly, fat tissue and tracheal air sacs were removed. Muscles close to the brain as well as the esophagus were transected, and the gut was removed through an abdominal incision in order to reduce brain movements. Hemolymph leakage was prevented by using a thread to tie off the abdomen. To further stabilize the brain, it was supported from posterior by a small metal wire platform. To ease electrode penetration the neural sheath above the central brain was removed using forceps. During animal preparation and intracellular recording the brain was immersed in locust saline (Clements and May, 1974) containing 0.09 mol l^{-1} saccharose.

Electrophysiology and visual stimulation

For intracellular recordings sharp glass microelectrodes were drawn from borosilicate

capillaries (Hilgenberg, Malsfeld, Germany) using a Flaming/Brown horizontal puller (P-97, Sutter Instrument, Novato, CA, USA). The electrode tip was filled with 4% Neurobiotin (Vector Laboratories, Burlingame, CA,USA) diluted in 1 mol l^{-1} KCl, the electrode shank with 1 mol l^{-1} KCl. Neural signals were amplified 10× with a custom-built amplifier and visualized with an oscilloscope (DS 1052Eh, Rigol Technologies, Beijing, China). A digitizer (CED1401plus, Cambridge Electronic Design, Cambridge, UK) was used to sample the signals at a rate of 20 kHz. The data were stored on a PC using Spike2 (Version 6.022, Cambridge Electronic Design, Cambridge, UK). After the recording Neurobiotin was injected into the neuron by applying constant positive current of about 1 nA for 3-4 minutes. During the recording the animal's body axis was oriented vertically with its head uppermost (Pfeiffer et al., 2005). The locust was stimulated with polarized blue light, generated by a blue light emitting diode (LED; Oslon SSL 80, LDCQ7P, 452 nm, Osram Opto Semiconductors, Regensburg, Germany, or LXML-PR01-0500, 447.5 nm, Philips Lumileds Lighting Company, San José, CA, USA). Light intensity was adjusted to a photon flux of 1.7×10^{13} photons cm^{-2} s^{-1}. The LED was positioned in the zenith (visual angle 32.5° or 18.6°). Its light passed through a diffusor and a polarizer (HNP'B, Polaroid, Cambridge, MA,USA), which rotated 360° clockwise or counterclockwise, with 40°/s or 36°/s velocity. A stimulation velocity of 30°/s was used in 4 experiments. Additionally, we stimulated the animal with unpolarized green and UV light spots. The green light spot was generated by a green LED (LED535-series, 535 nm, Roithner Lasertechnik, Vienna, Austria, or Oslon SSL 80, LT CP7P, 528 nm, Osram Opto Semiconductors, Regensburg, Germany; photon flux adjusted to 10^{14} photons cm^{-2} s^{-1}), the UV light spot by an ultraviolet LED (XSL-355-5E, 355 nm, Roithner Lasertechnik, or Nichia STS-DA1-2394D, NCSU033B(T), 365 nm, Nichia Corporation, Anan, Japan; photon flux adjusted to 10^{14} photons cm^{-2} s^{-1}). Their light passed through a diffusor. The unpolarized light stimuli covered a visual angle of 16.3°. They were moved around the head of the animal at an elevation of 45° and a velocity of 40°/s or 36°/s (Fig. 1B).

Histology

Brains were dissected in locust saline and immersed overnight at 4°C in fixative containing 4% paraformaldehyde, 0.25% glutaraldehyde, 2% saturated picric acid in 0.1 mol l^{-1} phosphate buffered saline (PBS). They were stored for up to 14 days in sodium phosphate buffer at 4°C. Brains were rinsed 4 × 15 minutes in 0.1 mol l^{-1} PBS and incubated for three days in Cy3-conjugated streptavidin (Dianova, Hamburg, Germany) diluted 1:1,000 in 0.1 mol l^{-1} PBS containing 0.3% Triton X-100 (PBT) at 4°C in the dark. After incubation they were rinsed 2 × in 0.1 mol l^{-1} PBT and 3 × in 0.1 mol l^{-1} PBS for 30 min. each, dehydrated in an increasing ethanol series (30%, 50%, 70%, 90%, 95%, 100% for 15 minutes each), cleared in a 1:1 mixture of 100% ethanol and methyl salicylate (Merck, Darmstadt, Germany) for 20 minutes, followed by pure methyl salicylate for one hour, and were finally mounted in Permount (Fisher Scientific, Waltham, MA, USA) between two coverslips. Neurons were visualized using a confocal laser scanning microscope (Leica TCS-SP5, Leica Microsystems, Wetzlar, Germany) with a DPSS Laser (561 nm) and AMIRA (version 5.4.5, FEI Visualization Science Group, Mérignac Cedex, France). Neurons were reconstructed two-dimensionally using Adobe Photoshop CC (version 2014.2.1, Adobe Systems, San José, CA, USA).

Data preprocessing

Physiological data were evaluated only from recordings of neurons that were clearly identified by means of their labeling. Recordings were preprocessed using Spike2 (Cambridge Electronic Design, Cambridge, UK). The quality of recording was determined by visual inspection. Recordings with strong fluctuations in baseline or with low spike amplitudes (< 5 mV) were rejected. In the selected recordings spikes were detected with threshold based event detection in Spike2. The data were then exported as a mat-file. All subsequent analysis was performed using MATLAB (Version 2016a, The MathWorks, Natick, MA, USA).

Background activity

To analyze neuronal responses during polarizer/light spot rotation we calculated the background activity (BA) of each neuron. Only stable parts of the recording during absence of stimulation or current injection were selected. Spikes were binned in 1 s bins. Spike counts of all bins were used to calculate the median, the lower and upper quartile as well as the 2.5^{th} and 97.5^{th} percentile of BA. To assess the role of BA we analyzed responses of neurons with high and low BA separately. A cell-type specific median BA was calculated out of all median BAs of the neurons belonging to that cell type. Median individual BAs lower than or equal to the cell type specific median BA were defined as low BA, whereas median individual BAs higher than the cell type specific BA were defined as high BA.

Stimulus responsiveness

For each stimulus presentation (i.e. 360° rotation of *E*-vector/light spot) the neuron's stimulus response curve was obtained by calculating the spike rate within each of 36 bins of 10°. From the stimulus response curves we tested the responses for unidirectionality (green/UV spot stimulus) by angular-linear correlation analysis (Zar, 1999; Berens, 2009). The angles of bin centers were used as the angular variable and the mean spiking activity in each bin as the linear variable. The responses to the rotating *E*-vector were tested for bidirectionality, thus the angular variable was doubled (Batschelet, 1981). The criterion for responsiveness to the plane of polarized light or the azimuth of unpolarized light spots was the significance of the resulting correlation coefficient r_{al} ($\alpha = 0.05$).

Stimulus response characteristics

Spike times were transformed into angles (hereafter referred to as spike angles) by multiplying them with the rotation velocity of the stimulus. In the case of significant angular-linear correlation these were used to calculate the preferred angle (Φ_{max}) (Batschelet, 1981). It indicates the preferred angular orientation of the polarizer (periodicity 180°), resp. the preferred azimuthal angles of the unpolarized light spots (periodicity 360°). The anti-preferred angle (Φ_{min}) was regarded as the angle perpendicular, i.e. 90° distant, to Φ_{max} in the case of polarized light stimulation, and as the angle 180° to Φ_{max} in the case of unpolarized light stimulation. The angular-linear correlation analysis of stimulus response curves gave a correlation coefficient (r_{al}). Its square, the coefficient of determination (r_{al}^2) ranges from zero to unity. It is an estimate of how much the change of spike rate can be explained by the change of *E*-vector/light spot angle during rotation (Bockhorst and Homberg, 2015). In order to characterize the tuning curves in more detail we calculated their amplitude and tuning width. We fitted a smoothing spline onto the stimulus response curve of significant responses, normalized to the median BA of the respective cell, using the MATLAB curve fitting toolbox (smoothing parameter set to 10^{-4}). We defined the amplitude as the difference in normalized

spike rate between peak and trough of the fit curve, and the tuning width as the angular distance between values at half amplitude.

Data plots

For circular histograms pooled stimulus response curves (10° bin width) were plotted on a circular scale using Origin 6.0 (MicroCal, Northhampton, MA, USA). Colored bars show the mean spiking activity in each bin. Error bars indicate standard deviation. For each recording equal numbers of responses to clockwise and counterclockwise stimulation were pooled, in order to avoid a shift in tuning due to direction selectivity. Boxes in boxplots range from the 25th (Q1) to 75th (Q3) percentile. Data points less than Q3 - 1.5 × (Q3 - Q1) and greater than Q3 + 1.5 × (Q3 - Q1) were drawn as outliers. Whiskers extend to the adjacent value that is the most extreme data point, which is not an outlier. Notches indicate the 95% confidence interval of the median. Two medians with non-overlapping confidence intervals were termed truly different at the 5% confidence level.

Results

General response properties

We analyzed the responses of 87 CX neurons, belonging to 13 morphological types, to blue light from dorsal direction passing a rotating polarizer and to unpolarized green and UV light spots moving around the head of the animal. Twelve of these cell types were shown previously to be sensitive to zenithal *E*-vector orientation (Heinze et al., 2009), but one cell type (TB3) has not been studied before. Table S1 provides an overview of cell-type specific responsiveness to all three stimulation regimes. Tangential neurons of the lower division of the central body (TL neurons) receive visual input from the AOTU and represent the input stage to the polarization network of the CX (Figs. 1C, 2; Heinze et al., 2009). Columnar neurons of the lower division of the central body (CL1 neurons) carry the signal to the protocerebral bridge (PB). Tangential neurons of the PB, termed TB neurons, distribute the signals throughout the 16 slices of the PB. CL1 and TB neurons represent the intermediate stage of processing (Figs. 1C, 3). Columnar neurons (CPU and CP neurons) with ramifications in the PB and axonal projections to subfields of the lateral accessory lobe (LAL) likely converge on interneurons contacting descending pathways (Figs. 1C, 4; Heinze and Homberg, 2009, Träger and Homberg, 2011). Therefore, these neuron types represent the output stage of visual processing of the CX.

Four types of TL neurons were studied (Fig. 2). They differ in the location of their input arborizations in the lateral accessory lobe (TL1, TL4), the medial and lateral bulb (TL2, TL3), and their axonal projections to specific layers of the CBL (Müller et al., 1997). TL1 neurons were recorded twice. One neuron responded to polarized light but not to the unpolarized light spots, whereas the other cell was responsive to all three stimuli (Fig. 2A). It was slightly excited and inhibited depending on *E*-vector orientation, but excited at all angles of the green and UV light spots. The second neuron did not respond to the unpolarized light spots, but to the orientation of the *E*-vector with excitation at all angles. TL2 neurons were recorded more frequently (n=7). They were excited and inhibited by the *E*-vector (Fig. 2B; Fig. 5A). The tunings to green and UV light showed pronounced spatial opponency, i.e. excitation at the preferred angle of the unpolarized light spot and inhibition when the stimulus appeared at the opposite side of the head (anti-preferred angle; Fig. 2B; Fig. 5A). A spike train of the TL2

neuron from Fig. 2B is shown in Fig. 1D. TL3 neurons were recorded twice. They showed polarization opponency, i.e. excitation at the preferred *E*-vector orientation and inhibition at the orthogonal *E*-vector (anti-preferred orientation; Fig. 2C; Fig 5A). In contrast, their tunings to green and UV light were only slightly modulated by the angle of the unpolarized light spots with weak excitation at a broad range around Φ_{max} (Fig. 2C; Fig. 5A). Only one TL4 neuron was recorded. It showed weak excitation at Φ_{max}, but no inhibition at Φ_{min} in response to polarized light, a strong inhibition at the anti-preferred angle of green light, and spatial opponency in response to UV light (Fig. 2D).

Four types of neuron, CL1, TB1, TB2, and TB3 of the intermediate processing stage were studied (Fig. 3). CL1 neurons connect individual slices of the CBL to slices of the PB. All CL1 neurons studied here had a mixture of fine and varicose arborizations in the CBL and claw-like varicose ramifications in the PB, characteristic of the CL1a subtype (Fig. 3A; Heinze and Homberg 2008). The appearance of arborizations may indicate the polarity of a neuron. As shown by ultrastructural studies, smooth or fine processes are largely postsynaptic, whereas varicose or claw-like neurites generally contain transmitter-filled vesicles and act presynaptically (Peters at al., 1986; Cardona et al., 2010; Homberg and Müller, 2016). Therefore, CL1a neurons are most likely pre- and postsynaptic in the CBL and exclusively presynaptic in the PB. TB1 neurons had varicose arborizations in the posterior optic tubercle (POTU), varicose ramifications in two slices of the PB, separated by 7 slices, and fine processes in several slices in between (Fig. 3B). One TB2 neuron recorded here had varicose arborizations in the outermost slice of the ipsilateral hemisphere and the innermost slices of both hemispheres of the PB and smooth processes in other slices in between. Fine processes clustered together extended to the POTU (Fig. 3C). The TB3 neuron is a novel cell type of the CX network. It had varicose ramifications in the POTU and its vicinity (Fig. 3D). In the PB it invaded the outermost and the two innermost slices of the ipsilateral hemisphere with varicose processes. Slices in between were invaded by fine processes. All neurons showed clear responses to the stimuli, but tuning characteristics were diverse. CL1 (n=20) and TB1 (n=16) neurons were recorded most frequently. Both cell types showed polarization and spatial opponency, but excitation and inhibition was more pronounced in the CL1 neurons (Fig. 3A,B; Fig. 5A). TB2 and TB3 neurons were recorded only once. The TB2 neuron was excited at Φ_{max} and inhibited at Φ_{min} in response to all three stimuli (Fig. 3C). Responses of the TB3 neuron were weak (Fig. 3D). The rotating polarizer elicited only slight excitation at Φ_{max} and slight inhibition at Φ_{min}. In response to the rotating light spots the neuron was clearly excited at Φ_{max}, and likewise inhibited at Φ_{min}.

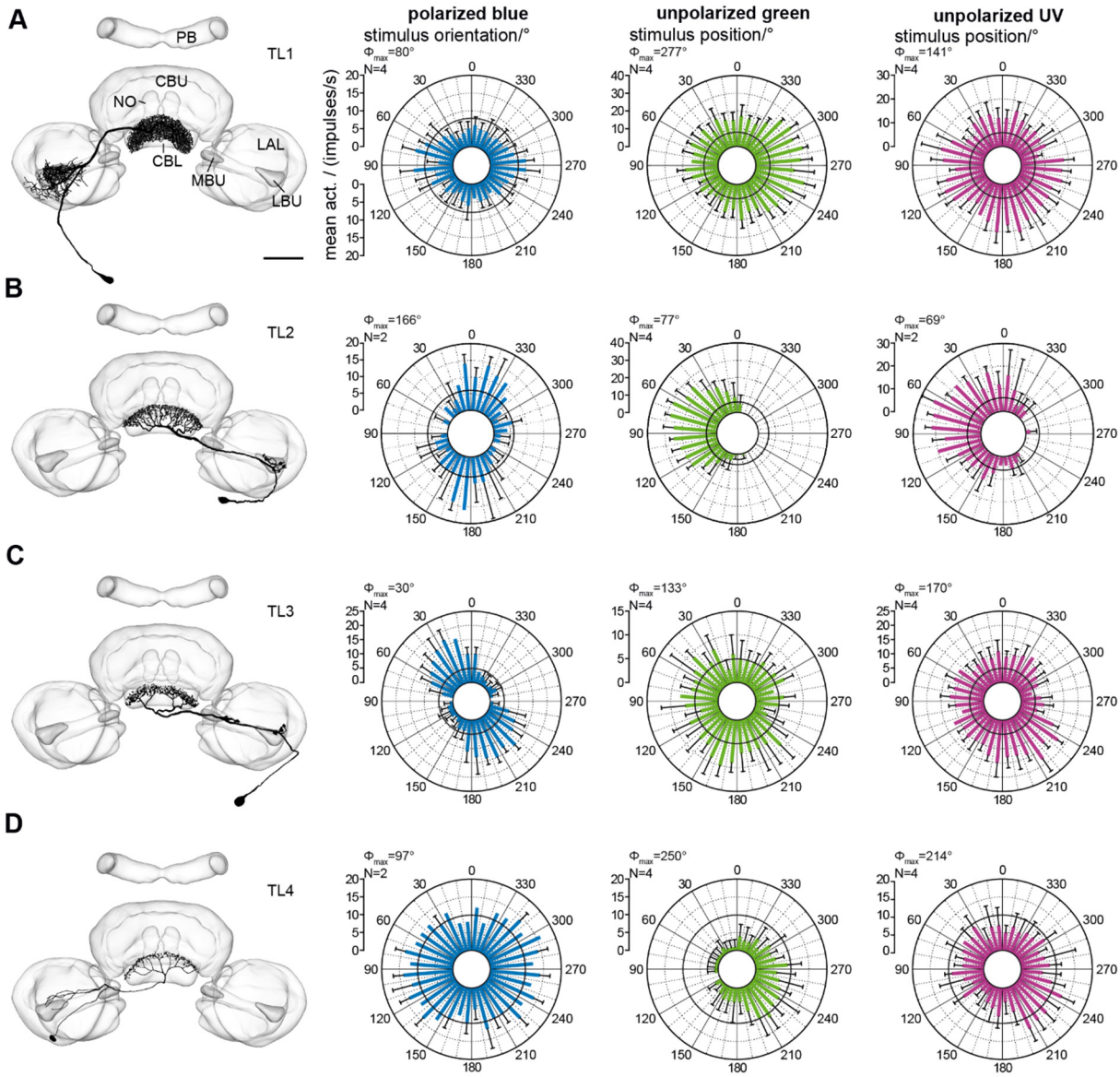

Fig. 2. Morphology and physiology of tangential neurons of the lower division of the central body (TL). (A-D) Reconstructions of a TL1 (B), TL2 (C), TL3 (D), and TL4 (E) neuron, projected onto the standard CX (el Jundi et al., 2010; posterior view; left panels) and circular histograms of stimulus responses (right panels) from the animals' perspective. *N* responses to 360°-rotations of the polarizer (polarized, blue), a green and a UV light spot (unpolarized green resp. UV) were pooled and plotted as means in 10°-bins. Black circles indicate median background activity. Error bars indicate SD. The preferred *E*-vector orientation or azimuth of the unpolarized light spots is indicated by Φ_{max}. Scale bar, 100 µm. CBL, central body lower division; CBU, central body upper division; LAL, lateral accessory lobe; LBU, lateral bulb; MBU, medial bulb; NO, noduli; PB, protocerebral bridge.

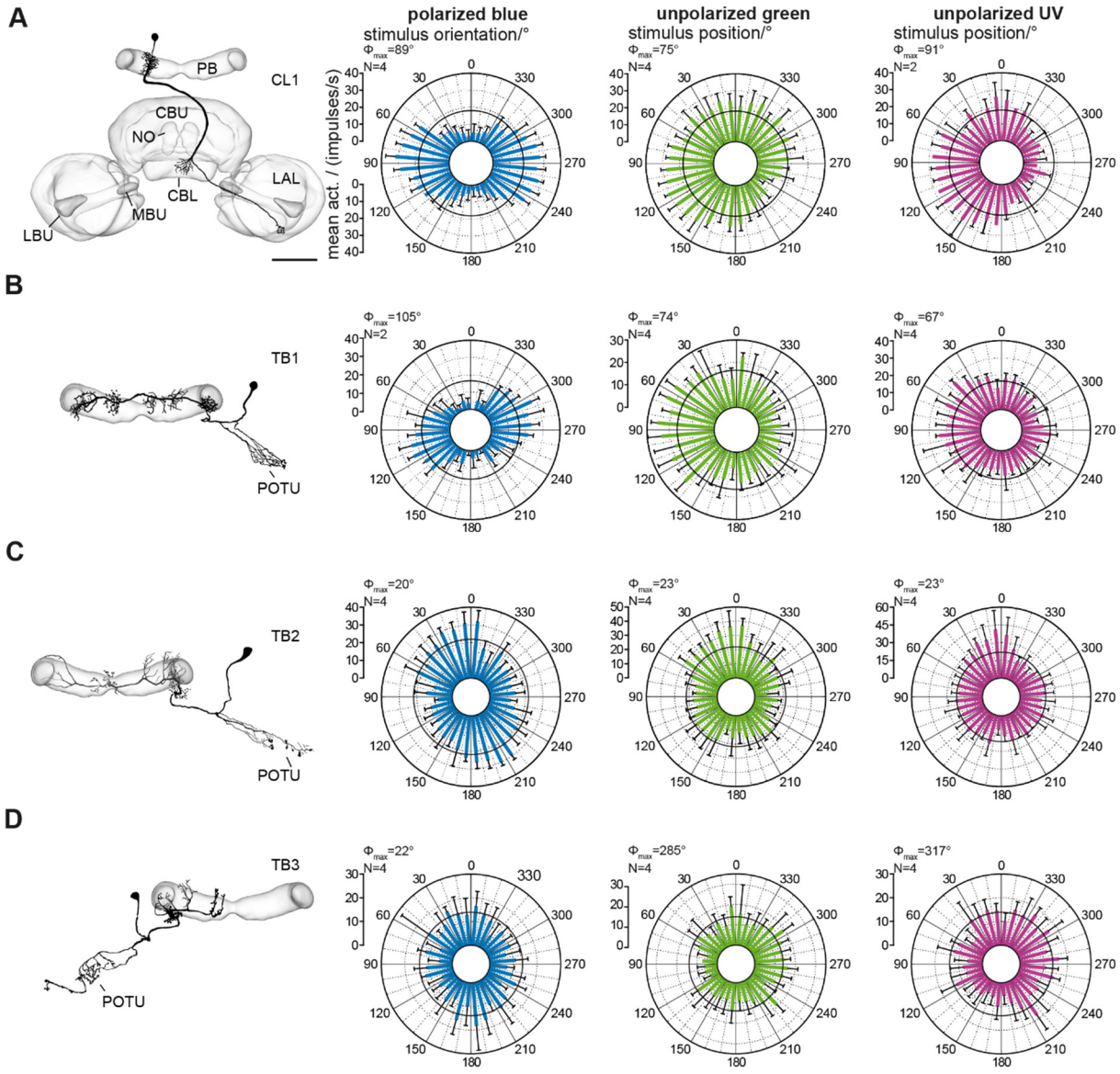

Fig. 3. Morphology and physiology of a columnar neuron of the lower division of the central body (CL1) and tangential neurons of the protocerebral bridge (TB). (A-D) Reconstructions of a CL1 (A), TB1 (B), TB2 (C) and TB3 (D) neuron, projected onto the standard CX (el Jundi et al., 2010; left panels) and circular histograms of stimulus responses (right panels). *N* responses to 360°-rotations of the polarizer (polarized, blue), a green and a UV light spot (unpolarized green resp. UV) were pooled and plotted as means in 10°-bins. Black circles indicate median background activity. Error bars indicate SD. The preferred *E*-vector orientation or azimuth of the unpolarized light spots is indicated by Φ_{max}. Scale bar, 100 µm. CBL, central body lower division; CBU, central body upper division; LAL, lateral accessory lobe; LBU, lateral bulb; MBU, medial bulb; NO, noduli; PB, protocerebral bridge; POTU, posterior optic tubercle.

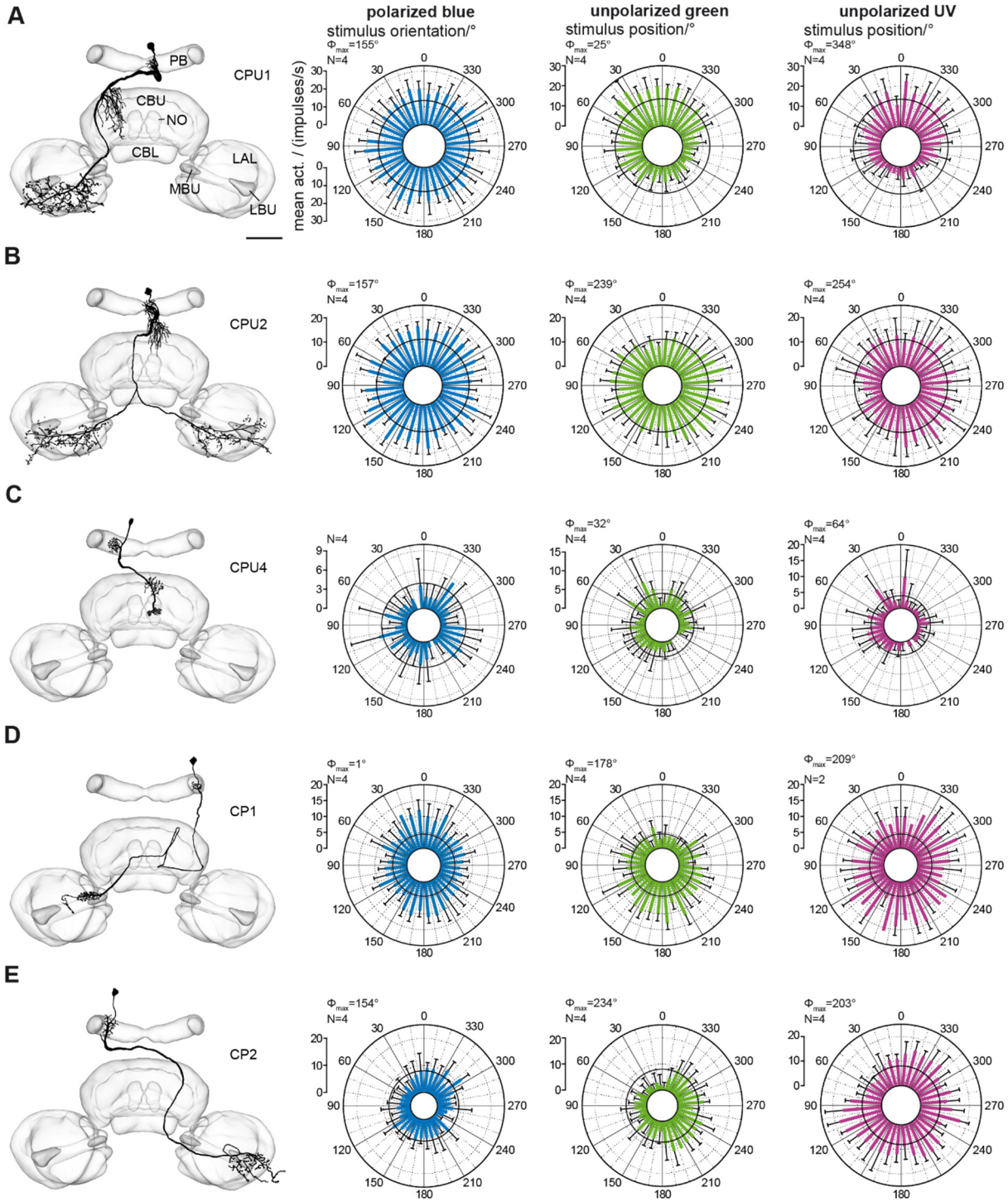

Fig. 4. Morphology and physiology of columnar neurons (types CPU and CP) of the protocerebral bridge. (A-E) Reconstructions of a CPU1 (A), CPU2 (B), CPU4 (C), CP1 (D) and CP2 (E) neuron, projected onto the standard CX (el Jundi et al., 2010; left panels) and circular histograms of neuronal responses (right panels). *N* responses to 360°-rotations of the polarizer (polarized, blue), a green and a UV light spot (unpolarized green resp. UV) were pooled and plotted as means in 10°-bins. Black circles indicate median background activity. Error bars indicate SD. The preferred *E*-vector orientation or azimuth of the unpolarized light spots is indicated by Φ_{max}. Note that the CPU4 neuron and the CP2 neuron were not responsive to the orientation of the polarizer. Scale bar, 100 µm. CBL, central body lower division; CBU, central body upper division; LAL, lateral accessory lobe; LBU, lateral bulb; MBU, medial bulb; NO, noduli; PB, protocerebral bridge.

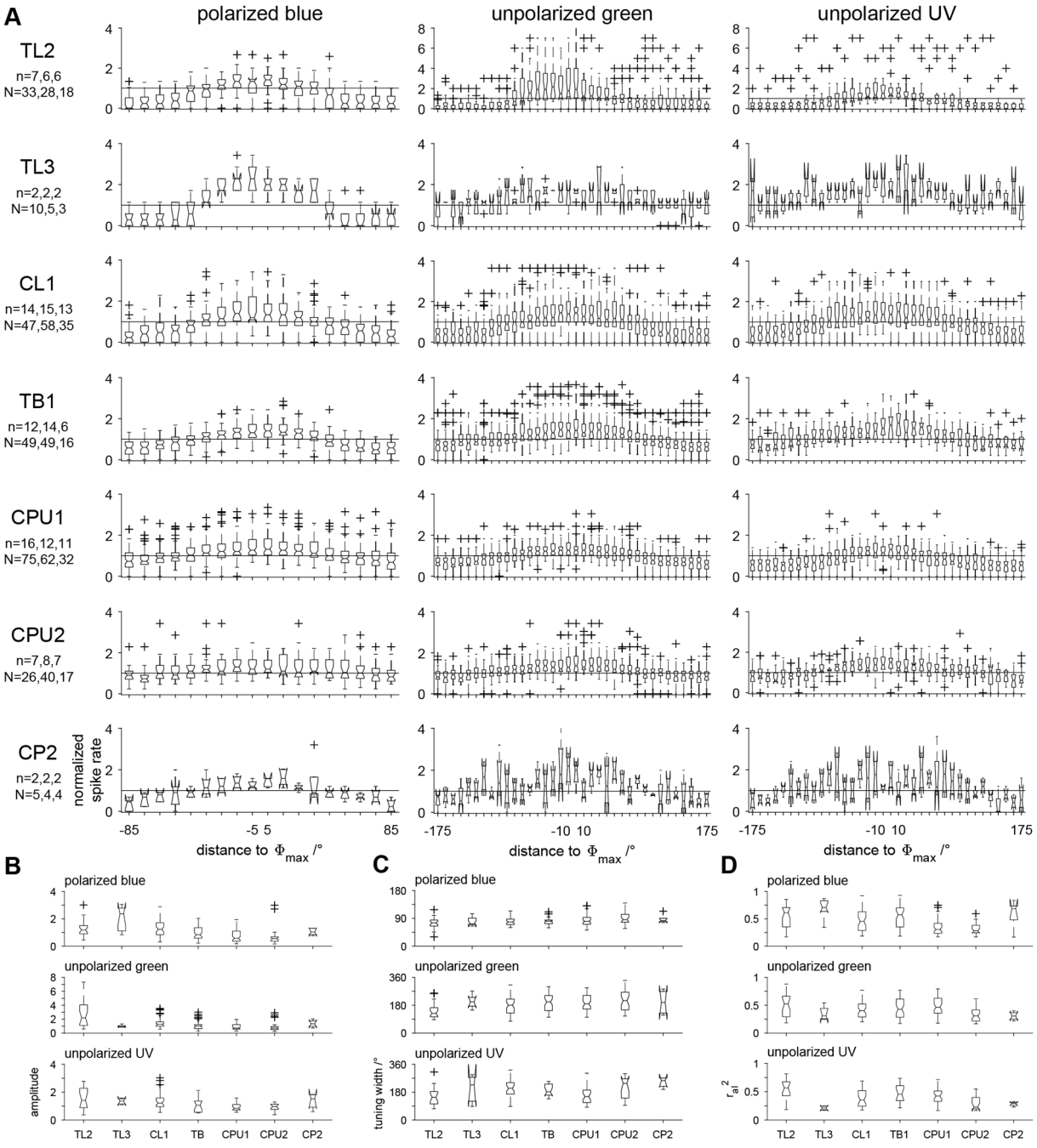

Fig. 5. Tuning curves and tuning characteristics of responses to the plane of polarized blue light and the azimuth of an unpolarized green and UV light spot. (A) Normalized stimulus response curves of N responses in n neurons to polarized blue light, unpolarized green and unpolarized UV light. Stimulus response curves were normalized to the median neuronal background activity (solid line at value 1). E-vector tuning was analyzed from Φmax-90° to Φmax+90°, unpolarized light spot tunings from Φmax-180° to Φmax+180°. (B-D) Amplitude (B), width (C) and ral2 (D) of responses in (A) are box-plotted for each cell type.

Finally, 4 types of columnar output neurons, CPU1, CPU2, CP1 and CP2 were investigated (Fig. 4). A fifth type of neuron, CPU4, was included in this group (Fig. 4C) because like the other cell types it had dendritic ramifications in the PB, but whether it acts as an output or an intrinsic element of the CX, remains to be shown. CPU1 and CPU2 neurons had smooth ramifications in the PB and varicose ramifications in the contralateral LAL (CPU1), or both LALs (CPU2). The CPU4 neuron had varicose ramifications in the upper division of the contralateral nodulus, and in several slices of the upper division of the central body (CBU). Ramifications in the PB were smooth, thus possibly dendritic. CP1 and CP2 neurons had likewise fine, thus likely dendritic processes in the PB, and varicose terminals in distinct parts of the LAL. CPU1 (n=19) and CPU2 (n=11) neurons were recorded most frequently. Both cell types showed spatial opponency in their responses to the unpolarized light spots (Fig. 4A,B; Fig. 5A). CPU4 neurons were recorded only once. The neuron was not responsive to polarized light, but to both unpolarized light spots (Fig. 4C). The tunings to green and UV light were spatially opponent. CP1 neurons were recorded twice. One cell was excited at the preferred E-vector angle and at the preferred azimuth of the green spot (Fig. 4D), but both responses lacked inhibition at the anti-preferred angle. In contrast the neuron was excited at many angles of the UV light spot. The second neuron was not responsive to UV light, but polarization opponent in its E-vector tuning and spatially opponent in its green light tuning. CP2 neurons (n=4) showed polarization opponency, however inhibition at Φmin was stronger than excitation at Φmax (Fig. 4E; Fig. 5A). Responses to the unpolarized light spots were spatially opponent, but here with stronger excitation at Φmax and weaker inhibition at Φmin (Fig. 4E; Fig. 5A).

Responsiveness and tuning characteristics

As shown in Figs. 2-4 and illustrated in Table S1, the majority of neurons of the CX polarization processing network responded to all three stimuli (Table S1). However, insensitivity to the rotating polarizer or the rotating green or UV light spots was found in neurons of all cell types and in a substantial number of tests (Table S1). Across the three stimuli some neurons of each type showed responses with significant correlation as well as responses that lacked significant correlation during the same recording This is indicated by comparison of the total number of neurons with those that responded to each stimulus and those that did not respond to any stimulus repetition (Table S1). The overall responsiveness to polarized light, green and UV light differed between cell types. TL1 neurons showed only weak responsiveness to all three stimuli. TL2 neurons were more often responsive to the azimuth of the green spot (88%) than to the orientation of the *E*-vector (77%) and azimuth of the UV spot (75%) (Table S1). TL3 neurons responded more reliably to the *E*-vector (83%) than to the unpolarized light spots (50% and 38%). In contrast, CL1 neurons responded more reliably to green and UV light (both 73%), but less reliably to polarized light (55%), whereas TB1 neurons responded most reliably to green light (72%). CPU1 neurons showed responsiveness between 60% and 70% to all three stimuli, and finally CPU2 neurons showed lowest responsiveness (36%) to polarized light, but high responsiveness to green (68%) and UV (77%) light.

To compare the tunings to the stimuli in more detail, we plotted for each cell type all stimulus response curves with significant correlation, normalized to the median BA of

the respective neuron (Fig. 5A). Because states of background activity (BA) have a duration of up to 7 s (Bockhorst and Homberg, 2015), a minimal BA duration of 14 s was required for normalization, otherwise responses were excluded from analysis as were neurons with low sample size (TL1 (n=2), TL4 (n=1), TB2 (n=1), TB3 (n=1), CPU4 (n=1), CP1 (n=2)).

Next we plotted tuning amplitudes and widths and the coefficient of determination (r_{al}^2) of the stimulus response curves. Amplitude and width indicate the strength of modulation during stimulation by the *E*-vector and the unpolarized light spots. Independent on response amplitude the correlation r_{al}^2 estimates how much the change in spike rate can be explained by the change of the stimulus angle. It therefore can be used to describe the shape of the stimulus response curve (e.g. the more a tuning to an unpolarized light spot looks like a sinewave the higher will be r_{al}^2). Neurons of the input stage (TL2 and TL3) differed substantially in their tuning characteristics to polarized and unpolarized light. TL2 neurons showed higher amplitude, lower tuning width and higher correlation in azimuth tunings to the green and UV light spots. In contrast, TL3 neurons responded with higher amplitude and correlation, but with the same tuning width as TL2 neurons to the rotating polarizer (Fig. 5B-D). In all cell types downstream of TL neurons the response amplitude decreased from CL1 to CPU2 neurons (in tunings to the UV spot to similar levels in CPU1 and CPU2 neurons; Fig. 5B). The overall tuning width was similar in *E*-vector responses of all cell types, as indicated by the overlapping notches of boxplots (Fig. 5C). The tuning width of responses to unpolarized light was generally larger and more variable in TL3, CL1, TB1, CPU1, CPU2, and CP2 than in TL2 neurons. The correlation between *E*-vector angle and firing rate was generally weaker in neurons of the output stage than in input stage neurons, except in CP2 neurons (Fig. 5D). CP2 neurons showed for all of the three stimuli a correlation similar to that of TL3 neurons (Fig. 5D).

Polarization opponency and spatial opponency

The background activity (BA) of a neuron can be highly variable during the recording despite constant recording quality (Bockhorst and Homberg, 2015). Whether a postsynaptic neuron can distinguish between states of BA or a stimulus response might depend on variability of BA. Therefore, we wanted to assess whether neurons were excited at Φ_{max} and inhibited at Φ_{min} (i.e. polarization/spatial opponency) beyond the occurring variations in BA. We calculated effective tuning amplitudes by normalizing firing rates at Φ_{max} (+/-10°) to very high (97.5 percentile) BA, and at Φ_{min} (+/-10°) to very low (2.5 percentile) BA (Fig. S2). The results are summarized in Table 1. In response to polarized light TL3, TB1, CPU1 and CP2 neurons were excited at Φ_{max} and inhibited at Φ_{min} (Table 1, Fig. S2). Of these, TB1 and CP2 neurons showed the strongest polarization opponency. In contrast, TL2 and CL1 neurons were inhibited at $\Phi_{min,}$ but not excited at Φ_{max}. CPU2 neurons were neither excited at Φ_{max} above high BA nor inhibited at Φ_{min} below low BA. In response to the rotating green light spot TL2, TB1 and CP2 neurons were excited at Φ_{max} and inhibited at Φ_{min}, thus showed spatial opponency (Tab. 1, Fig. S2). CL1 and CPU1 neurons showed no excitation at $\Phi_{max,}$ but inhibition at Φ_{min}, whereas TL3 neurons were excited but lacked inhibition. CPU2 neurons were again neither excited at Φ_{max} nor inhibited at Φ_{min}. Responses to the rotating UV light spot of TL2, TL3, TB1, CPU1 and CP2 neurons were spatially opponent (Table 1, Fig. S2).

As for polarized and green light stimulation CL1 neurons showed no excitation at the preferred angle and CPU2 neurons no inhibition at the anti-preferred angle.

Dependency on background activity

Background firing may be highly variable between different recordings of the same neuron type (Heinze and Homberg, 2009), and it has already been suggested that in CPU neurons low BA might indicate strong responses to polarized light (Bockhorst and Homberg, 2015). To compare responses that occurred during high BA to responses that occurred during low BA, we sorted recordings of each cell type according to their median BA into those with high BA and those with low BA (for detailed description see Methods). The calculated cell-type specific BA of TL2, CL1, TB1, CPU1 and CPU2 neurons was 9, 8, 20, 17 and 11 spikes/s, respectively. Across all stimulation regimes and cell types the tuning shape was dependent on BA (Figs. 6A, S3A, S4A). In TL2, CL1, TB1 and CPU1 neurons the amplitude of responses to the rotating green light spot and its variability were significantly higher during low BA than during high BA (Fig. 6B).

Table 1: Polarization / spatial opponency in CX neurons. Effective excitation at Φ_{max} and effective inhibition at Φ_{min} for responses with significant correlation to polarized blue, unpolarized green, and unpolarized UV stimulation. Robust excitation (inhibition) is marked by ++ (--), partial excitation (inhibition) by + (-). 0 means no effective excitation / inhibition.

Cell type	Excitation at Φ_{max}	Inhibition at Φ_{min}
polarized blue		
TL2	0	--
TL3	++	-
CL1	0	--
TB1	++	--
CPU1	+	-
CPU2	0	0
CP2	++	--
unpolarized green		
TL2	+	--
TL3	+	0
CL1	0	-
TB1	+	-
CPU1	0	-
CPU2	0	0
CP2	++	-
unpolarized UV		
TL2	+	--
TL3	+	-
CL1	0	-
TB1	+	-
CPU1	+	-
CPU2	+	0
CP2	+	-

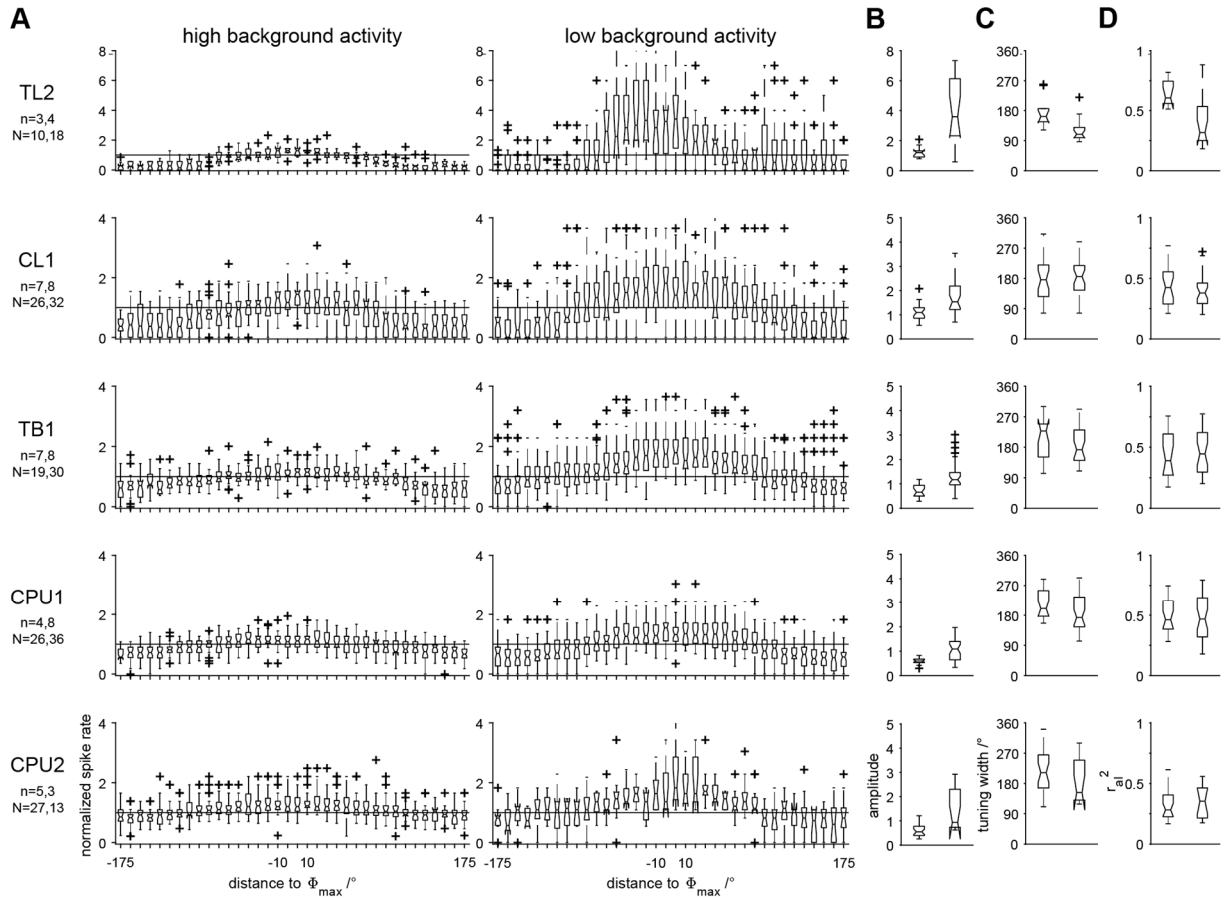

Fig. 6. Comparison of tuning characteristics to green light during high and low background activity. (A) Normalized stimulus response curves of *N* responses in *n* neurons to unpolarized green light during high and low neuronal background activity. Stimulus response curves were normalized to the median neuronal background activity (solid line at value 1). *E*-vector tunings were analyzed from Φ_{max}-90° to Φ_{max}+90°, green/UV light spot tunings from Φ_{max}-180° to Φ_{max}+180°. (B-D) Box plots showing amplitude, width and r_{al}^2 of responses in (A) for each cell type during high (left) and low (right) BA.

In CPU2 neurons only the variability of amplitude was increased in neurons with low BA. In contrast the range of tuning width was generally independent of BA, but the median width was shifted toward 180° in TB1, CPU1 and CPU2 neurons (Fig. 6C). The distribution of ral2 in neurons with high BA was similar to the distribution of ral2 in neurons with low BA in CL1, TB1, CPU1 and CPU2 neurons, but significantly decreased in TL2 neurons with low BA (Fig. 6D). CPU2 neurons showed lowest ral2 independent of BA. Tunings to the rotating UV light spot showed similar properties (Fig. S3). The amplitude was higher in TB1, CPU1 and CPU2 neurons with low BA than in cells with high BA (Fig. S3B). Again the width of tuning was statistically equal in all cell types during high and low BA, but the median shifted toward 180° in TL2, TB1, CPU1 and CPU2 neurons during low BA (Fig. S3C). The ral2 of UV tunings was independent of BA in all cell types (Fig. S3D). In responses of TB1, CPU1 and CPU2 neurons to the rotating polarizer the amplitude was higher in cells with low BA than in cells with high BA (Fig. S4A,B). Amplitude variability was increased in all cell types. As in the other stimulation regimes tuning widths were equal during high BA and low BA across all cell types (Fig. S3C). The correlation between E-vector orientation and firing rate was higher in CPU2 neurons during low BA than during high BA, and not affected by BA in all other cell types (Fig. S3D).

Table 2: Polarization and spatial opponency in CX neurons with low and high BA. Effective excitation at Φ_{max} and effective inhibition at Φ_{min} for responses with significant correlation to polarized blue, unpolarized green, and unpolarized UV stimulation. Responses were divided into those from neurons with high BA and those from neurons with low BA. Robust excitation (inhibition) is marked by ++ (--), partial excitation (inhibition) by + (-). 0 means no effective excitation / inhibition.

	Responses from neurons with high BA		Responses from neurons with low BA	
Cell type	Excitation at Φ_{max}	Inhibition at Φ_{min}	Excitation at Φ_{max}	Inhibition at Φ_{min}
polarized blue				
TL2	+	--	+	--
CL1	0	--	+	-
TB1	++	-	++	--
CPU1	0	0	++	-
CPU2	0	-	++	0
unpolarized green				
TL2	+	--	++	--
CL1	0	-	0	-
TB1	0	--	++	-
CPU1	0	-	+	-
CPU2	0	0	0	0
unpolarized UV				
TL2	+	--	+	--
CL1	0	-	0	-
TB1	0	--	++	-
CPU1	+	-	+	--
CPU2	+	0	++	-

We next investigated whether polarization opponency and spatial opponency also depended on BA. Thus, we plotted again the firing rates at Φ_{max} and Φ_{min} normalized to very high and very low levels of BA, respectively, in the two populations of neurons (Fig. S5). The main findings are shown in Table 2. In response to polarized light during high BA only TL2 and TB1 neurons showed polarization opponency (Table 2). In contrast, CL1 and CPU2 neurons were inhibited at Φ_{min}, but not excited at Φ_{max}, respectively. CPU1 neurons were neither excited at Φ_{max} above high BA nor inhibited at Φ_{min} below low BA. In contrast, during low BA all cell types, except CPU2 neurons, showed polarization opponency. Only TL2 neurons showed spatial opponency in green light spot responses at high BA. All other cell types lacked excitation at Φ_{max}. In contrast, during low BA TL2, TB1 and CPU1 neurons were spatially opponent. CL1 neurons were again inhibited at Φ_{min}, but not excited at Φ_{max}, and CPU2 neurons were neither excited at Φ_{max} above high BA nor inhibited at Φ_{min} below low BA. Responses to the rotating UV light spot during high BA showed spatial opponency in TL2 and CPU1 neurons. Again CL1 neurons were inhibited at Φ_{min}, but not excited at Φ_{max}. In contrast, during low BA all cell types except CL1 neurons responded in a spatially opponent manner. In general cells were mainly inhibited, when they had high BA. In contrast, they were strongly excited during low BA, but the inhibition at Φ_{min} remained, although weaker than during

high BA, so that polarization and spatial opponency was more distinct.

Rotation direction sensitivity

For the calculation of general response characteristics of a neuron, like the preferred tuning angle, rotation-direction specific effects were eliminated by pooling equal numbers of clockwise and counterclockwise rotations. Here, we address possible differences in response parameters depending on the direction of rotation. We calculated for each neuron the angular distances between Φ_{max} values of individual responses to clockwise and counterclockwise rotations to the pooled Φ_{max} of responses to all rotations. Neurons usually showed either delayed responses during single rotations (Fig. S6) or advanced responses (Fig. 7) in comparison to the pooled Φ_{max} from equal numbers of clockwise and counterclockwise rotations. Neurons showing a mixture of advanced and delayed responses were excluded from analysis. In anticipatory *E*-vector tunings of all cell types time shifts were rather similar, except in CP2 neurons (Fig. 7).

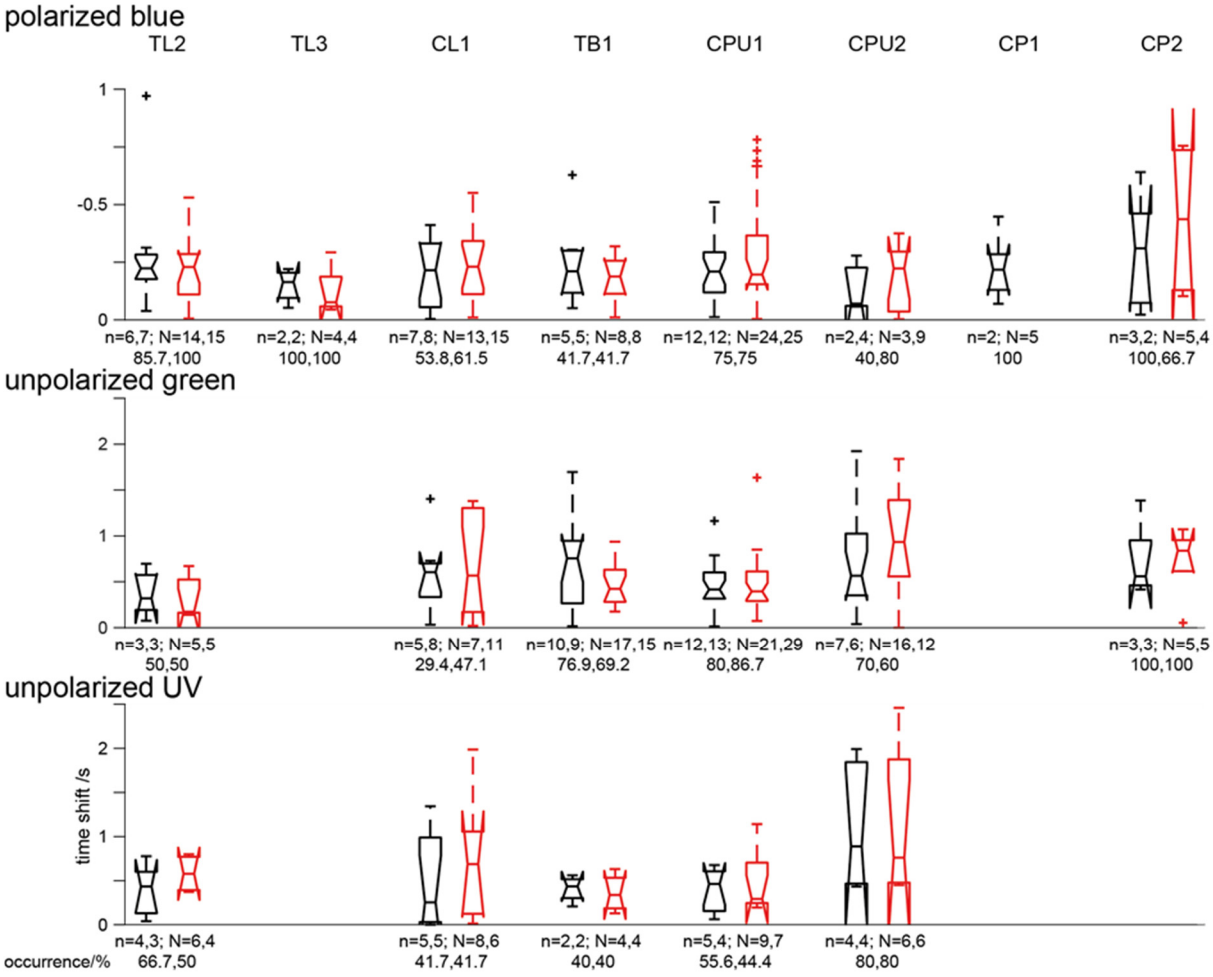

Fig. 7. Response advances in responses to clockwise and counterclockwise stimulation. Box plots showing phase advance shifts in Φ_{max} from individual responses to clockwise (black) and counterclockwise (red) rotations when compared to the pooled Φ_{max} of responses to all rotations. *n*, number of neurons. *N*, number of clockwise and counterclockwise rotations. Only cell types with N > 2 are included. In recordings with different numbers of clockwise and counterclockwise responses, redundant responses were excluded from analysis randomly.

In contrast, responses to the green light spot showed increasingly longer time shifts from the input toward the output processing stage. Especially in CPU2 neurons time shifts were more negative than in all other cell types. Also the overall time shifts of all cell types were commonly twice as long in green and UV responses than in E-vector tunings. In neurons showing a delayed Φmax in single rotations compared to the pooled Φmax, the delays were

generally shorter in E-vector and green light tunings than the advances of anticipating cells (Figs. S6; 7). In UV light spot tunings time delays were similar in absolute value to time advances of anticipating cells. The overall occurrence of advances and delays was similar in CL and TB neurons, but in TL2 and all neurons of the output stage, phase advances in Φmax dominated.

Angular distance between tunings to different stimuli

Although the solar position changes over the course of the day, there is a fixed relationship between sun position and sky polarization (Fig. 1). Important for navigational purposes, the *E*-vector in the zenith is always 90° distant (orthogonal) from the solar azimuth (Fig. 1A). To assess whether this is reflected in the tuning of CX neurons, we calculated the angular distance between the azimuth of green tuning and the azimuth of UV tuning, and between the orientation of polarization tuning and the azimuth of green/UV tuning. Distances between Φ_{max} green and Φ_{max} UV were clustered around 0° in CL1, TB, CPU1 and CPU2 neurons (Fig. 8A). In TL neurons the dispersion was higher, so that the Rayleigh test did not reveal any clustering. In certain cell types (CL1, CPU1) single distances were close to 180°. Comparison of *E*-vector and light-spot tuning showed that most TL neurons had a tuning distance close to 90° (Fig. 8B).

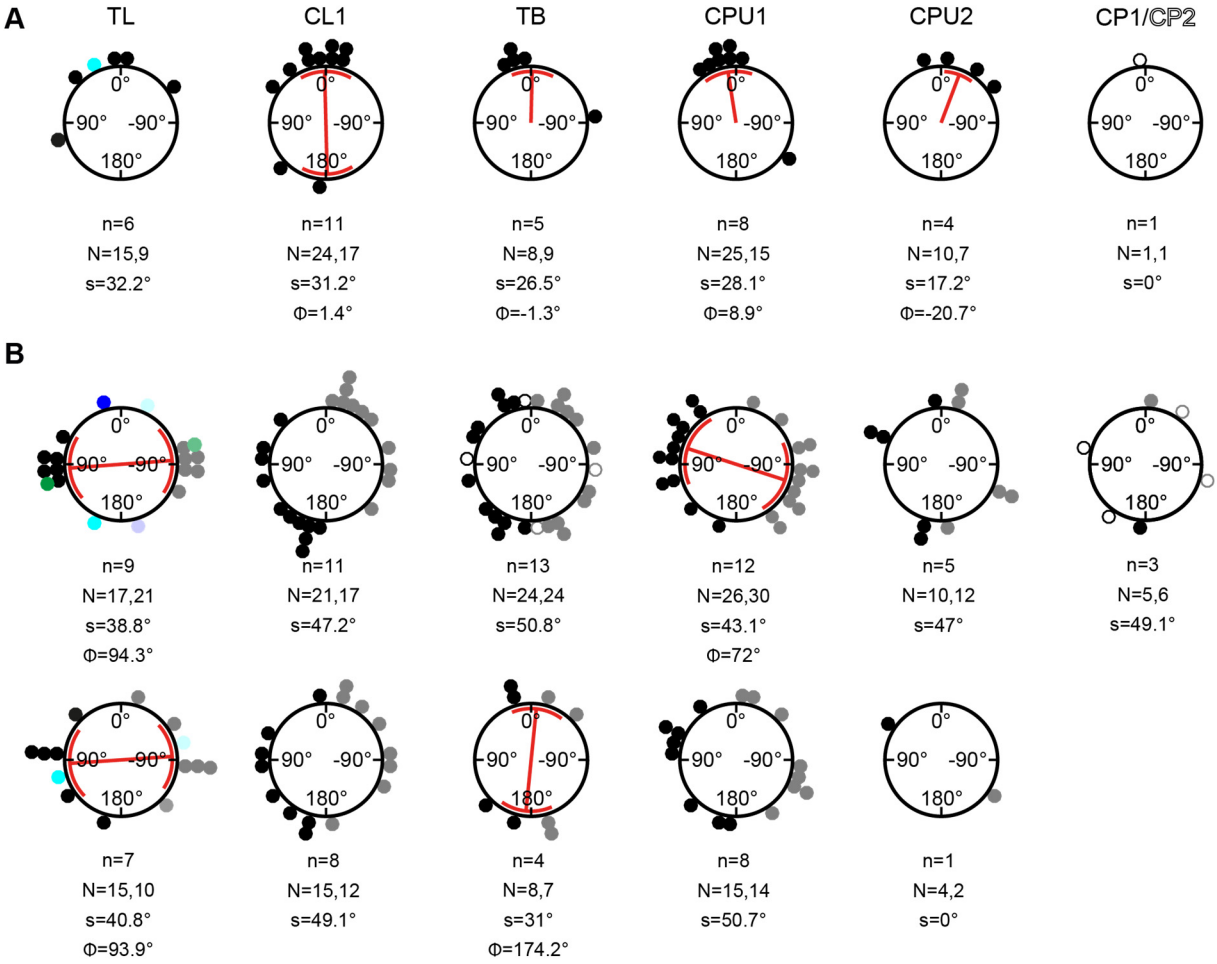

Fig. 8. Distance between tunings to polarized light, unpolarized green and UV light spots. (A) Relative distances between Φmax green and Φmax UV from n neurons. Pooled Φmax were calculated from N responses to clockwise stimulation and N responses to counterclockwise stimulation (green, UV). (B) Positive relative angular distances (filled black/coloured circles) and negative angular distances (filled grey/light coloured circles) between the Φmax of E-vector tuning and the Φmax of unpolarized green tuning (upper panel) and between the Φmax E-vector tuning and the Φmax of unpolarized UV tuning (lower panel) from n neurons. Pooled Φmax values were calculated from N responses to clockwise stimulation and N responses to counterclockwise

stimulation (polarized blue, unpolarized green / polarized blue, unpolarized UV). Values of CP2, TB2 and TB3 neurons are plotted in open circles, those of TL1 in blue, TL2 in black, TL3 in green, and TL4 neurons in cyan circles. The distribution of angular distances was statistically tested for uniformity using the Rayleigh test (Batschelet, 1981). In (B) angles were doubled in all cases and in (A) whenever the distribution appeared bidirectional. In the case of significance ($p<0.05$) the direction of the mean vector (Φ) is given and plotted (red line). s, circular standard deviation (red), plotted in significant cases only.

However, most of the TL neurons clustered around 90°, belonged to the TL2 or TL3 subtypes, whereas the TL1 and TL4 neurons showed different tuning distances of 17° (TL1) and 153° (TL4). In contrast, angular distances in CL1 neurons between *E*-vector and unpolarized light spot tuning ranged from 0° to 180°. In TB neurons the distribution of distances was non-directional when comparing *E*-vector tuning with green tuning, but directed toward 0° when comparing *E*-vector tuning with UV tuning. CPU2 and CP neurons showed non-directional distribution of angular distances. In CPU1 neurons distances were clustered around 70°, but only for comparison of *E*-vector tuning with green tuning. CPU2 and CP1/CP2 neurons showed no clustering of angular distances.

Discussion

Contribution of chromatic cues to the internal E-vector compass

We analyzed the responses of locust CX neurons to zenithal *E*-vectors and to unpolarized green and UV light spots moving on a circular path around the head of the animal. All types of CX neurons that were sensitive to zenithal *E*-vector orientation were also sensitive to the azimuth of the unpolarized light spots. Therefore, CX neurons are well suited to code for solar azimuth. Similar responses of CX neurons to a moving bright object have been demonstrated in flies (Seelig and Jayaraman, 2015; Kim et al., 2017), cockroaches (Varga and Ritzmann, 2016), monarch butterflies (Heinze and Reppert, 2011) and two species of dung beetle (el Jundi et al., 2015). In the locust tuning to unpolarized UV light was similar to tuning to green light across all cell types. Neurons of the AOTU, located upstream of CX neurons, showed color opponent tuning to green and UV (Pfeiffer and Homberg, 2007). Commissural neurons connecting the right and left AOTUs (types LoTu1 and TuTu1) were inhibited by UV light and excited by green light at the same azimuth and vice versa (Pfeiffer and Homberg, 2007). These neurons thus were assumed to encode for the chromatic differences in the solar and antisolar hemisphere of the sky. In all types of CX neurons, however, tuning to the green and UV light spots were highly similar. We therefore assume that these neurons, in addition to celestial *E*-vector orientation, code for the azimuth of bright light sources, possibly representing the sun, largely ignoring wavelength information. This consistent with wavelength independent azimuth coding in the CX of the monarch butterfly (Heinze and Reppert, 2011), and in a small subset of locust CX neurons (el Jundi et al., 2014a).

The tuning of TL2 and TL3 neurons showed a 90° distance between the Φ_{max} of the zenithal *E*-vector and Φ_{max} of the green light spot, reflecting the relationship between solar azimuth and zenithal *E*-vector in the sky (Fig. 1A). In all cell types downstream in the network this relationship occurred only in a minority of recorded cells. TL neurons integrate *E*-vector orientations across the entire sky in a matched-filter like manner for particular solar positions (Bech et al., 2014). Therefore, the 90° relationship of solar

azimuth and zenithal *E*-vector orientation strongly supports the animal's internal polarization compass at the input stage of the CX. Neurons of the AOTU were reported to show a daytime compensation in the angular distance between *E*-vector and light spot tuning (Pfeiffer and Homberg, 2007). In contrast tuning distances may be daytime independent in TL2 and TL3 neurons. TL1 and TL4 neurons showed striking deviations from a 90° tuning relation with tuning distances close to 0° and 180°, but their receptive field organizations are not known. For all other CX neurons of the polarization network receptive fields for *E*-vector orientations have, likewise not been analyzed in detail, so that it is still unknown whether the 'matched filter' properties of TL neurons are maintained in all neurons downstream in the network. Because of the mean distance between polarization and azimuth tuning of 70°, receptive fields of CPU1 neurons are likely to differ from those of TL neurons. In the monarch butterfly angular distances between the preferred *E*-vector and the preferred azimuth of a green spot were less than 45° in TL neurons (Heinze and Reppert, 2011), while in dung beetles they ranged from 0° to 90° across all recorded cell types (TL, CL1, TB1, CPU1) (el Jundi et al., 2015). In neither species have the receptive fields for polarized light been characterized in CX neurons yet.

Signal processing from input to output of the CX network

At least two parallel input pathways to the CBL exist in the fruit fly (Omoto et al., 2017), the honeybee (Held et al., 2016), and the locust (Homberg et al., 2003). In *Drosophila*, two types of AOTU neurons making connections to two distinct types of ring neurons (TL neurons) responded differently to a moving unpolarized light spot. Equivalent cell types in the locust may be the two subtypes of TULAL1 neurons, making synapses with TL2 neurons in the lateral bulb (TULAL1a) and with TL3 neurons in the lateral and medial bulb (TULAL1b) (Träger et al., 2008). In our experiments TL2 and TL3 showed remarkably different response amplitudes to polarized and unpolarized light, but the sample size for TL3 neurons was low, so that further experiments on TL3 neurons are necessary to substantiate this observation. In contrast to TL2 and TL3 neurons, the role of TL1 and TL4 neurons is unknown. Their dendritic arbors spread widely through the LAL and, thus, might receive input from a variety of neurons. Both recorded TL1 neurons were responsive to the orientation of the *E*-vector, but only one of them to the azimuth of the unpolarized light spots. The TL4 neuron was tuned to the zenithal *E*-vector and to the azimuth of the unpolarized green and UV light spots. Hence all subtypes of TL neurons studied here seem to be involved in sky compass coding, but may differ in the relative contribution and combination of different celestial signals.

In all cell types downstream of TL neurons the responses to the polarized and the unpolarized light stimuli were generally similar, indicating that polarization and azimuth information are processed together. Bockhorst and Homberg (2015) reported high variability in *E*-vector tuning at the output processing stage (CPU2 neurons) ranging from strong polarization opponency to unresponsiveness. In the present study, CPU2 neurons showed overall lowest responsiveness to *E*-vector orientation. Moreover, their tunings to all three stimuli were generally of low amplitude and showed weak correlation with little variability. A high incidence of unresponsiveness of CPU2 neurons to zenithal *E*-vectors (50%) was also observed by Heinze and Homberg (2009). They suggested that CPU2 neurons are recruited to the polarization processing network depending on the animal's

internal state (Heinze and Homberg, 2009). It is thus conceivable that in CPU2 neurons context information plays a major role, so that the moving visual scenery as presented to the animal by Bockhorst and Homberg (2015) may have resulted in a higher incidence of pronounced responses.

CX neurons usually show some variability in background spiking over the course of a recording (Bockhorst and Homberg, 2015). We thus analyzed spiking at Φ_{max} and Φ_{min} to different levels of background activity (BA). Polarization and spatial opponency occurred in all cell types except CL1 and CPU2 neurons. The exclusive inhibition of CL1 neurons by polarized light and the resultant lack of polarization opponency have already been shown (Bockhorst and Homberg, 2015). It is therefore likely that polarization and spatial opponency in the PB emerge from mutual inhibition of TB1 neurons with opposite *E*-vector (Bockhorst and Homberg, 2015) and green/UV light spot tuning. Polarization opponency was reported by Bockhorst and Homberg (2015) to be absent in CX neurons upstream of TB1 neurons, however they considered only CL1 and TL2 neurons. Here we show that *E*-vector tunings of another type of TL neuron (TL3) are polarization opponent. In contrast to TL3 neurons, TL2 neurons were exclusively inhibited by polarized light, but spatially opponent in their responses to green light. This raises the question of how polarization opponency in TL2 neurons and spatial opponency in TL3 neurons leads to exclusive inhibition of CL1 neurons under rigorous criteria. CL1 neurons likely receive input from six morphological types of TL neuron. At least four of them (TL1-4) are likely involved in shaping *E*-vector and azimuth tuning of CL1 neurons. TL2, TL3 and TL4 neurons are GABA-immunoreactive (Homberg et al., 1999) and, therefore, probably inhibit CL1 neurons. Although the TL2 neurons shown here were strongly inhibited by all stimuli at Φ_{min}, the total excitation of TL3 and possibly TL4 neurons might be dominant, resulting in an overall inhibition of the postsynaptic CL1 neurons.

Parallels to the mammalian brain

We compared responses of neurons with high and low BA. In all cell types low BA was accompanied by enhanced response amplitudes to all stimuli, as well as enhanced variability in response amplitude. Likewise, neuronal BA influences behavioral performance in human vision (Boly et al., 2007) and somatosensation (Hesselmann et al., 2008). Two models explaining the interaction of BA and stimulus-evoked activity are under discussion. BA may be superimposed on the evoked neuronal response as shown in the cat V1 cortex (Arieli et al., 1996; Azouz and Gray, 1999) and in human extrastriate areas (Becker et al., 2011). In contrast, a recent study indicates that ongoing activity in human cerebral cortex negatively correlates with evoked activity, such that evoked responses are of higher amplitude whenever pre-stimulus activity is low (He, 2013). Neurons of the locust CX polarization vision network seem to share the latter characteristics, suggesting that they integrate different stimuli in a non-linear way. As in the cat and human cortex this interaction between background and evoked firing might be interpreted as some kind of attention related to the internal neuronal state. In most neurons polarization and spatial opponency were enhanced at low BA. This suggests that background firing in the locust CX strongly interacts with navigational task-evoked responses.

All recorded cell types showed a shift in Φ_{max} of unpolarized light spot or *E*-vector tuning depending on the direction of stimulus rotation (clockwise or counterclockwise), as already demonstrated for polarized light (Bockhorst and Homberg, 2015; Träger and

Homberg, 2011). Cells either responded with phase advances to *E*-vector orientation and light spot azimuth, or their firing was phase delayed when comparing clockwise and counterclockwise stimulation. These phenomena appear similar to the anticipatory firing observed in rat head-direction cells of the anterodorsal thalamus (AND) and postsubiculum (PoS) (Taube and Muller, 1998). Cells of the AND anticipate future headings, but cells of the PoS are tuned to past headings. In the locust TL, CL, TB1, CPU1 and CPU2 neurons might encode both, future headings or past headings. The two phenomena occurred equally often in CL and TB1 neurons, but in all output neurons, phase advances were clearly more prominent. In rat head-direction cells anticipation is assumed to arise from motor efference copies and vestibular input (van der Meer et al., 2007). Because the locust was fixed during the experiments, anticipation in the CX might arise solely from stimulus history or the velocity of stimulus rotation. Rotation velocity might influence anticipation, because CPU2 neurons anticipated future *E*-vector orientations by more than 500 ms with a rotation velocity of 30°/s (Bockhorst and Homberg, 2015), but only about 250 ms at rotation velocities of 40°/s and 36°/s, as used here. Stimulus anticipation was also dependent on the type of stimulus. In most cell types anticipatory time shifts of the preferred azimuth of the green/UV spot (360° periodicity) were twice as long as those of the preferred *E*-vector orientation (180° periodicity). This dependence on stimulus periodicity also points to a mechanism based on stimulus history. Nonetheless, for elucidating the origin of anticipation in locust compass cells it will be essential to study anticipation in actively and passively moving animals, and to test various stimulus velocities.

Acknowledgements

We thank Joss von Hadeln for providing the drawings of the TB2 and TB3 neurons and Martina Kern for maintaining locust cultures.

Author contributions

K.P. and U.H. designed the experiments. U.P. performed experiments. U.P. analyzed the data. U.P., K.P. and U.H. interpreted the results, U.P. prepared figures and provided the first draft of the paper, U.P., K.P. and U.H. revised the paper.

Funding

This work was supported by the Deutsche Forschungsgemeinschaft (grant HO 950/23-1).

References

Arieli, A., Sterkin, A., Grinvald, A. and Aertsen, A. (1969). Dynamics of ongoing activity: explanation of the large variability in evoked cortical responses. *Science* **273**, 1868-1871.

Azouz, R. and Gray, C.M. (1999). Cellular mechanisms contributing to response variability of cortical neurons *in vivo*. *J. Neurosci.***19**, 2209-2223.

Batschelet, E. (1981). *Circular Statistics in Biology*. London, UK: Academic Press.

Bech, M., Homberg, U. and Pfeiffer, K. (2014). Receptive fields of locust brain neurons are matched to polarization patterns of the sky. *Curr. Biol*. **24**, 2124-2129.

Becker, R., Reinacher, M., Freyer, F., Villringer, A. and Ritter, P. (2011). How ongoing oscillations account for evoked fMRI variability. *J. Neurosci.* **31**, 11016-11027.

Berens, P. (2009). CircStat: A MATLAB toolbox for circular statistics. *J. Stat. Softw.* **31**, 1-21.

Bockhorst, T. and Homberg, U. (2015). Amplitude and dynamics of polarization-plane signaling in the central complex of the locust brain. *J. Neurophysiol*. **113**, 3291-3311.

Boly, M., Balteau, E., Schnakers, C., Degueldre, C., Moonen, G., Luxen, A., Philips, C., Peigneux, P., Maquet, P. and Laureys, S. (2007). Baseline brain activity fluctuations predict somatosensory perception in humans. *Proc. Natl. Acad. Sci. U S A* **104**, 12178-12192.

Brines, M.L. and Gould, J.L. (1979). Bees have rules. *Science* **206**, 571-573.

Cardona, A., Saalfeld, S., Preibisch, S., Schmid, B., Cheng, A., Pulokas, J., Tomancak, P. and Hartenstein, V. (2010). An integrated micro- and macroarchitectural analysis of the *Drosophila* brain by computer-assisted serial section electron microscopy. *PLoS Biol.* **8,** e1000502.

Clements, A.N. and May, T.E. (1974). Studies on locust neuromuscular physiology in relation to glutamic acid. *J. Exp. Biol.* **60**, 673–705.

Coemans, M.A., Vos, H.J.J. and Nuboer, J.F. (1994). The relation between celestial color gradients and the position of the sun, with regard to the sun compass. *Vision. Res.* **34**, 1461-1470.

Dacke, M., Nordström, P. and Scholtz, C.H. (2003). Twilight orientation to polarized light in the crepuscular dung beetle *Scarabaeus zambesianus*. *J. Exp. Biol.* **206**, 1535-1543.

el Jundi, B., Heinze, S., Lenschow, C., Kurylas, A., Rohlfing, T. and Homberg, U. (2010). The locust standard brain: a 3D standard of the central complex as a platform for neural network analysis. *Front. Syst. Neurosci.* **3**, 3-21.

el Jundi, B., Pfeiffer, K., Heinze S. and Homberg, U. (2014a). Integration of polarization and chromatic cues in the insect sky compass. *J. Comp. Physiol. A.* **200**, 575-589.

el Jundi, B., Pfeiffer, K. and Homberg, U. (2011). A distinct layer of the medulla integrates sky compass signals in the brain of an insect. *PLoS One.* **6**, e27855.

el Jundi, B., Smolka, J., Baird, E., Byrne, M.J. and Dacke, M. (2014b). Diurnal dung beetles use the intensity gradient and the polarization pattern of the sky for orientation. *J. Exp. Biol.* **217**, 2422-2429.

el Jundi, B., Warrant, E.J., Byrne, M.J., Kjaldy, L., Baird, E., Smolka, J. and Dacke, M. (2015). Neural coding underlying the cue preference for celestial orientation. *Proc. Natl. Acad. Sci. U S A* **112**, 11395-11400.

Frost, B.J. and Mouritsen, H. (2006). The neural mechanisms of long distance animal navigation. *Curr. Opin. Neurobiol.* **16**, 481-488.

Gould, J.L. (1998). Sensory bases of navigation. *Curr. Biol.* **8**, R731-R738.

He, B.J. (2013). Spontaneous and task-evoked brain activity negatively interact. *J. Neurosci.* **33**, 4672-4682.

Heinze, S. and Homberg, U. (2007). Maplike representation of celestial *E*-vector orientations in the brain of an insect. *Science* **315**, 995-997.

Heinze, S. and Homberg, U. (2008). Neuroarchitecture of the central complex of the desert locust: intrinsic and columnar neurons. *J. Comp. Neurol*. **511**, 454-478.

Heinze, S., Gotthardt, S. and Homberg, U. (2009). Transformation of polarized light information in the central complex of the locust. *J. Neurosci.* **29**, 11783-11793.

Heinze, S., and Homberg, U. (2009). Linking the input to the output: New sets of neurons complement the polarization network in the locust central complex. *J. Neurosci.* **29**, 4911-4921.

Heinze, S. and Reppert, S.M. (2011). Sun compass integration of skylight cues in migratory monarch butterflies. *Neuron* **69**, 345-358.

Held, M., Berz, A., Hensgen, R., Muenz, T.S., Scholl, C., Rössler, W., Homberg, U. and Pfeiffer K. (2016). Microglomerular synaptic complexes in the sky-compass network of the honeybee connect parallel pathways from the anterior optic tubercle to the central complex. *Front. Behav. Neurosci.* **10**, 186.

Hesselmann, G., Kell, C.A., Eger, E. and Kleinschmidt, A. (2008). Spontaneous local variations in ongoing neural activity bias perceptual decisions. *Proc. Natl. Acad. Sci. U S A* **105**, 10984-10989.

Homberg, U. and Müller, M. (2016). Ultrastructure of GABA- and tachykinin-immunoreactive neurons in the lower division of the central body of the dessert locust. *Front. Behav. Neurosci.* **10**, 230.

Homberg, U., Heinze, S., Pfeiffer, K., Kinoshita, M. and el Jundi, B. (2011). Central neural coding of sky polarization in insects. *Phil. Trans. R. Soc. B* **366**, 680-687.

Homberg, U., Vitzthum, H., Müller, M. and Binkle, U. (1999). Immunocytochemistry of GABA in the central complex of the locust *Schistocerca gregaria*: Identification of immunoreactive neurons and colocalization with neuropeptides. *J. Comp. Neurol.* **409**, 495-507.

Homberg, U., Hofer, S., Pfeiffer K. and Gebhardt, S. (2003). Organization and neural connections of the anterior optic tubercle in the brain of the locust, *Schistocerca gregaria*. *J. Comp. Neurol.* **462**, 415-430.

Kennedy, J.S. (1951). The migration of the desert locust (*Schistocerca gregaria* Forsk.). I. The behavior of swarms. II. A theory of long-range migrations. *Philos. Trans. R. Soc. B*. **235**, 163-290.

Kim, S.S., Rouault, H., Druckmann, S. and Jayaraman, V. (2017). Ring attractor dynamics in the *Drosophila* central brain. *Science* **356**, 849-853.

Kinoshita, M., Pfeiffer, K. and Homberg, U. (2007). Spectral properties of identified polarized-light sensitive interneurons in the brain of the desert locust *Schistocerca gregaria*. *J. Exp. Biol.* **210**, 1350-1361.

Labhart, T. and Meyer, E.P. (1999). Detectors for polarized skylight in insects: a survey of ommatidial specializations in the dorsal rim area of the compound eye. *Microsc. Res. Tech.* **47**, 368-379.

Müller, M., Homberg, U. and Kühn, A. (1997). Neuroarchitecture of the lower division of the central body in the brain of the locust (*Schistocerca gregaria*). *Cell Tissue Res*. **288**, 159-176.

Neuser, K., Triphan, T., Mronz, M., Poeck, B. and Strauss, R. (2008). Analysis of a spatial orientation memory in *Drosophila*. *Nature* **453**, 1244-1247.

Ofstad, T.A., Zuker, C.S. and Reiser, M.B. (2011). Visual place learning in *Drosophila melanogaster*. *Nature* **474**, 204-207.

Omoto, J.J., Keleş, M.F., Nguyen, B.C.M., Bolanos, C., Lovick, J.K., Frye, M.A. and Hartenstein, V. (2017). Visual input to the *Drosophila* central complex by developmentally and functionally distinct neuronal populations. *Curr. Biol.* 27, 1098-1110.

Peters, B.H., Römer, H. and Marquart, V. (1986). Spatial segregation of synaptic inputs in a locust auditory interneurone. *J. Comp. Neurol.* **254**, 34-50.

Pfeiffer, K. and Homberg, U. (2007). Coding of azimuthal directions via time-compensated combination of celestial compass cues. *Curr. Biol.* **17**, 960-965.

Pfeiffer, K., Kinoshita, M. and Homberg, U. (2005). Polarization-sensitive and light-sensitive neurons in two parallel pathways passing through the anterior

optic tubercle in the locust brain. *J. Neurophysiol.* **94**, 3903-3915.

Reppert, S.M., Zhu, H. and White, R.H. (2004). Polarized light helps monarch butterflies navigate. *Curr. Biol.* **14**, 155-158.

Rossel, S. (1993). Navigation by bees using polarized skylight. *Comp. Biochem. Physiol. A* **104**, 695-708.

Rossel, S., Wehner, R. and Lindauer, M. (1978). E-vector orientation in bees. *J. Comp. Physiol. A.* **125**, 1-12.

Sakura, M., Lambrinos, D. and Labhart, T. (2008). Polarized skylight navigation in insects: model and electrophysiology of e-vector coding by neurons in the central complex. *J. Neurophysiol.* **99**, 667-682.

Seelig, J.D. and Jayaraman, V. (2015). Neural dynamics for landmark orientation and angular path integration. *Nature* **521**, 168-191.

Stalleicken, J., Mukhida, M., Labhart, T., Wehner, R., Frost, B. and Mouritsen, H. (2005). Do monarch butterflies use polarized skylight for migratory orientation? *J. Exp. Biol.* **208**, 2399-2408.

Taube, J.S. and Muller, R.U. (1998). Comparisons of head direction cell activity in the postsubiculum and anterior thalamus of freely moving rats. *Hippocampus* **8**, 87-108.

Träger, U. and Homberg, U. (2011). Polarization-sensitive descending neurons in the locust: Connecting the brain to thoracic ganglia. *J. Neurosci.* **31**, 2338-2247.

Träger, U., Wagner, R., Bausenwein, B. and Homberg, U. (2008). A novel type of microglomerular synaptic complex in the polarization vision pathway of the locust brain. *J. Comp. Neurol.* **506**, 288-300.

Van der Meer, M.A., Knierim, J.J., Yoganarasimha, D., Wood, E.R. and van Rossum, M.C. (2007). Anticipation in the rodent head direction system can be explained by an interaction of head movements and vestibular firing properties. *J. Neurophysiol.* **98**, 1883-18897.

Varga, A.G. and Ritzmann, R.E. (2016). Cellular basis of head direction and contextual cues in the insect brain. *Curr. Biol.* **26**, 1816-1828.

von Frisch, K. (1949). Die Polarisation des Himmelslichtes als orientierender Faktor bei den Tänzen der Bienen. *Experientia* **5**, 142-148.

Wehner, R. (2001). Polarization vision – a uniform sensory capacity? *J. Exp. Biol.* **204**, 2589-2596.

Wehner, R. and Müller, M. (2006). The significance of direct sunlight and polarized skylight in the ant's celestial system of navigation. *Proc. Natl. Acad. Sci. U S A* **103**, 12575-12579.

Weir, P.T. and Dickinson, M.H. (2012). Flying *Drosophila* orient to sky polarization. *Curr. Biol.* **22**, 21-27.

Weir, P.T. and Dickinson, M.H. (2015). Functional divisions for visual processing in the central brain of flying *Drosophila*. *Proc. Natl. Acad. Sci. U S A* **112**, 5523-5532.

Wernet, M.F., Perry, M.W. and Desplan, C. (2015). The evolutionary diversity of insect retinal mosaics: common design principles and emerging molecular logic. *Trends Genet.* **31**, 316-328.

Zar, J.H. (1999). *Biostatistical Analysis* (4th ed.). Upper Saddle River, NJ: Prentice Hall.

Supplemental information

Table S1: Responsiveness of central-complex neurons to the plane of polarized blue light and the azimuth of an unpolarized green and UV light spot. n_{total}, total number of neurons; $n_{sig.}$, number of neurons with significant responses to all stimuli repetitions; $n_{n.s.}$, number of neurons that did not respond to any of the stimulus repetitions; N_{total}, total number of stimulus presentations; $N_{sig.}$, number of significant responses; $\%N_{sig.}$, percentage of significant responses.

	n_{total}	$n_{sig.}$	$n_{n.s.}$	N_{total}	$N_{sig.}$	$\%N_{sig.}$
polarized blue						
TL1	2	0	0	18	8	44
TL2	7	6	0	43	33	77
TL3	2	1	0	12	10	83
CL1	20	7	3	118	65	55
TB1	16	9	2	86	54	63
CPU1	19	4	2	130	84	65
CPU2	11	3	2	87	31	36
CP1	2	1	0	12	11	92
CP2	4	2	0	30	12	40
unpolarized green						
TL1	2	0	1	18	7	43
TL2	7	5	1	32	28	88
TL3	2	0	0	10	5	50
CL1	20	10	1	108	79	73
TB1	16	8	1	76	55	72
CPU1	19	10	2	113	79	70
CPU2	11	3	0	73	50	68
CP1	2	1	0	8	6	75
CP2	4	2	0	16	12	75
unpolarized UV						
TL1	2	0	1	8	1	12
TL2	7	5	1	24	18	75
TL3	2	0	0	8	3	38
CL1	18	10	2	60	44	73
TB1	10	5	3	36	20	56
CPU1	16	8	4	60	36	60
CPU2	8	4	0	26	20	77
CP1	2	0	0	6	2	33
CP2	4	0	0	14	6	43

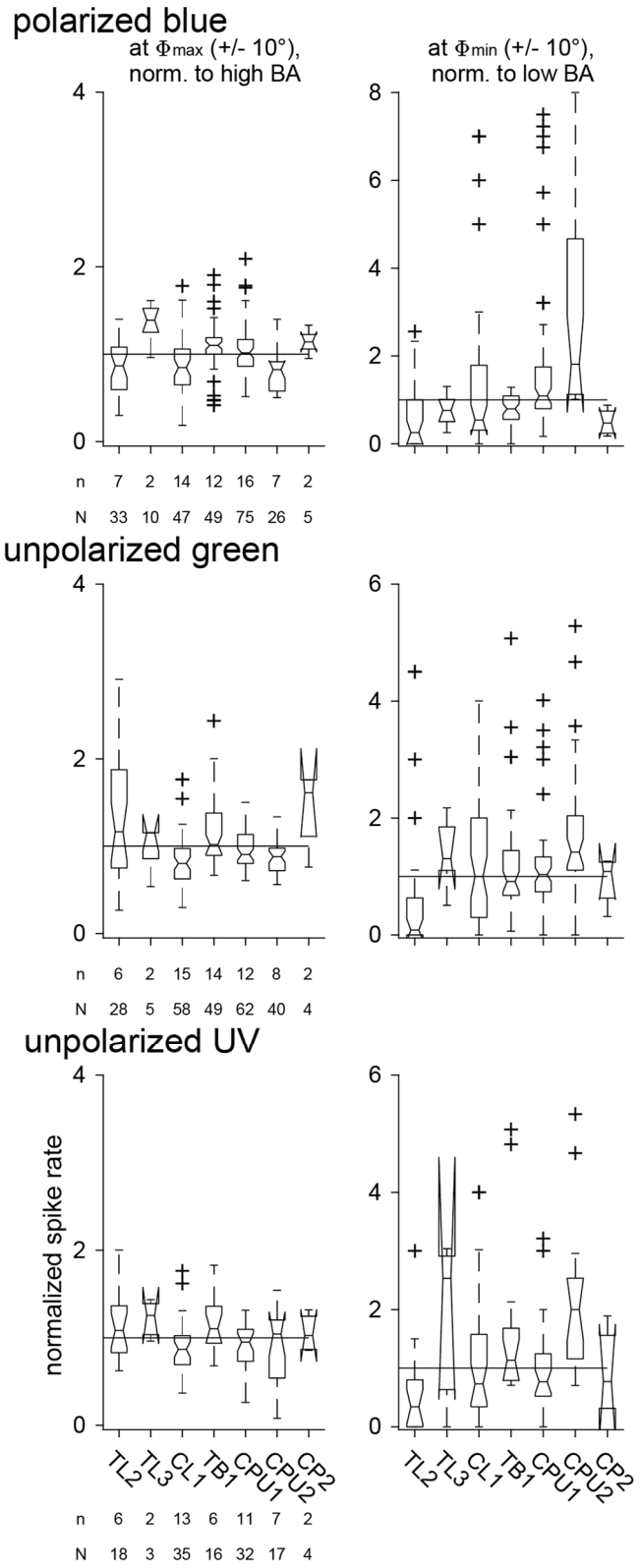

Fig. S2. Effective amplitudes of tunings to the plane of polarized blue light and the azimuth of an unpolarized green and UV light spot. Mean spiking activities at Φ_{max} +/- 10° and Φ_{min} +/- 10° are plotted from *N* responses of *n* neurons to polarized blue light, unpolarized green light, and unpolarized UV light. Spike rates are normalized to very high BA (the 97.5th percentile) or very low BA (the 2.5th percentile), respectively. Solid lines mark a value of 1. The upper limit of confidence interval exceeding unity in the left panels indicates excitation at Φ_{max}, the whole confidence interval exceeding unity indicates robust excitation at Φ_{max}. The lower limit of confidence interval undershooting unity in the right panels indicates inhibition at Φ_{min}, the whole confidence interval undershooting unity indicates robust inhibition at Φ_{min}.

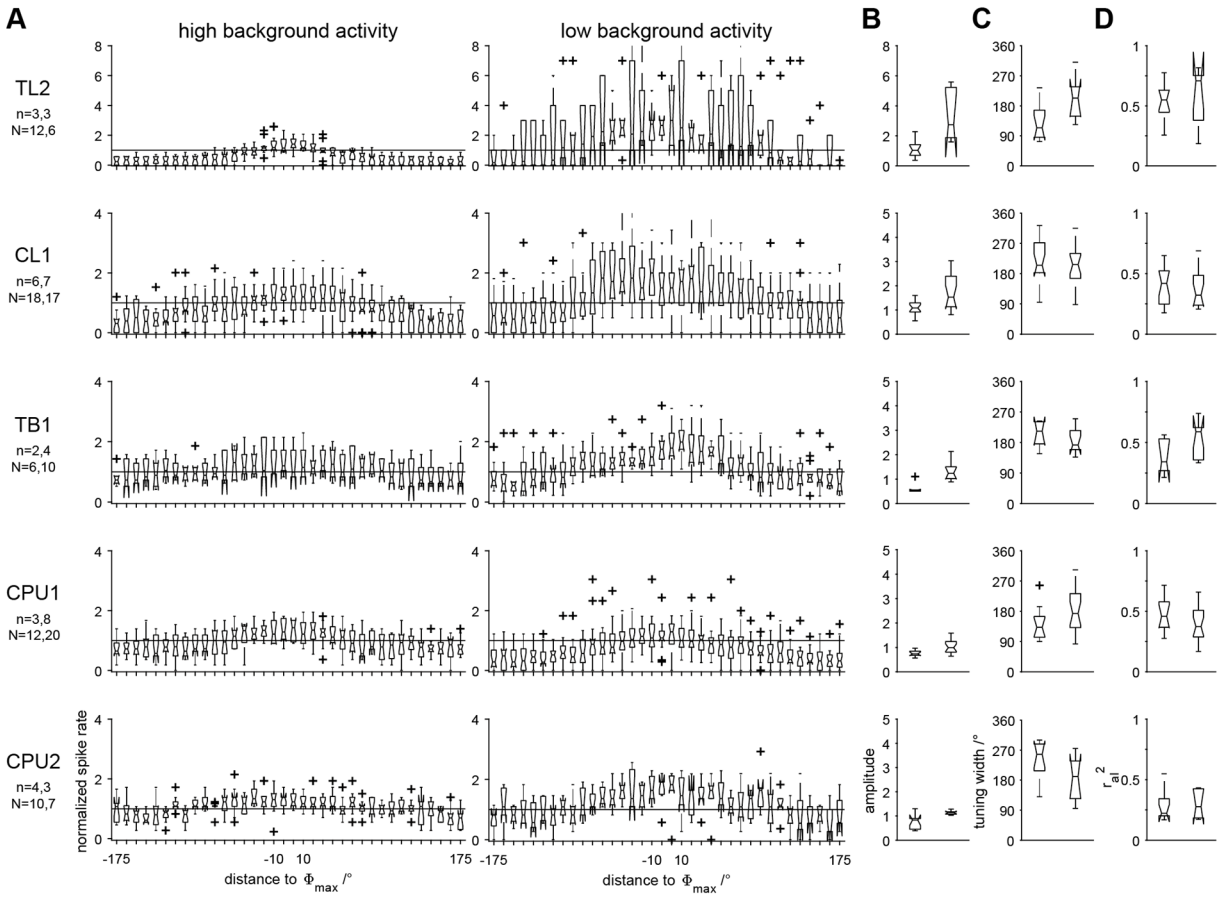

Fig. S3. Comparison of tuning characteristics to unpolarized UV light during high and low background activity. (A) Normalized stimulus response curves of N responses and n neurons to unpolarized UV light during high and low neuronal background activity. Spike angles (i.e. were shifted to Φmax and binned in 10° wide bins. Stimulus response curves were normalized to the median neuronal BA (solid line at value 1). (B-D) Box plots showing amplitude, width and ral2 of each response in (A) for each cell type during high and low BA.

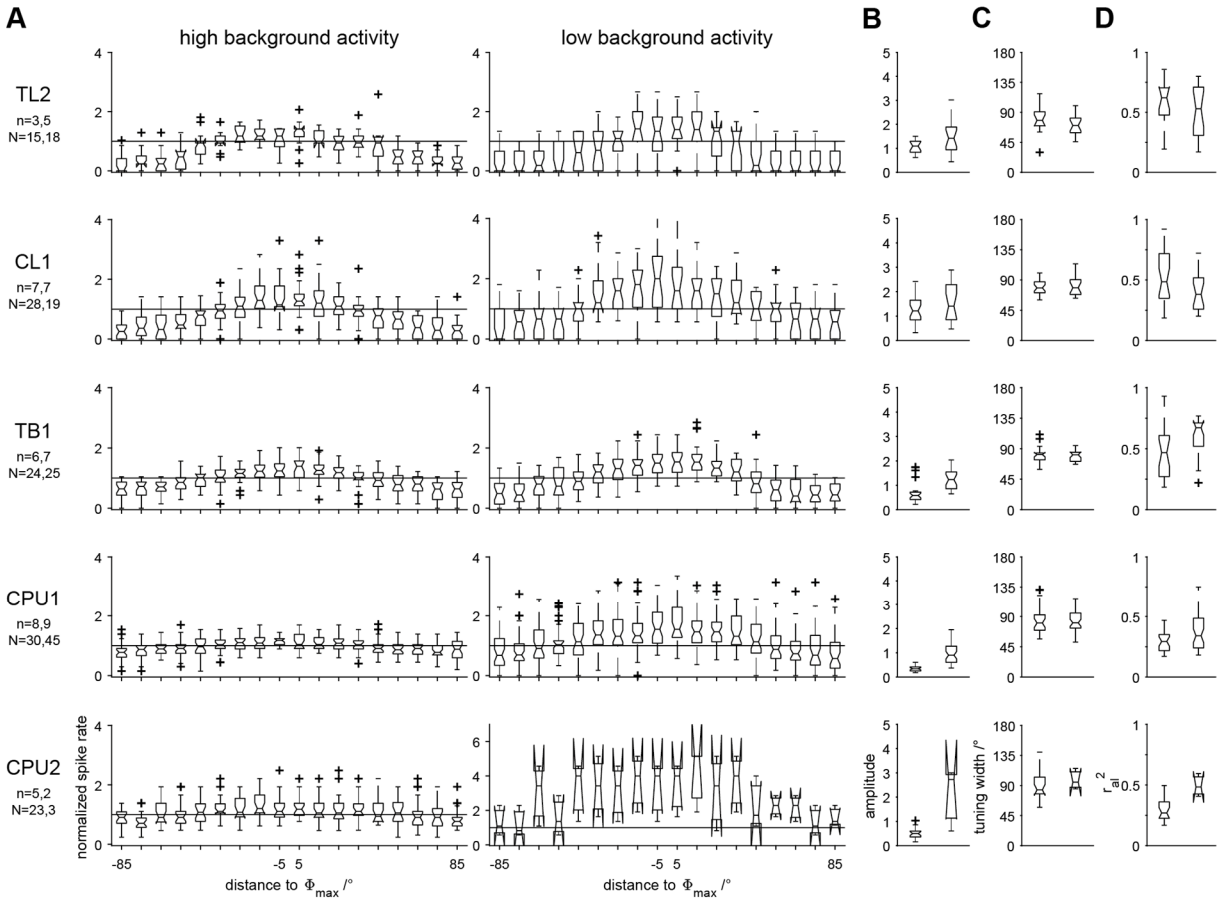

Fig. S4. Comparison of tuning characteristics to polarized light during high and low background activity. (A) Normalized stimulus response curves of N responses and n neurons to polarized blue light during high and low neuronal background activity. Spike angles were shifted to Φmax and binned in 10° wide bins. Stimulus response curves were normalized to the median neuronal BA (solid line at value 1). (B-D) Box plots showing amplitude, width and ral2 of each response in (A) for each cell type during high and low BA. Note that in (D) ral² of responses during high BA decreases from TL toward CPU2 neurons.

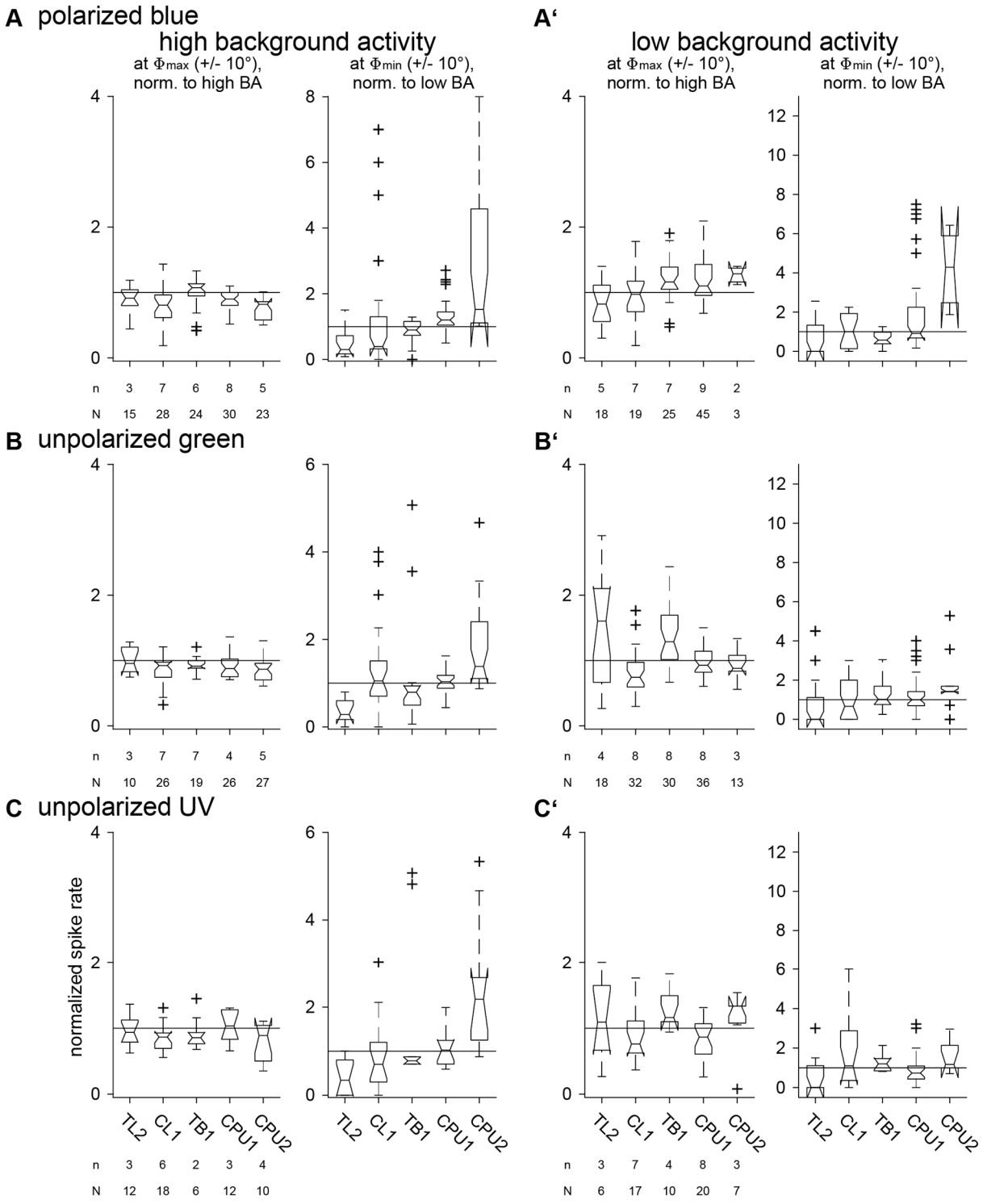

Fig. S5. Comparison of effective amplitudes of responses to three different stimulation regimes in neurons with high and low background activity. Mean spiking activities at Φmax +/- 10° and Φmin +/- 10° are plotted from N responses of n neurons to polarized blue light (A,A'), unpolarized green light (B,B'), and unpolarized UV light (C,C') during high and low BA. Spike rates were normalized to very high BA (i.e. the 97.5th percentile of BA), or very low BA (i.e. the 2.5th percentile of BA), respectively. Solid line marks a value of 1.

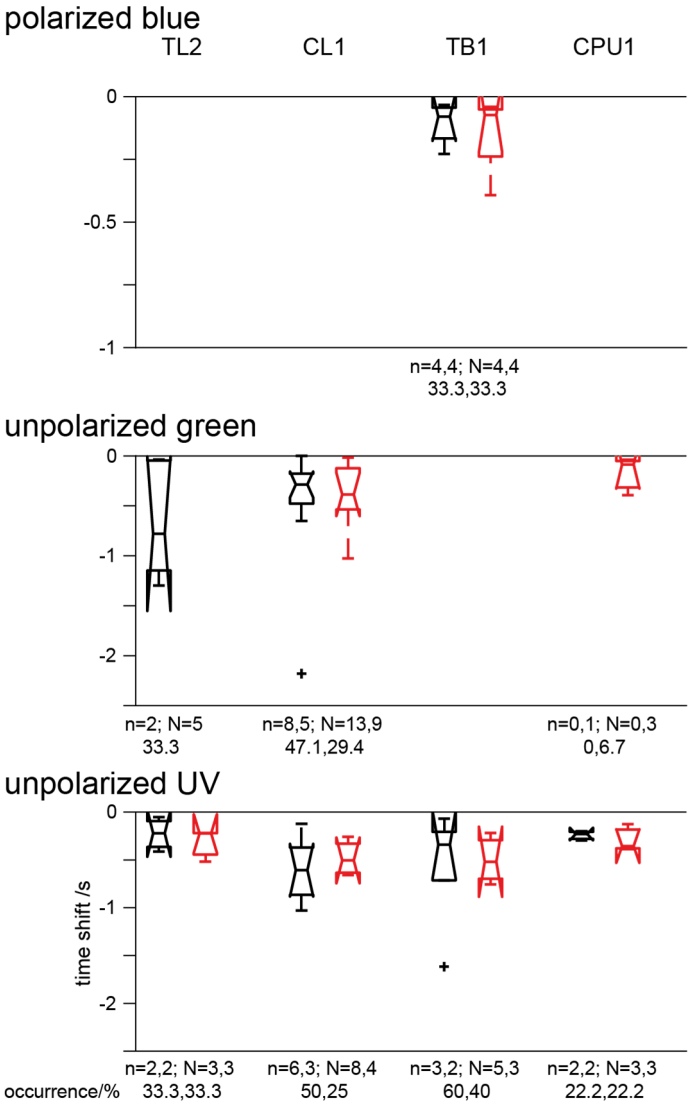

Fig. S6. Response delays in responses to clockwise and counterclockwise stimulation. Boxplots showing delays in Φ_{max} of individual responses to clockwise (black) and counterclockwise (red) rotations when compared to the pooled Φ_{max} of responses to all rotatons. *n*, number of neurons, *N*, number of clockwise and counterclockwise rotations. Only cell types with N>2 are included. In recordings with different numbers of clockwise and counterclockwise responses, redundant responses were randomly excluded from analysis.

Chapter 2

Two compasses in the central complex of the locust brain

Two compasses in the central complex of the locust brain

Uta Pegel, Keram Pfeiffer, Christine Scholtyssek, Uwe Homberg

Many migratory insects rely on a celestial compass for spatial orientation. Several features of the sky, all generated by the sun, can be exploited for navigation. Two of these are the position of the sun, specified by azimuth and elevation, and the pattern of polarized skylight. Neurons of the central complex (CX), a group of neuropils in the central brain of insects, have been shown to encode sky compass cues. In desert locusts the CX holds a topographic, compass-like representation of the plane of polarized light (*E*-vector), presented from dorsal direction. In addition, these neurons also encode the azimuth of an unpolarized light spot, likely representing the sun. Here we investigate whether, in addition to *E*-vector orientation, the solar azimuth is represented topographically in the CX. We recorded intracellularly from 8 types of CX neuron, while stimulating the animal with polarized blue light from zenithal direction and an unpolarized green light spot, rotating around the animal's head at different elevations. CX neurons did not code for elevation of the unpolarized light spot. However, all types of columnar neuron showed a linear correlation between innervated slice in the CX and azimuth tuning to the unpolarized green light spot, consistent with an internal compass representation of solar azimuth. Columnar outputs of the CX also showed a topographic representation of zenithal *E*-vector orientation but both compasses were not linked to each other. Combined stimulation with unpolarized green and polarized blue light suggest that the two compass interact in a non-linear way.

Significance statement

In the brain of the desert locust, neurons sensitive to the plane of celestial polarization are arranged like a compass in the slices of the central complex. These neurons, in addition, code for the horizontal direction of an unpolarized light cue possibly representing the sun. We show here that horizontal directions are, in addition to *E*-vector orientations from dorsal direction, represented in a compass-like manner across the slices of the central complex. However, both compasses are not linked to each other but seem to interact in a cell specific non-linear way. Our study confirms the role of the central complex in signaling heading directions signaling and shows that different cues are employed for this task.

Introduction

Many animals rely on visual cues for navigation. Some of them, including certain insects, exploit global compass cues of the sky to extract heading information and maintain directions during walking and flight (Wehner, 1984; Merlin et al., 2012; Homberg, 2015). Sky compass cues are highly reliable due to their persistent presence during locomotion (Gould, 1998; Frost and Mouritsen, 2006). Besides direct sunlight, the polarization pattern and the chromatic gradient across the sky, both generated by scattering of sunlight in the atmosphere, provide reference to the position of the sun. In addition to sky compass cues, insects also rely on landmarks and perhaps even map-like mechanisms of orientation, especially in familiar terrain (Collett, 1992; Menzel et al., 2005; Zars, 2009; Wystrach and Graham, 2012). Large landscape features, like coastlines or mountain ranges may also serve as guiding cues for long distance migrators (Reppert et al., 2016).

Several insect species show orientation behavior dependent on sky compass cues or, under laboratory settings, signals that mimic zenithal sky polarization or solar position. These include honey bees (Brines and Gould, 1997; von Frisch, 1949), desert ants (Wehner and Müller, 2006), dung beetles (Dacke et al., 2003; el Jundi et al., 2014b), fruit flies (Weir and Dickinson, 2012), field crickets (Brunner and Labhart, 1987), and locusts (Mappes and Homberg, 2004). All of these species possess specialized photoreceptors, working as *E*-vector analyzers, located in the dorsal rim areas of their compound eyes (Labhart and Meyer, 1999; Schmeling et al., 2014).

Visual pathways from the dorsal rim areas of both compound eyes converge on the central complex (CX), a group of midline-spanning neuropils in the brain (Homberg et al., 2011; Heinze, 2014). The CX consists of the upper and lower division of the central body (CBU, CBL), the paired noduli (NO) and the protocerebral bridge (PB; Fig. 1*A*). In the desert locust, the CBU, CBL and PB are structured in rows of 16 vertical slices. Many CX neurons arborize in adjacent bilateral structures, the lateral accessory lobes, and the medial and lateral bulbs. Several types of CX neuron are involved in the processing of polarized light. These include tangential neurons of the CBL (TL2) serving as input-neurons to the CX and contacting columnar neurons of the CBL (CL1; Fig. 1*A*). CL1 neurons arborize in distinct slices of the PB, where they might contact tangential neurons (TB1; Fig. 1*B*). Columnar neurons, termed CPU1, CPU2, CP1 and CP2 have smooth arborizations in the PB and are regarded as output neurons of the network (Fig. 1*B*,*C*). The CX is involved in the control of navigational tasks (Ofstad et al., 2011; Varga et al., 2017). In locusts and fruit flies the CX holds an internal representation of head orientation relative to a visual reference. Whereas in fruit flies head orientation relative to bright landmarks is represented in the ellipsoid body (corresponding to the CBL in other species; Seelig and Jayaraman, 2013) and the PB (Green et al., 2017), a topographic representation of zenithal *E*-vectors is present in the PB of the locust (Heinze and Homberg, 2007). In dung beetles and monarch butterflies CX neurons code for the orientation of zenithal polarized light as well as for the azimuth of an unpolarized green light spot, likely representing the sun (el Jundi et al., 2015; Heinze and Reppert, 2011). Similar responses to polarized and unpolarized stimuli were also demonstrated in CX neurons of the locust (el Jundi et al., 2014a; Pegel et al., 2018). This raises the question, whether the azimuth of the sun, like the *E*-vector angle, is represented in a topographic fashion in the slices of the locust CX and which neuron types

are involved in this representation. We show here by using intracellular recordings in the locust CX that several types of columnar neuron of the PB represent not only celestial *E*-vectors, but also azimuth angles of unpolarized light cues in a compass-like manner.

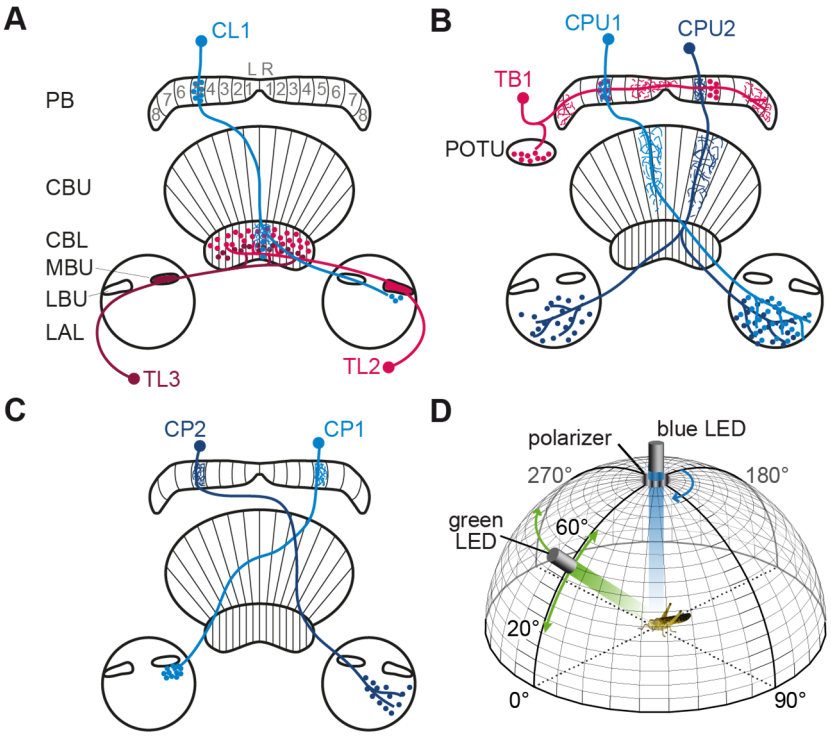

Figure 1. Neuronal cell types and visual stimulation. ***A-C,*** Schematic illustration of tangential (red) and columnar (blue) neurons of the sky compass network in the locust central complex. Vertical lines mark the edges of slices occupied by arborizations of columnar neurons. Slices are termed R1-8 (right hemisphere) and L1-8 (left hemisphere). Fine processes illustrate likely dendritic input regions of the neuron, dots represent varicose arborizations und thus likely presynaptic output regions. The filled lateral and medial bulb (LBU, MBU) in ***A*** indicate input synapses arranged in microglomerular complexes. Neuropil abbreviations: CBL, central body lower division; CBU, central body upper division; LAL, lateral accessory lobe; LBU, lateral bulb; MBU, medial bulb; POTU, posterior optic tubercle. Abbreviations of neuron types: CL1, columnar neuron of the CBL type 1; CP1, columnar neuron of the PB type 1; CP2, columnar neuron of the PB type 2; CPU1, columnar neuron of the CBU and the PB type 1; CPU2, columnar neuron of the CBU and PB type 2; TB1, tangential neuron of the PB type 1; TL2, tangential neuron of the CBL type 2; TL3, tangential neuron of the CBL type 3. ***D,*** Schematic illustration of visual stimulation. The light of a blue LED, positioned in the zenith, was passed through a rotating polarizer. A green LED appeared to the animal as an unpolarized light spot. It rotated around the animal's head (green horizontal arrow) at elevations ranging from 20° to 60° (green vertical arrow).

Materials and methods

Animals and preparation

Desert locusts (*Schistocerca gregaria*) were reared under crowded conditions in a 12:12 h light:dark cycle. Only sexually mature animals, at least one week after final moult, were used for experiments. Animals were mounted onto a metal holder using dental wax, with their anterior-posterior body axis oriented vertically (Pfeiffer et al., 2005). Wings and legs were cut off. The head capsule was opened from anterior and fat tissue, tracheal air sacs, and gut were removed in order to reduce body movements. Mouthparts, leg stumps, and abdomen were immobilized by wax. Muscles close to the brain were cut for further stabilization. A small twisted metal wire was used to support the brain from posterior. The neural sheath covering the central brain was removed to allow access for the electrode. During preparation and intracellular recording the brain was immersed in locust saline (Clements and May, 1974) containing 0.09 mol l^{-1} saccharose.

Electrophysiology and visual stimulation

Sharp glass microelectrodes were drawn from borosilicate capillaries (Hilgenberg) using a Flaming/Brown horizontal puller (P-97, Sutter Instrument). Electrode tips were filled with 4% Neurobiotin (Vector Laboratories) diluted in 1 mol l^{-1} KCl. Electrode shanks were filled with 1 mol l^{-1} KCl. Neuronal signals were amplified 10× by a custom-built amplifier (University of Regensburg), visualized by an oscilloscope (DS 1052Eh, Rigol Technologies), digitized by an analog-to-digital converter (CED1401 plus, Cambridge Electronic Design) at a rate of 20 kHz, and stored on a PC using the software Spike2 (Version 6.02, Cambridge Electronic Design). Neuronal responses to polarized and unpolarized light stimuli were studied (Fig. 1*D*). Polarized light was generated by passing light of a blue LED (Oslon SSL 80, LDCQ7P, 452 nm, Osram Opto Semiconductors, or LXML-PR01-0500, 447.5 nm, Philips Lumileds Lighting Company) through a polarizer (HNP'B, Polaroid). Both were positioned in the zenith to stimulate the dorsal part of the eye. The polarized light stimulus covered a visual angle of 32.5° or 18.6° and had an intensity of 1.7×10^{13} photons cm^{-2} s^{-1}. The polarizer was rotated at angular velocities of 40°/s or 36°/s. The unpolarized light spot was generated by light from a green LED (LED535-series, 535 nm, Roithner Lasertechnik, or Oslon SSL 80, LT CP7P, 528 nm, Osram Opto Semiconductors) passing through a diffusor. The unpolarized light stimulus appeared at a visual angle of 16.3° and had an intensity of 10^{14} photons cm^{-2} s^{-1}. It was moved around the animal's head at an elevation of 45° and an angular velocity of 40°/s or 36°/s. In experiments testing for elevation-dependent coding the elevation of the light spot could be changed to 20°, 30°, 40°, 50° and 60° (Fig. 1*D*). At the end of the recording Neurobiotin was injected into the neuron by applying a positive constant current of approximately 1 nA for 1-4 min.

Histology and image processing

Brains were dissected in locust saline, immersed over night at 4°C in fixative containing 4% paraformaldehyde (PFA), 0.25% glutaraldehyde and 0.2% saturated picric acid diluted in 0.1 mol l^{-1} phosphate buffered saline (PBS). Brains were stored for up to 2 weeks at 4°C in sodium phosphate buffer. Subsequently they were incubated in PBS with 0.3% Triton X-100 and Cy3 conjugated streptavidin (1:1000) for three days, dehydrated in an ascending ethanol series (30%, 50%, 70%, 90%, 95%, 100%) with 15 min steps, and cleared in a 1:1 mixture of 100% ethanol and methyl salicylate for 20

min, followed by 1 h in 100% methyl salicylate. Finally, brains were embedded in Permount (Fisher Scientific) between two cover slips. For synapsin immunostaining brains were rehydrated in a decreasing ethanol series (100%, 95%, 90%, 70%, 50%, 30%) with 15 min steps, embedded in albumin/gelatin, fixed overnight in 8% formaldehyde (FA) at 4°C, and sectioned in 130 µm slices using a vibrating-blade microtome (VT 1000S, Leica). Sections were preincubated overnight in PBS with 5% Triton X-100 and 5% normal goat serum (NGS) and then incubated for 5 days at 4°C in PBS with 5% Triton X-100, 1% NGS and anti-synapsin antibody (1:50). The monoclonal anti-synapsin antibody was generated in mouse against fusion proteins consisting of glutathione-S-transferase and the *Drosophila* Syn1 protein (Klagges et al., 1996). It was kindly provided by Drs. Erich Buchner and Christian Wegener (University of Würzburg). The antibody labels synapse-rich neuropils in various insect species (Brandt et al., 2005; Kurylas et al., 2008; Held et al., 2016). Following incubation in anti-synapsin sections were incubated in PBS with 5% Triton X-100, 1% NGS and the secondary antibody (goat anti-mouse) conjugated with Cy5 (1:300) for three days at 4°C. The sections were finally dehydrated in an increasing ethanol series (as described above), cleared in methyl salicylate (as described above) and mounted in Permount between two cover slips. For more detailed description of the protocol see Heinze and Homberg (2008). Preparations were scanned with a confocal laser scanning microscope (Leica) using a DPSS laser (561 nm) for detection of Cy3 and a He-Ne laser (633 nm) for detection of Cy5. Scans were visualized in AMIRA (version 5.4.5, FEI Visualization Sciences Group). Images were processed in Adobe Illustrator CC (version 2017.1.0, Adobe Systems).

Pre-processing of physiological data

Recording traces were visualized using Spike2. Action potentials were detected as events with a threshold based mechanism. The data were exported to a mat-file. All subsequent analysis was performed using custom functions written in MATLAB (Version 2017a, The MathWorks).

Experimental design and statistical analysis

For each stimulus presentation a stimulus response curve was obtained by calculating the mean spiking activity in 10° bins. To assess the response of a neuron to a stimulus condition the stimulus response curves of all presentations were averaged. At least one clockwise and one counterclockwise rotation of the polarizer / unpolarized light spot were averaged. Responses to clockwise and counterclockwise tests were always pooled in equal numbers to avoid a shift in the preferred calculated angle due to rotation direction. A directed modulation of spike rate by the orientation of the *E*-vector or the azimuth of the unpolarized light spot was determined by an angular-linear correlation analysis (Zar, 1999). The responsiveness of the neuron to a stimulus was indicated by the significance (α=0.05) of the correlation coefficient (r_{al}). The coefficient of determination (r_{al}^2) describes the strength of correlation between *E*-vector orientation or light spot azimuth and the spike rate (for detailed description see Pegel et al., 2018). To calculate the preferred *E*-vector or azimuth (Φ_{max}) spike times were transformed into angles by multiplying them with the stimulus rotation velocity. From these angles the mean vector Φ was calculated (Batschelet, 1981) and defined as the preferred angle (Φ_{max}). The anti-preferred angle (Φ_{min}) was defined as the angle 180° to Φ_{max} (azimuth tuning) or 90° to Φ_{max} (*E*-vector tuning). For all analyses of axial data (*E*-vector stimulation) the angles were doubled (Batschelet, 1981). Background activity was

determined by selecting parts of the recording without any stimulation and dividing them into 1-s bins. In each bin the spikes were counted. Spike counts were used to calculate the median background activity. The correlation between the location of arborization in the PB and Φ_{max} was assessed by a circular-linear correlation analysis as described by Kempter et al. (2012), which gave a correlation coefficient (ρ) and a regression line. Here the slice of PB arborization was used as the linear variable (values ranging from 0 to 15) and Φ_{max} as the circular variable.

For figures 5 and 6 stimulus response curves were smoothed. The stimulus response curve was normalized to the median background activity of the neuron. A smoothing spline was fitted onto the curve using the MATLAB curve fitting toolbox (smoothing parameter set to 10^{-4}, 360 array elements). For experiments with different light spot elevations additional characteristics of the stimulus response curve were calculated using the smoothed stimulus response curve: the tuning amplitude and the tuning width. The amplitude was determined by calculating the difference in normalized spike rate between the peak and the trough of the fit curve. The tuning width was defined as the angular difference between two points on the fit curve at half amplitude.

For experiments with combined stimulation (Fig. 5) a hypothetical response to combined stimulation was calculated following the equation $f(x) = POL \cdot x1 + green \cdot x2$, where *POL* is the stimulus response curve of tuning to the *E*-vector, *green* the stimulus response curve of tuning to the green light spot, and $x1$ and $x2$ their respective weighting factors. We used the smoothed stimulus response curves of *E*-vector, azimuth and combined stimulation tuning to calculate the weighting factors $x1$ and $x2$ following the equations

$$x1 = \frac{combM - green \cdot x2}{POL}$$

$$\text{and } x2 = \frac{combM - POL \cdot x1}{green},$$

where *combM* is the measured stimulus response curve of tuning to the combined stimulation. The equation describing $x2$ was inserted into that for $x1$ in order to reduce the number of unknown variables to one. The difference between the resulting estimation of the response to combined stimulation and the measured response to combined stimulation was minimized using the MATLAB built-in function fminbnd with $x1$ in the interval $-10 < x1 < +10$.

Results

Most data analyzed here are from recordings presented previously (Pegel et al., 2018). In that study we analyzed basic response features of the neurons, including their tuning to the plane of polarized light, unpolarized green and UV light spots, response amplitudes, tuning widths, and tuning differences when comparing clockwise and counterclockwise rotations of the stimuli. Here we asked whether morphological characteristics of the neurons such as the innervated layer in the CBL and columnar domains in the PB, CBU and CBL correspond to tuning properties of the neurons.

Tuning properties of TL neurons innervating different layers of the CBL

Six types of tangential neuron termed TL1-TL6 have been distinguished in the CBL of the locust (Müller et al., 1997; Bockhorst and Homberg, 2015a). Of these, TL2 and TL3 neurons were analyzed here. They receive input via microglomerular complexes in the lateral and medial bulb, respectively (Träger et al., 2008). In the CBL they invade specific

layers. TL2 neurons arborize in layer 2 or 3, and TL3 in layers 4 and 5 or in layers 2 and 6 (Müller et al., 1997). The functional significance of layering in the CBL is not known. We recorded from eight TL2 and three TL3 neurons. Five TL2 neurons invaded layer 2 of the CBL and are termed here TL2a (Fig. 2*A*). Two TL2 neurons invaded layer 3 and are termed here TL2b (Fig. 2*A*). The three TL3 neurons arborized in layers 4 and 5 (Müller et al., 1997). Corresponding to the innervated layers in the CBL, TL2a, TL2b and TL3 neurons also differed in their innervation of the bulb (Fig. 2*B*). Whereas TL2a neurons innervated microglomeruli in dorsal parts of the lateral bulb, TL2b neurons innervated microglomeruli of more ventral parts. Microglomerular arborizations of TL3 neurons were located in the medial bulb, but one neuron additionally invaded a few microglomeruli at the most medio-dorsal tip of the lateral bulb (Fig. 2*B*). All TL2 neurons responded with excitation at Φ_{max} and inhibition at Φ_{min}. TL3 neurons were generally tuned only weakly to the azimuth of the green spot and either showed exclusively excitation at Φ_{max} (Fig. 2*C*), inhibition at Φ_{min}, or both. In all TL2a neurons the preferred azimuth of the green light spot was on the contralateral side (Fig. 2*C*,*D*). In contrast, in the two TL2b neurons, the preferred azimuth was on the ipsilateral side (Fig. 2*C*,*D*). The three TL3 neurons showed mixed responses, with Φ_{max} on the ipsilateral side in two neurons, and on the contralateral side in the third neuron (Fig. 2*C*,*D*).

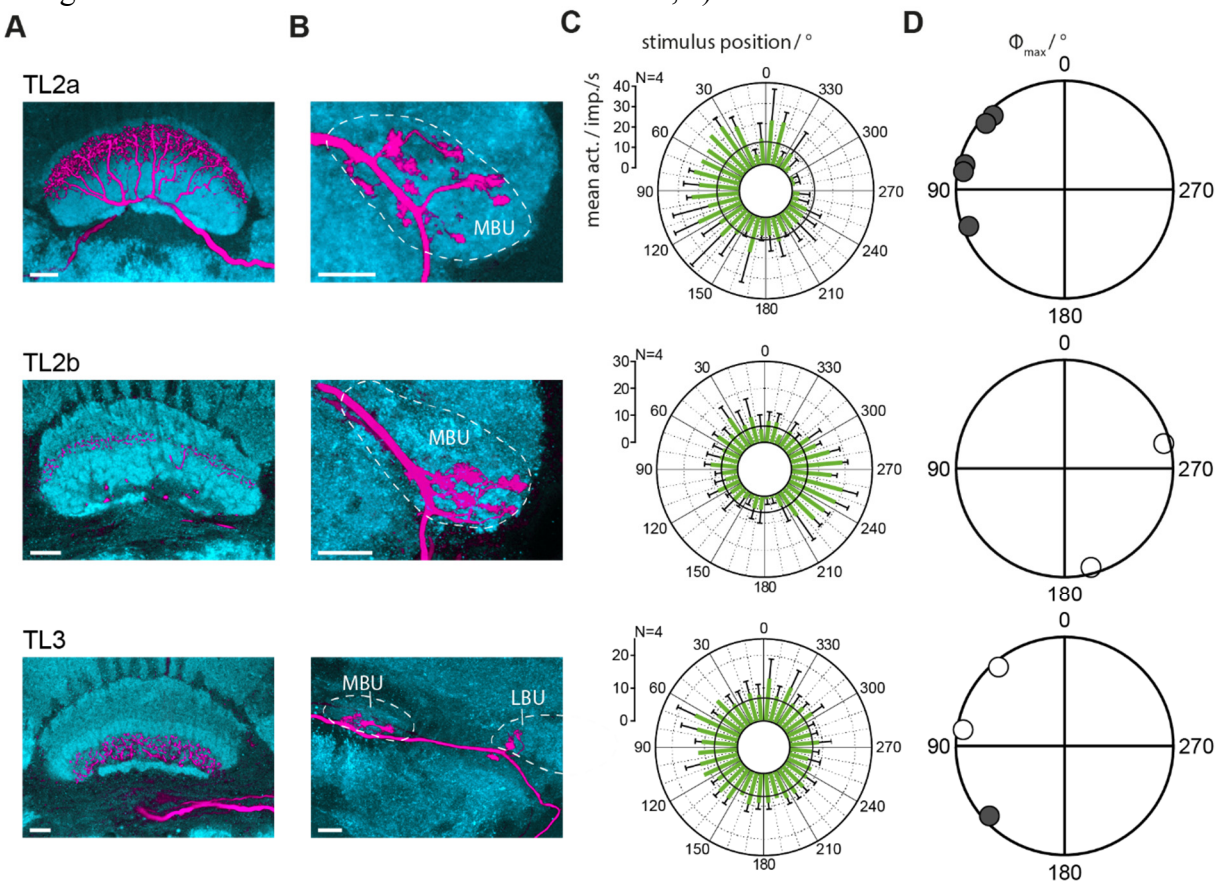

Figure 2. Morphology and physiology of TL neurons. ***A-B,*** Cy3-stainings of TL neurons (magenta). Neuropils were visualized by synapsin immunostaining (cyan). Scale bars, 20 µm. ***A,*** Arborizations of a TL2a neuron (upper row), a TL2b neuron (middle row) and a TL3 neuron (lower row) in the CBL; single optical sections. ***B,*** Arborizations of the neurons in the lateral (LBU) or medial bulb (MBU); projections of stacks of several optical sections. ***C,*** Circular histograms showing the average response of the TL2a (Φ_{max} = 76°), TL2b (Φ_{max} = 284°), and TL3 (Φ_{max} = 133°) neuron, presented in ***A*** and ***B***, to a rotating green light spot (elevation = 45°). Green bars indicate mean spiking activity. Error bars show SD. Black circles indicate median background activity. N, number of stimulus presentations. ***D,*** Preferred azimuth angles for the green spot from all recorded TL2a, TL2b and TL3 neurons. Open circles indicate a preferred azimuth on the ipsilateral side, filled grey circles indicate a preferred angle on the contralateral side.

Topographic representation of E-vector and azimuth angles in the PB

In the PB zenithal *E*-vectors are topographically represented, indicating that the PB acts as an internal sky polarization compass (Heinze and Homberg, 2007). This representation was found for TB1, CPU1, CP1 and CP2 neurons (Heinze and Homberg, 2007), but not for CL1 neurons (Heinze and Homberg, 2009). We asked here whether a topographic representation of azimuth of unpolarized light, respresenting the sun is, likewise, present across the PB. We recorded from CL1, TB1, CPU1, CP1 and CP2 neurons, and from an additional cell type, CPU2 neurons (Fig. 1*A*-*C*). Neurons were tested for *E*-vector coding by presenting polarized light from the zenith, and for azimuth coding by presenting an unpolarized green light spot, rotating at an elevation of 45° around the animals' head. The preferred angles were plotted against the slice of arborization in the PB. Because TB1 neurons have varicose arborizations in one PB slice of each brain hemisphere (separated by 7 slices), their preferred angles were plotted only for the left brain hemisphere. In CL1 neurons the preferred *E*-vector was not correlated with the slice of arborization in the PB (Fig. 3*A*). These observations are in line with previous results (Heinze and Homberg, 2009). TB1 neurons showed a correlation between preferred *E*-vector and slice of arborization, but the correlation coefficient was low compared to all other data sets (Fig. 3*B*). The data confirm the results of Heinze and Homberg (2007), who showed a topographic representation of *E*-vectors for TB1 neurons. Like in Heinze and Homberg (2007) the fit line had a positive slope and covered an angular range of 462° across the PB, which differs from the value of 364° found by Heinze and Homberg (2007). Due to small sample size, CPU2, CP1 and CP2 columnar output neurons were plotted together. In CPU1 and CPU2/CP1/CP2 neurons the preferred *E*-vector angle was significantly correlated with the slice of arborization in the PB (Fig. 3*C,D*), indicating an internal compass for zenithal *E*-vectors in the PB (Fig. 3*C'',D''*). The circular-linear fits covered a circular space of 360° in CPU1 neurons from L8 to R8, and 277.7° in CPU2/CP1/CP2 neurons. The steepness of fitlines were considerably different to those of Heinze and Homberg (2007), who reported a representation of 410° in CPU1 neurons and 411° in CP1/CP2 neurons.

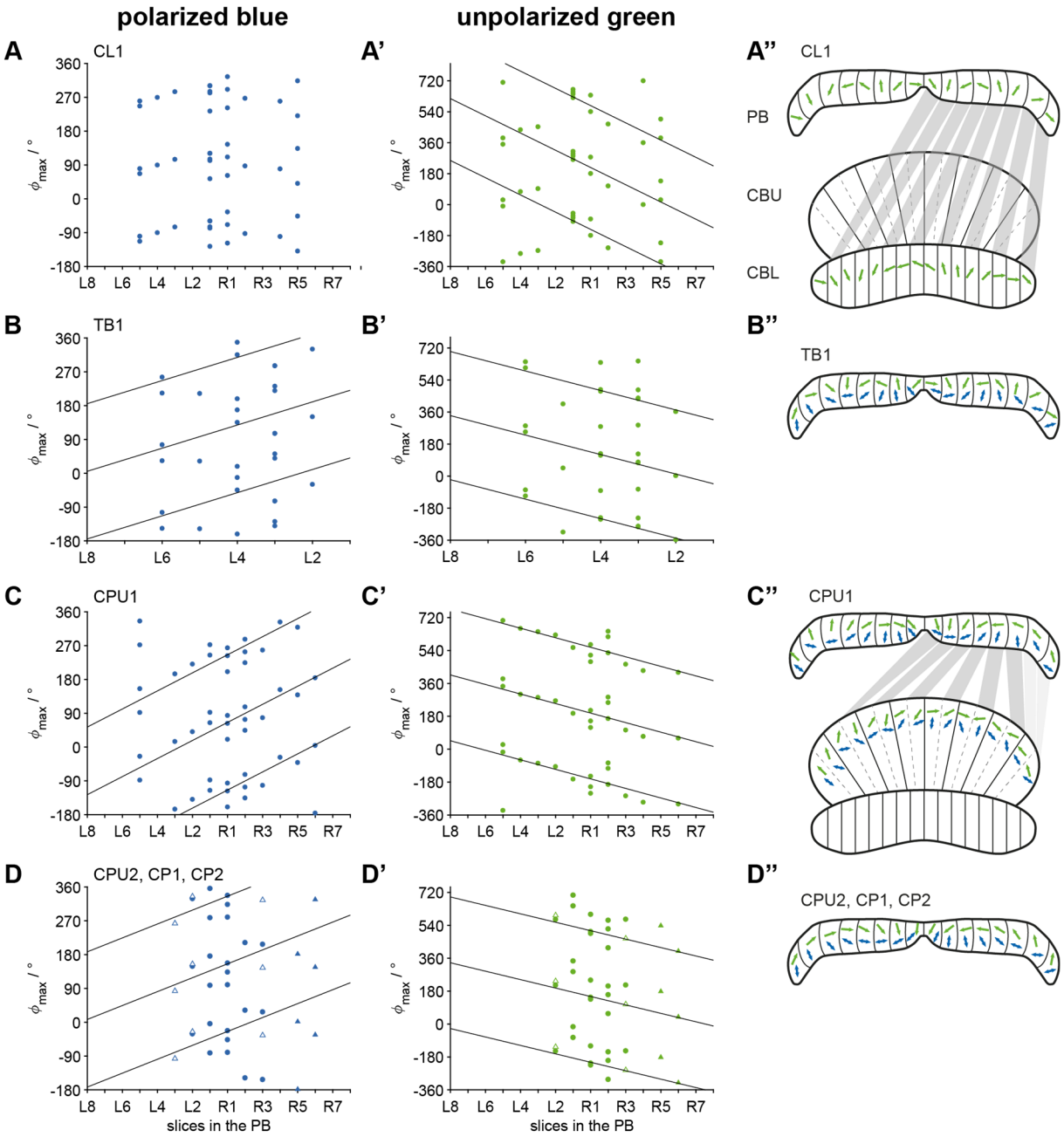

Figure 3. Internal representation of zenithal *E*-vector and azimuth in the CX. Preferred *E*-vector angles (***A, B, C, D***, blue markers) and preferred azimuth angles of the unpolarized light spot (***A', B', C', D'***, green markers) are plotted against the slice of arborization of the respective neuron in the PB. Data sets are plotted three times: ± 180° for preferred *E*-vectors and ± 360° for preferred azimuths. Solid lines show the best fit line, only in cases with significant correlation. Light spot elevation was at 45°. ***A'', B'', C'', D'',*** Mean *E*-vectors (blue double arrows) and mean azimuth angles (green arrows), taken from the circular-linear fits. For neurons arborizing additionally in the CB, the mean preferred angles were transferred from the PB to the CB, according to the wiring schemes as shown by Heinze and Homberg (2008). Wiring is indicated by shades of grey for the right brain hemisphere. Light grey indicates unknown and, thus, hypothetical connections. ***A, A',*** Preferred angles of CL1 neurons. Circular-linear regression does not show significant correlation between innervated slice and preferred angles for polarized blue light ($\rho = 0.11$, $p = 0.45$, $n = 16$), but significant correlation between innervated slice and unpolarized green light ($y = -50.1x + 256.5$, $\rho = -0.71$, $p = 1\times10^{-6}$, $n = 14$). ***B, B',*** Preferred angles of TB1 neurons. Significant correlation exists for polarized blue light ($y = 30.8x + 5$, $\rho = -0.48$, $p = 0.007$, $n = 11$) and for unpolarized green light ($y = -54.7x + 339.7$, $\rho = -0.54$, $p = 6\times10^{-3}$, $n = 11$). Due to similar location of varicose arborizations of TB1 neurons in the left and right PB hemisphere, only data of the left hemisphere are shown. ***C, C',*** Preferred angles of CPU1 neurons. Significant correlation exists for polarized blue light ($y = 24x - 126.7$, $\rho = 0.33$, $p = 0.008$, $n = 16$) and unpolarized green light ($y = -26.1x + 46.4$, $\rho = -0.54$, $p = 4\times10^{-4}$, $n = 15$). ***D, D',*** Preferred angles of CPU2 (filled circles), CP1 (filled triangles) and CP2 neurons (open triangles) plotted together. Significant correlation exists for polarized blue light ($y = 18.5x + 7.3$, $\rho = -0.46$, $p = 0.002$, $n=13$), and for unpolarized green light ($y = -23.1x + 335.4$, $\rho = -0.51$, $p = 3\times10^{-4}$, $n = 14$).

A correlation between the slice of arborization in the PB and the preferred azimuth of the unpolarized light spot was found in all cell types (Fig. 3*A'-D'*). This indicates that, in addition to the *E*-vector of polarized light, the azimuth of the green spot is topographically represented in the PB (Fig. 3*A''-D''*). However, in contrast to the positive correlation between *E*-vector and PB slice, the correlation between azimuth and PB arborization was negative in all cell types. The fits for the preferred azimuth of the unpolarized green spot covered 751.5° in CL1 neurons, 820.5° in TB1 neurons, 391.5° in CPU1 neurons, and 346.5° in CPU2/CP1/CP2 neurons across the PB. Because CPU1 and CL1 neurons arborize not only in slices of the PB but also in distinct slices of the central body we transferred the mean preferred angle (i.e. the y-value of the fit line in the center of each slice) from the PB to the CB following the wiring scheme of the respective neuron type (Heinze and Homberg, 2008). In CL1 neurons mean preferred azimuth angles resulted in a representation of 391.5° across the CBL (Fig. 3*B''*). CPU1 neurons innervating PB slices L6-R6 arborize in two neighbouring slices of the CBU. For the PB slices L8, L7, R8 and R7, however, the wiring scheme is not known, because CPU1 neurons arborizing in these slices have never been stained. By extrapolating the logic of connections from the central slices, Heinze and Homberg (2008) suggested that they invade corresponding outermost slices of the CBU. Following that scheme, mean *E*-vector angles across the eight double-slices covered a range of 166.5° in the CBU (Fig. 3*C''*). Interestingly, the mean azimuth angles of CPU1 neurons in double-slices of the CBU were almost spatially opponent to each other, except for the outermost double-slices, where they were roughly parallel (Fig. 3*C''*).

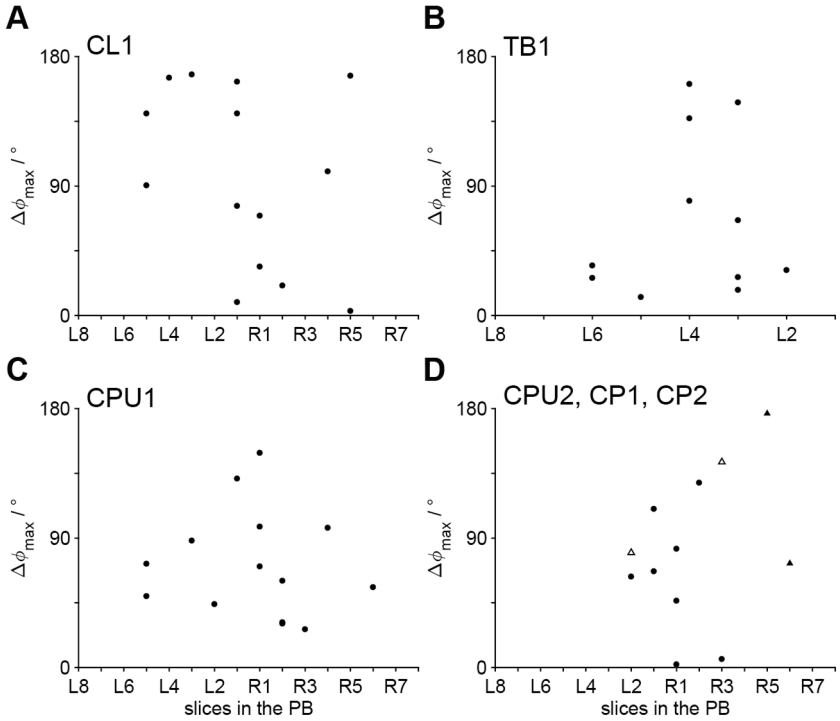

Figure 4. Distances between preferred *E*-vectors and azimuth angles. ***A-D,*** Distances between preferred *E*-vector angles and preferred azimuth angles (black markers) plotted against the slice of arborization in the PB. Distances were calculated by subtracting the preferred *E*-vector angle from the preferred azimuth of the green spot. ***A,*** Distances of CL1 neurons (n = 14). ***B,*** Distances of TB1 neurons (n = 11). ***C,*** Distances of CPU1 neurons (n = 14). ***D,*** Distances of CPU2 (filled circles), CP1 (filled triangles) and CP2 (open triangles) neurons plotted together (n = 12).

We next asked whether the angular distance between the tuning to both stimuli (*E*-vector and green azimuth) and the slice of arborization in the PB were correlated in any way. Across all cell types distances were independent of the slice of PB arborization (Fig. 4) and varied greatly for a given slice. In CL1 neurons distances were widely dispersed from 0° to 180° (Fig. 4*A*). In contrast, in most TB1 neurons distances were smaller than 90° (Fig. 4*B*). In CPU1 neurons the distances clustered between 45° and 90° (Fig. 4*C*). Most CPU2 neurons showed distances less than 90°, whereas in CP1 and CP2 neurons the distances were between 45° and 180° (Fig. 4*D*).

Interaction between polarized and unpolarized light stimulus

In some recordings we presented the unpolarized light spot together with the zenithal *E*-vector (Fig. 5). The relative angle between both stimuli was set to 90°, corresponding to the relationship between solar azimuth and zenithal *E*-vector in the sky. We analyzed the responses of two TL2, three CL1, 4 TB1, 6 CPU1, two CPU2 neurons and one CP1 neuron. A response curve of best fit to combined stimulation was calculated, to estimate the relative contribution of the single stimuli (*E*-vector or light spot) to the measured response to combined stimulation. The absolute values and the ratio of weighting factors varied from neuron to neuron and could not be related to cell type, slice of PB innervation, or distance between tuning to the *E*-vector and green light spot. Weighting factors for azimuth tuning ranged from 0 to 1.7, and for *E*-vector tuning, from -2 to 1.2. Their ratio ranged from -1.1 to 11.5. Some neurons showed a strong preference in the combined response for the *E*-vector or the unpolarized light spot, as shown for a CPU1 neuron preferring the *E*-vector (Fig. *5A*). Other cells showed a less pronounced preference for the *E*-vector as shown for a CL1 and a TB1 neuron (Fig. 5*B,C*), or for the azimuth of the green spot, as shown for a CPU1 and a CPU2 neuron (Fig. 5*D,E*). Some neurons showed responses to combined stimulation, in which the contribution of *E*-vector tuning and light spot tuning were similar (CL1, Fig. 5*F*). Nonetheless, in neurons not showing a strong preference the response to combined stimulation always revealed one higher peak or one deeper trough in spike rate modulation across 360°.

Influence of elevation on azimuth tuning

In some recordings of CL1, TB1 and CPU1 neurons we tested different elevations of the unpolarized green light spot. Only few of them showed an impact of elevation on the azimuth tuning. One CL1 neuron showed a second peak in azimuth tuning when stimulated at low elevations (Fig. 6*A*). At higher elevations of 50° or 60° the second peak disappeared, so that the tuning was more directed toward Φ_{max}. Another phenomenon occurred in a CPU1 neuron. Here the tuning curve was flat at high elevations and of higher amplitude at low elevations (Fig. 6*B*). Of all recordings these two neurons showed the strongest influence of elevation on azimuth tuning. The general effects on the correlation strength of the tunings were small (Fig. 6*C*). Different elevations changed the significance of the correlation coefficient only in one CL1 (red), one TB1 (blue) and one CPU1 neuron (purple). All other neurons were either responsive to all tested elevations (n = 10) or to none of them (n = 1). Elevations different from 45° were often tested later in the recording so that tuning parameters might have been altered by a change of neuronal background state. Across all cell types the correlation strength was most dispersed between elevations, whereas tuning amplitude and width were only slightly affected. Nonetheless, no common systematic change of tuning parameters occurred in any neuron type.

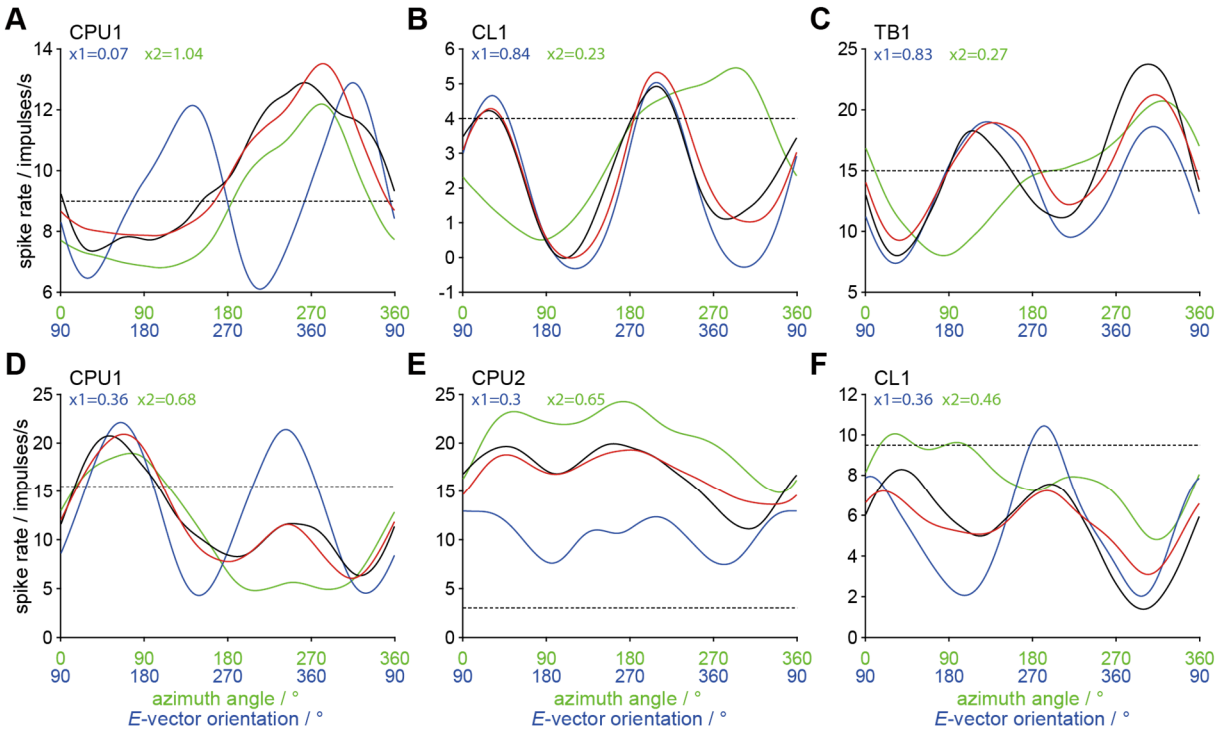

Figure 5. Responses to combined stimulation with polarized light and an unpolarized light spot. ***A-F,*** Tunings of central complex neurons to the *E*-vector (blue), the azimuth of the unpolarized light spot (green), and to both stimuli presented simultaneously (black). Tunings are presented as smoothed stimulus response curves. During combined stimulation the *E*-vector was adjusted at 90° angular distance from the green light spot. Therefore, the x-axis shows the orientation of the *E*-vector (blue) separated from the azimuth angle (green). Responses to the *E*-vector alone are shifted by 90°. Solid red lines show the best fit curves resulting from summation of *E*-vector tuning and light spot tuning multiplied by a weighting factor (*x*1 for the *E*-vector tuning, *x*2 for the azimuth tuning). Dotted lines indicate background activity. ***A,*** Responses of a CPU1 neuron showing a strong preference for the green light spot. *E*-vector tuning: Φ_{max} = 40°; p = $6 \cdot 10^{-5}$. Azimuth tuning: Φ_{max} = 264°; p = $2 \cdot 10^{-5}$. Combined response bidirectional tuning: p = 0.83. Combined response unidirectional tuning: Φ_{max} = 249°; p = $1 \cdot 10^{-3}$. ***B-F,*** Responses of CL1 neurons (***B,F***), a TB1 neuron (***C***), a CPU1 neuron (***D***) and a CPU2 neuron (***E***) to combined stimulation with less pronounced preference for the *E*-vector or the azimuth of the green spot. ***B,*** Responses of a CL1 neuron showing a preference for polarized light. *E*-vector tuning: Φ_{max} = 120°; p = $3 \cdot 10^{-6}$. Azimuth tuning: Φ_{max} = 261°; p = $2 \cdot 10^{-6}$. Combined response bidirectional tuning: Φ_{max} = 117°; p = $2 \cdot 10^{-5}$. Combined response unidirectional tuning: p = 0.64.***C,*** Responses of a TB1 neuron. *E*-vector tuning: Φ_{max} = 39°; p = $2 \cdot 10^{-5}$. Azimuth tuning: Φ_{max} = 285°; p = $4 \cdot 10^{-5}$. Combined response bidirectional tuning: Φ_{max} = 36°; p = $2 \cdot 10^{-4}$. Combined response unidirectional tuning: p = 0.2. ***D,*** Responses of a CPU1 neuron. *E*-vector tuning: Φ_{max} = 152°; p = $2 \cdot 10^{-7}$. Azimuth tuning: Φ_{max} = 69°; p = $8 \cdot 10^{-7}$. Combined response bidirectional tuning: Φ_{max} = 154°; p = $3 \cdot 10^{-3}$. Combined response unidirectional tuning: Φ_{max} = 73°; p = $2 \cdot 10^{-3}$. ***E,*** Responses of a CPU2 neuron. *E*-vector tuning: Φ_{max} = 99°; p = $4 \cdot 10^{-3}$. Azimuth tuning: Φ_{max} = 145°; p = $2 \cdot 10^{-4}$. Combined response bidirectional tuning: Φ_{max} = 116°; p = $1 \cdot 10^{-2}$. Combined response unidirectional tuning: Φ_{max} = 121°; p = $1 \cdot 10^{-3}$. ***F***, Responses of a CL1 neuron. *E*-vector tuning: Φ_{max} = 104°; p = $2 \cdot 10^{-5}$. Azimuth tuning: Φ_{max} = 92°; p = $5 \cdot 10^{-3}$. Combined response bidirectional tuning: Φ_{max} = 119°; p = $1 \cdot 10^{-3}$. Combined response unidirectional tuning: Φ_{max} = 117°; p = $3 \cdot 10^{-3}$.

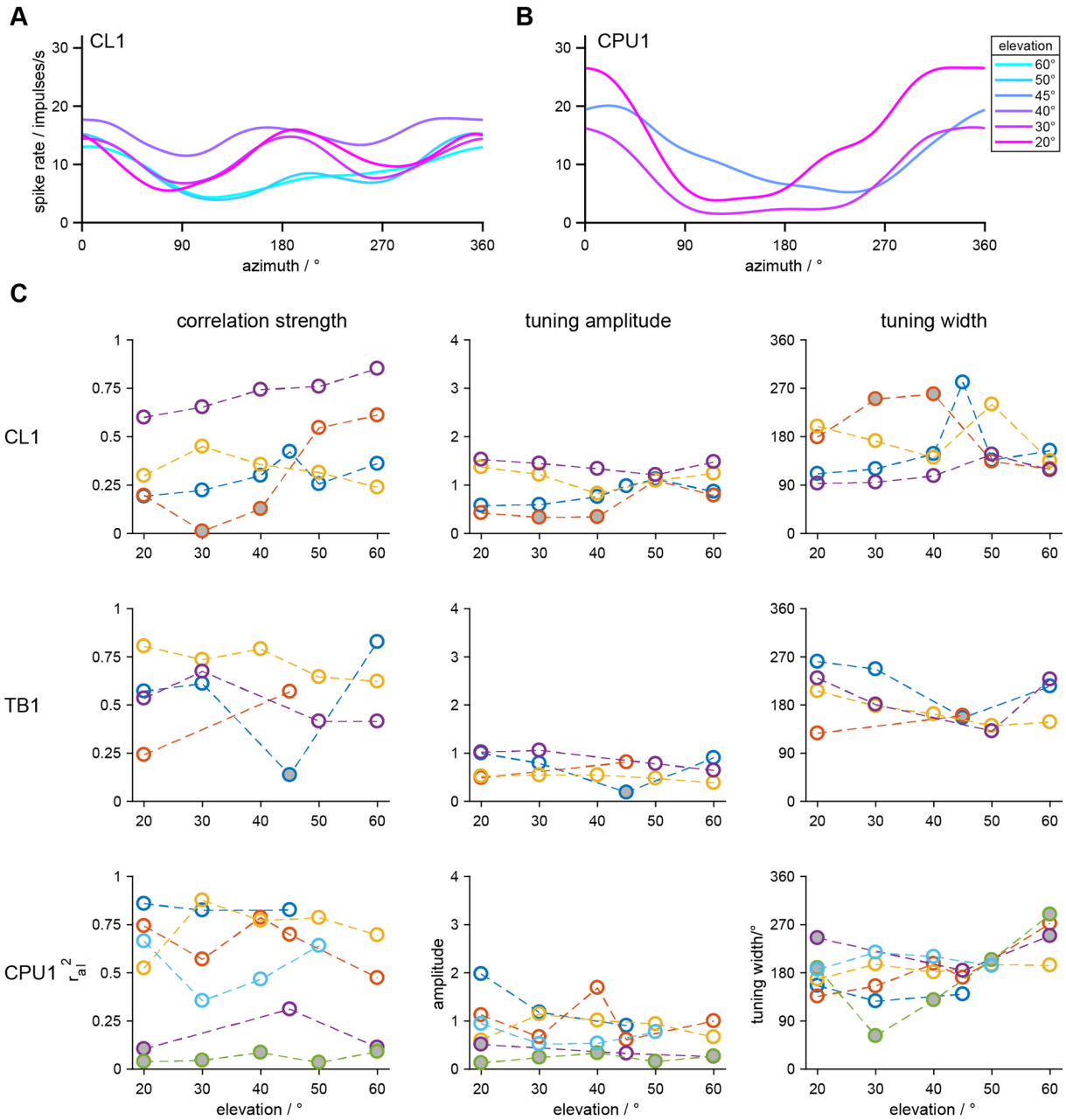

Figure 6. Influence of stimulus elevation on tuning parameters of CL1, TB1 and CPU1 neurons. ***A, B,*** Smoothed stimulus response curves of a CL1 neuron (***A***) and a CPU1 neuron (***B***) to rotation of the green light spot presented at different elevations. ***C,*** Tuning parameters of all recorded CL1, TB1 and CPU1 neurons. Tuning amplitude, tuning width and correlation strength (r_{al}^2) of the average stimulus response curve of each neuron plotted against the tested elevation. Colors code for individual neurons of the respective cell type. Open circles indicate data from significant responses, circles filled in grey indicate data from non-significant responses. Data from the CL1 neuron coded in red are from the same neuron as data in ***A***, and data from the CPU1 neuron coded in dark blue are from the same neuron as data in ***B***.

Discussion

We show here that zenithal *E*-vector orientations and azimuthal directions are represented in a compass-like fashion across the slices of the locust CX. Columnar output neurons of the CX network represent 360° of *E*-vectors across the PB. In addition, the azimuth of an unpolarized green light spot is represented, covering a circular space of nearly 2 × 360° in CL1 and TB1 neurons and roughly 360° in columnar output neurons. Although both compasses were found in

identical neuron populations, there is no constant angular relationship between them.

Side specific azimuth representation in tangential inputs to the CBL

Sky compass signals from both eyes converge in the CX via TL2 and TL3 tangential neurons. These neurons connect microglomeruli of the lateral (TL2) and medial (TL3) bulbs of the lateral complex to specific layers of the CBL (Müller et al., 1997; Vitzthum et al., 2002; Träger et al., 2008). We show here that TL2a neurons innervating dorsal microglomeruli of the lateral bulb target the dorsal layer 2 of the CBL, while TL2b neurons connect ventral microglomeruli of the lateral bulb to the more ventral layer 3 of the CBL. TL2a neurons preferred the green cue on the ipsilateral side, TL2b neurons, in contrast, preferred the green cue on the contralateral side. TL3 neurons with ramifications in the medial bulb and the dorsal tip of the lateral bulb showed a preferred azimuth of the unpolarized green light spot either on the ipsi- or contralateral side. These data are highly similar to the situation in the fruit fly *Drosophila*. Here, R neurons (equivalent to locust TL neurons) connect topographically distinct microglomeruli of the bulbs to different layers of the ellipsoid body (Omoto et al., 2017). R neurons arborizing in ventral parts of the bulb have contralateral receptive fields for visual cues and innervate outer layers of the ellipsoid body, while R neurons connecting microglomeruli in dorsal parts of the bulb to inner layers of the ellipsoid body respond to ipsilateral targets (Shiozaki and Kazama, 2017). The latter also encode the recent visual experience of targets. These data suggest that different layers of the CBL/ellipsoid body not only receive input from different parts of the visual field, but also different types of information related to memory and decision-making.

Compass representations in CX slices

A compass-like representation of zenithal *E*-vectors in the PB has been shown by Heinze and Homberg (2007) for TB1, CPU1 and CP1/CP2 neurons. These findings are confirmed here. Like in Heinze and Homberg (2007), all regression lines had a positive slope and, in TB1 and CPU1 neurons, covered roughly 360° of compass directions from L8 – R8. The representation of *E*-vectors in CPU2/CP1/CP2 neurons covered only 280°, but this may be owing to the lack of values for L8 – L4. We found no correlation between preferred *E*-vector and PB slice in CL1 neurons, again confirming the findings of Heinze and Homberg (2009).

The circular-linear correlation coefficient was generally lower for *E*-vector correlations than for azimuth correlations, especially in TB1 neurons. Heinze and Homberg (2007) calculated coefficients using a linear-linear correlation analysis. We used here a circular-linear approach, which affects the results in a negative way: (1) With small sample size ($n<10$) the correlation has only low reliability (Kempter et al., 2012). Our sample size of TB1 neurons was just above this number. (2) For the analysis of axial data, like the preferred *E*-vectors, the angles need to be doubled to convert them into a circular variable. This procedure artificially increases the dispersion of data, thus decreasing the likelihood of correlation or, in the case of correlation, its strength. Nonetheless, the circular-linar analysis used here has a strong advantage. As data points are already present multiple times on the y-axis, to analyze the circularity of data, there is no need for a shift by 180° (*E*-vectors) or 360° (azimuth angles), which is necessary for the linear-linear correlation analysis, strongly influencing its result.

In addition to *E*-vector topography, we found a topographical representation of azimuth (green light spot) in CL1, TB1, CPU1

and CPU2/CP1/CP2 neurons. In all of these cell types, the regression line had a negative slope from L8 – R8, opposite to that for *E*-vector coding. It covered a range of roughly 720° in CL1 and TB1 neurons, with slight overrepresentation in TB1 neurons. These findings coincide with the twofold representation of 360° space of E-PG neurons (equivalents to locust CL1 neurons) in the fly (Green et al., 2017), which was also a necessary assumption for a computational model of path integration in bees (Stone et al., 2017). In contrast, columnar output neurons represented only 360° of azimuthal directions. As CPU1, CP1 and CP2 neurons from one PB hemisphere (8 slices) have their presynaptic arborizations in the same LAL, it seems reasonable that they represent 180°, so that they might elicit turning behavior either to the left or to the right.

Elevation independence

In contrast to the azimuth, elevation of the green light spot is not encoded in locust PB neurons, as in most recordings neurons were either responsive to all elevations or to none. Our results did not reveal directedness or preference for a specific elevation in any neuron type. However, we were not able to test TL neurons for different elevations, so that a direct comparison with receptive fields of *Drosophila* ring neurons (Seelig and Jayaraman, 2013) is not possible. In the fly, microglomeruli in the bulb innervated by R neurons are topographically organized with regard to preferred azimuth and preferred elevation (Seelig and Jayaraman, 2013). However, neurons of the *Drosophila* CX downstream of R neurons have not been tested so far for different elevations. In the locust polarization-sensitive neurons of the medulla are the first elements of the polarization vision pathway integrating polarized light and azimuth information (el Jundi et al., 2011). Interestingly, their dendritic arborizations in the medulla extend from dorsal to ventral, already suggesting an elevation independent coding.

Biological significance

Terrestial landmarks as well as sky compass cues are exploited by insects for spatial orientation. Because locust CX neurons represent zenithal *E*-vectors in a topographic manner, the azimuth of the unpolarized light spot might, likewise, indicate a celestial compass signal, the solar azimuth. Azimuth-dependent responses to a bright light spot have been observed in the CX of dung beetles (el Jundi et al., 2015) and monarch butterflies (Heinze and Reppert, 2011), and were assumed to encode solar azimuth. Dung beetles, in fact, completely ignore landmark information but solely rely on celestial cueas such as sky polarization and the position of the moon or sun for spatial orientation (Dacke et al., 2013). In *Drosophila*, however, the preference for a certain azimuth of a bright spot or bar has been suggested to represent a landmark (Seelig and Jayaraman, 2013, 2015). Omoto et al. (2017) analyzing neurons presynaptic to R neurons discussed the receptive fields for bright bars more broadly as either a landmark or sunlight. Landmarks usually appear dark against a bright background, while the sun is generally the brightest visible spot. In the locust, responses of CX neurons to moving dark objects were typically triggered by the initiation of object motion followed by strong adaptation, but were independent of stimulus azimuth (Bockhorst and Homberg, 2015b).

The two internal compasses for *E*-vector orientation and azimuth angle differ not only in their orientation but also in the total space they represent across the PB. Moreover, there is no 90° distance between preferred *E*-vector and preferred azimuth in any of the PB slices, so that the natural distance between zenithal *E*-vector and sun is not encoded,

assuming that these neurons have zenith-centered receptive fields. These results show that the representations of the two cues (*E*-vector and light spot) are not linked to each other. This suggestion is additionally supported by the variety of weighting factors for the two cues leading to the response to combined stimulation. Although the preference for the *E*-vector or the light spot is highly variable the responses to combined stimulation showed either a pronounced peak or trough in the estimated firing rate, matching a peak or trough of the response to the *E*-vector or light spot alone. This may indicate that also in cases of a small ratio between the two weighting factors, one of the stimuli, and thus, one of the compasses, is still dominant. In general our findings are in line with observations by Wehner and Müller (2006) in ants. In behavioral experiments on homing they presented conflicting combinations of direct sunlight and celestial polarization and showed that the ants form two separate systems of navigation, with dominance of the polarization compass over the sun compass.

In conclusion our results support the assumption that CX neurons are involved in navigation, not only by using a sky-polarization compass but also an azimuth compass, possibly representing the sun. Both internal compasses emerge in neurons of the PB and are present in all columnar output neurons. Our data suggest that both compasses code directions separately from each other, rather than being linked to increase the robustness of head-direction coding.

Acknowledgements

This work was supported by Deutsche Forschungsgemeinschaft grants HO 950/23-1 and HO 950/24-1. We are grateful to Drs. Erich Buchner and Christian Wegener (University of Würzburg) for supplying anti-synapsin antibodies. Furthermore we thank Frederick Zittrell for providing Matlab code and Martina Kern for maintaining locust cultures.

References

Batschelet E (1981) Circular Statistics in Biology. London, UK: Academic Press.

Bockhorst T, Homberg U (2015a) Amplitude and dynamics of polarization-plane signaling in the central complex of the locust brain. J Neurophysiol 113:3291-3311.

Bockhorst T, Homberg U (2015b). Compass cells in the brain of an insect are sensitive to novel events in the visual world. PLoS One 10:e0144501.

Brandt R, Rohlfing T, Rybak J, Krofczik S, Maye A, Westerhoff M, Hege HC, Menzel R (2005) Three-dimensional average-shape atlas of the honeybee brain and its applications. J Comp Neurol 492:1–19.

Brines ML, Gould JL (1979) Bees have rules. Science 206:571-573.

Brunner D, Labhart T (1987) Behavioural evidence for polarization vision in crickets. Physiol Entomol 12:1-10.

Clements AN, May TE (1974). Studies on locust neuromuscular physiology in relation to glutamic acid. J Exp Biol 60:673–705.

Collett TS (1992) Landmark learning and guidance in insects. Philos Trans R Soc Lond B 337:295-303.

Dacke M, Byrne M, Smolka J, Warrant E, Baird E (2013) Dung beetles ignore landmarks for straight-line orientation. J Comp Physiol A 199:17-23.

Dacke M, Nordström P, Scholtz CH (2003) Twilight orientation to polarized light in the crepuscular dung beetle *Scarabaeus zambesianus*. J Exp Biol 206:1535-1543.

el Jundi B, Pfeiffer K, Heinze S, Homberg U (2014a) Integration of polarization and chromatic cues in the insect sky compass. J Comp Physiol A 200:575-589.

el Jundi B, Pfeiffer K, Homberg U (2011) A distinct layer of the medulla integrates sky compass signals in the brain of an insect. PLoS One 6:e27855.

el Jundi B, Smolka J, Baird E, Byrne MJ, Dacke M (2014b) Diurnal dung beetles use the intensity gradient and the polarization pattern of the sky for orientation. J Exp Biol 217:2422-2429.

el Jundi B, Warrant EJ, Byrne MJ, Kjaldy L, Baird E, Smolka J, Dacke M (2015) Neural coding underlying the cue preference for celestial orientation. Proc Natl Acad Sci U S A 112: 11395-11400.

Frost BJ, Mouritsen H (2006) The neural mechanisms of long distance animal navigation. Curr Opin Neurobiol 16:481-488.

Gould JL (1998) Sensory bases of navigation. Curr Biol 8:R731-R738.

Green J, Adachi A, Shah KK, Hirokawa JD, Magani PS, Maimon G (2017) A neural circuit architecture for angular integration in *Drosophila*. Nature 546:101-106.

Heinze S (2014) Polarized-light processing in insect brains: recent insights from the desert locust, the Monarch butterfly, the cricket, and the fruit fly. In: Polarized light and polarization vision in animal sciences (Horváth G, ed), pp61-111. Berlin, Heidelberg: Springer.

Heinze S, Homberg U (2007) Maplike representation of celestial *E*-vector orientations in the brain of an insect. Science 315:995-997.

Heinze S, Homberg U (2008) Neuroarchitecture of the central complex of the desert locust: intrinsic and columnar neurons. J Comp Neurol 511:454-478.

Heinze S, Homberg U (2009) Linking the input to the output: New sets of neurons complement the polarization network in the locust central complex. J Neurosci 29:4911-4921.

Heinze S, Reppert SM (2011) Sun compass integration of skylight cues in migratory monarch butterflies. Neuron 69:345-358.

Held M, Berz A, Hensgen R, Muenz TS, Scholl C, Rössler W, Homberg U, Pfeiffer K (2016) Microglomerular synaptic complexes in the sky-compass network of the honeybee connect parallel pathways from the anterior optic tubercle to the central complex. Front Behav Neurosci 10:186.

Homberg U (2015) Sky sompass orientation in desert locusts - evidence from field and laboratory studies. Front Behav Neurosci 9:247.

Homberg U, Heinze S, Pfeiffer K, Kinoshita M, el Jundi B (2011) Central neural coding of sky polarization in insects. Philos Trans R Soc Lond B 366:680-687.

Kempter R, Leibold C, Buzsáki G, Diba K, Schmidt R (2012) Quantifying circular-linear associations: hippocampal phase precession. J Neurosci Methods 207:113-124.

Klagges BR, Heimbeck G, Godenschwege TA, Hofbauer A, Pflugfelder GO, Reifegerste R, Reisch D, Schaupp M, Buchner S, Buchner E (1996) Invertebrate synapsins: a single gene codes for several isoforms in *Drosophila*. J Neurosci 16:3154-3165.

Kurylas AE, Rohlfing T, Krofczik S, Jenett A, Homberg U (2008) Standardized atlas of the brain of the desert locust, *Schistocerca gregaria*. Cell Tissue Res 333:125-145.

Labhart T, Meyer EP (1999) Detectors for polarized skylight in insects: a survey of ommatidial specializations in the dorsal rim area of the compound eye. Microsc Res Tech 47:368-379.

Mappes M, Homberg U (2004) Behavioral analysis of polarization vision in tethered flying locusts. J Comp Physiol A 190:61-68.

Menzel R, Greggers U, Smith A, Berger S, Brandt R, Brunke S, Bundrock G, Hülse S, Plümpe T, Schaupp F, Schüttler E, Stach S, Stindt J, Stollhoff N, Watzl S (2005) Honey bees navigate according to a map-like spatial memory. Proc Natl Acad Sci U S A 102:3040-3045.

Merlin C, Heinze S, Reppert SM. (2012) Unraveling navigational strategies in migratory insects. Curr Opin Neurobiol 22:353-361.

Müller M, Homberg U, Kühn A (1997) Neuroarchitecture of the lower division of the central body in the brain of the locust (*Schistocerca gregaria*). Cell Tissue Res 288:159-176.

Ofstad, TA, Zuker CS, Reiser MB (2011) Visual place learning in *Drosophila melanogaster*. Nature 474:204-207.

Omoto, JJ, Keleş MF, Nguyen BCM, Bolanos C, Lovick JK, Frye MA, Hartenstein V (2017) Visual input to the *Drosophila* central complex by developmentally and functionally distinct neuronal populations. Curr Biol 27:1098-1110.

Pegel U, Pfeiffer K, Homberg U (2018) Integration of celestial compass cues in the central complex of the locust brain. J Exp Biol 221: jeb171207.

Pfeiffer K, Kinoshita M, Homberg U (2005) Polarization-sensitive and light-sensitive neurons in two parallel pathways passing through the anterior optic tubercle in the locust brain. J Neurophysiol 94:3903-3915.

Reppert SM, Guerra PA, Merlin C (2016) Neurobiology of monarch butterfly migration. Annu Rev Entomol 61:25-42.

Reppert SM, Zhu H, White RH (2004) Polarized light helps monarch butterflies navigate. Curr Biol 14:155-158.

Schmeling F, Wakakuwa M, Tegtmeier J, Kinoshita M, Bockhorst T, Arikawa K, Homberg U (2014) Opsin expression, physiological characterization and identification of photoreceptor cells in the dorsal rim area and main retina of the desert locust, *Schistocerca gregaria*. J Exp Biol 217:3557-3568.

Seelig JD, Jayaraman V (2013) Feature detection and orientation tuning in the *Drosophila* central complex. Nature 503:262-266.

Seelig JD, Jayaraman V (2015) Neural dynamics for landmark orientation and angular path integration. Nature 521:168-191.

Shiozaki HM, Kazama H (2017) Parallel encoding of recent visual experience and self-motion during navigation in *Drosophila*. Nat Neurosci 20:1395-1403.

Stalleicken J, Mukhida M, Labhart T, Wehner R, Frost B, Mouritsen H (2005) Do monarch butterflies use polarized skylight for migratory orientation? J Exp Biol 208:2399-2408.

Stone T, Webb B, Adden A, Weddig NB, Honkanen A, Templin R, Wcislo W, Scimeca L, Warrant E, Heinze S (2017) An anatomically constrained model for path integration in the bee brain. Curr Biol 27:3069-3085.

Träger U, Wagner R, Bausenwein B, Homberg U (2008) A novel type of microglomerular synaptic complex in the polarization vision pathway of the locust brain. J Comp Neurol 506:288-300.

Varga AG, Kathman ND, Martin JP, Guo P, Ritzmann RE (2017) Spatial navigation and the central complex: Sensory acquisition, orientation, and motor control. Front Behav Neurosci 11:4.

Vitzthum H, Müller M, Homberg U (2002) Neurons of the central complex of the locust *Schistocerca gregaria* are sensitive to polarized light. J Neurosci 22:1114-1125.

von Frisch K (1949) Die Polarisation des Himmelslichtes als orientierender Faktor bei den Tänzen der Bienen. Experientia 5:142-148.

Wehner R (1984) Astronavigation in insects. Annu Rev Entomol 29:277-298.

Wehner R, Müller M (2006) The significance of direct sunlight and polarized skylight in the ant's celestial system of navigation. Proc Natl Acad Sci U S A 103:12575-12579.

Weir PT, Dickinson MH (2012) Flying *Drosophila* orient to sky polarization. Curr Biol 22:21-27.

Wystrach A, Graham P (2012) View-based matching can be more than image matching: The importance of considering an animal's perspective. Iperception 38:547-549.

Zar JH (1999) Biostatistical Analysis (4th ed.). Upper Saddle River, NJ: Prentice Hall.

Zars T (2009) Spatial orientation in *Drosophila*. J Neurogenet 23:104-110.

Chapter 3

Influence of wide-field motion on the signalling of sky compass cues in the locust central complex

Influence of wide-field motion on the signalling of sky compass cues in the locust central complex

Uta Pegel, Uwe Homberg, Ronny Rosner

Visual cues are essential for animal navigation and spatial orientation. Many insects rely on celestial cues for spatial orientation, including the sky polarization pattern. In desert locusts neurons encoding the plane of polarized light (*E*-vector) are located in the central complex (CX), a group of midline-spanning neuropils. Several types of CX neuron signalling heading direction represent zenithal *E*-vectors in a topographic manner across the slices of the CX and, likely, act as an internal sky compass. Because animals experience optic flow stimulation during flight, we asked whether progressive wide-field motion affects the responses of CX neurons to polarized light. In most neurons, progressive motion disadapted the response to the preferred *E*-vector (i.e. the *E*-vector eliciting strongest firing), whereas the response to the anti-preferred *E*-vector remained comparatively unaffected. This suggests context-dependent gain modulation in sky compass signalling. Three types of compass neuron were responsive to motion simulating body rotation around the yaw axis. Depending on arborization domains in the CX and rotation direction these neurons were strongly excited or inhibited. As proposed for *Drosophila*, they may be involved in shifting compass signal activity across the slices of the CX as the animal turns enabling it to keep track of its heading.

Introduction

Many animals use visual cues to navigate through their environment. Insects use a variety of sky compass signals for spatial orientation during homing or seasonal migrations. While ants and bees use the sky polarization pattern, the azimuth of the sun, and the chromatic gradient to find their way home (1-4), nocturnal dung beetles, in addition, exploit the position of the moon and the orientation of the milky-way to roll their dung pile on a straight path (5,6). For migratory locusts the polarization of skylight may be an important cue to keep a constant flight course (7). Sky compass cues are processed in the central complex (CX), a group of midline-spanning neuropils in the insect brain (8-11). The CX consists of the upper and lower divisions of the central body (CBU, CBL), the protocerebral bridge (PB), and the paired noduli (Fig. 1a). The PB and the CBL are prominently involved in an internal representation of horizontal spatial directions. In both brain areas, neurons signalling heading direction in the fruit fly (12) and in the desert locust (13,14) are organized topographically across arrays of vertical slices. In addition to directional information from landmarks or a compass, insects experience optic flow and frontal wind stimulation during flight. CX neurons are sensitive to approaching objects (locust: 15), small moving targets (locust: 16), and wide-field motion (cockroach: 17,18). In flying insects those signals are important to maintain flight stability (19-23) but in a resting animal they might be less meaningful. Thus, the responsiveness of neurons to such visual stimuli may be dependent on the animal's current behaviour. An enhancement of responses in the CX during flight or walking has, indeed, been shown in the fruit fly (24,25,18). Visual responses of descending neurons of the locust are as well dependent on the animal's motor state (26), but also on the presence of optic flow (20). Optic flow modulates flight rhythm and likely serves as visual context for responses of descending neurons detecting deviations from straight flight (22,20,). Moreover it initiates flight similar to frontal wind (22).

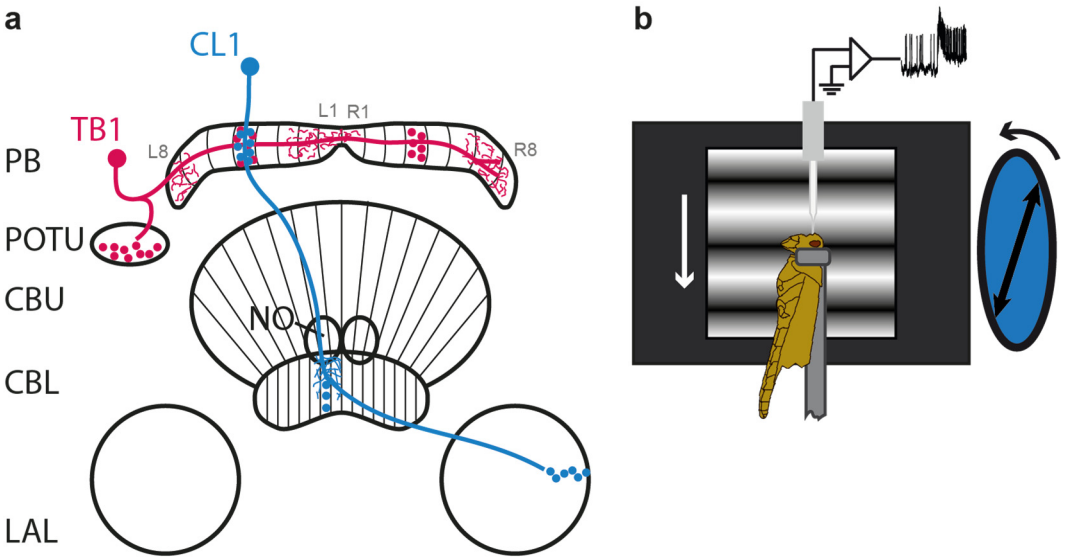

Figure 1. Neuronal cell types and visual stimulation. (a) Schematic illustration of one type of tangential (red) and one type of columnar neuron (blue) of the sky compass network in the locust central complex. Vertical lines mark the edges of slices occupied by arborizations of columnar neurons. Slices are termed R1-8 (right hemisphere) and L1-8 (left hemisphere). Circles indicate somata, thick colored lines indicate neurites, thin lines indicate smooth, likely dendritic, arborizations, and dots represent varicose, likely presynaptic, arborizations. Neuropil abbreviations: CBL, central body lower division; CBU, central body upper division; LAL, lateral accessory lobe; NO, noduli; PB,

protocerebral bridge. Abbreviations of neuron types: CL1, columnar neuron of the CBL type 1; TB1, tangential neuron of the PB type 1. **(b)** Illustration of visual stimulation. The locust was stimulated from dorsal direction by blue light passing a rotating or stationary polarizer and from both sides with sinusoidal gratings presented on LCD screens. Only the screen on the right side of the animal is shown. White arrow indicates progressive (front to back) motion of the sine wave grating. Black double arrow shows current orientation of the polarizer (*E*-vector). A sharp micro-electrode was used to penetrate the brain from above.In the present study, we used wide-field motion to simulate progressive self-motion as experienced by an animal during flight. To test whether sky compass signalling in the CX is dependent on the visual context, we recorded the activity of locust CX neurons during presentation of progressive wide-field motion in combination with a compass signal.

Results

We recorded intracellularly from 15 neurons of the locust CX belonging to the sky compass network. Neurons were identified by injection of Neurobiotin and subsequent staining. 9 neurons were identified as tangential neurons of the PB (TB1), 3 as columnar neurons of the PB and CBL (CL1), two as columnar neurons of the PB, CBL and noduli (CL2), and one as a columnar neuron of the CBU (CPU1). CL1 neurons connect slices of the CBL with slices of the PB (Fig. 1a). The CL1 subtype studied most often (CL1a) shows smooth processes with a varicose core in the CBL, whereas arborizations are claw-like in the PB and varicose in the LAL (27). CL2 neurons connect single slices of the PB and CBL as well, however, they follow a wiring scheme different from that of CL1 neurons (27). Arborizations are smooth in the PB and in the contralateral nodulus and varicose in the CBL. TB1 neurons in turn connect different slices of the PB with the posterior optic tubercle (POTU). They invade two slices of the PB, separated by 7 slices, with varicose processes and several slices inbetween with fine processes (Fig. 1a; 13). Arborizations in the POTU are varicose. CPU1 neurons connect slices of the PB and CBU with the lateral accessory lobe (LAL) of the contralateral brain hemisphere. Arborizations in the PB and the CBU are smooth and, in the LAL, of varicose appearance. In the following paragraph responses of CL1 and TB1 neurons are analyzed (Fig. 1a).

Responsiveness to progressive wide-field motion and polarized light

Animals were stimulated with polarized light presented from dorsal direction and, additionally, with progressive (front-to-back) motion of sinewave gratings presented on two LCD screens, one located on each side of the animal (Fig. 1b). All TB1 and CL1 neurons had a preferred *E*-vector orientation (i.e. the neurons had higher spiking activity at the preferred angle, Φ_{max}, and lower activity 90° distant to Φ_{max}, at Φ_{min}). The CPU1 neuron was not sensitive to polarized light and was, therefore, excluded from further analysis. Responses of a CL1 neuron and a TB1 neuron are shown in Fig. 2. Both neurons showed strong modulation caused by the rotation of the polarizer (Fig. 2a,b). As shown before (28) their preferred *E*-vector angle was dependent on rotation direction of the polarizer. Because the TB1 neuron was excited only weakly by progressive motion, only the CL1 neuron was responsive (Fig. 2a',b'). Overall, one out of three CL1 neurons (Fig. 3a), and 4 out of 9 TB1 neurons showed responsiveness to progressive motion (Fig. 3b). Therefore, these neurons responded to both the polarization stimulus and the progressive motion stimulus. Next we asked how the processing of sky compass and motion signals interact in the locust CX.

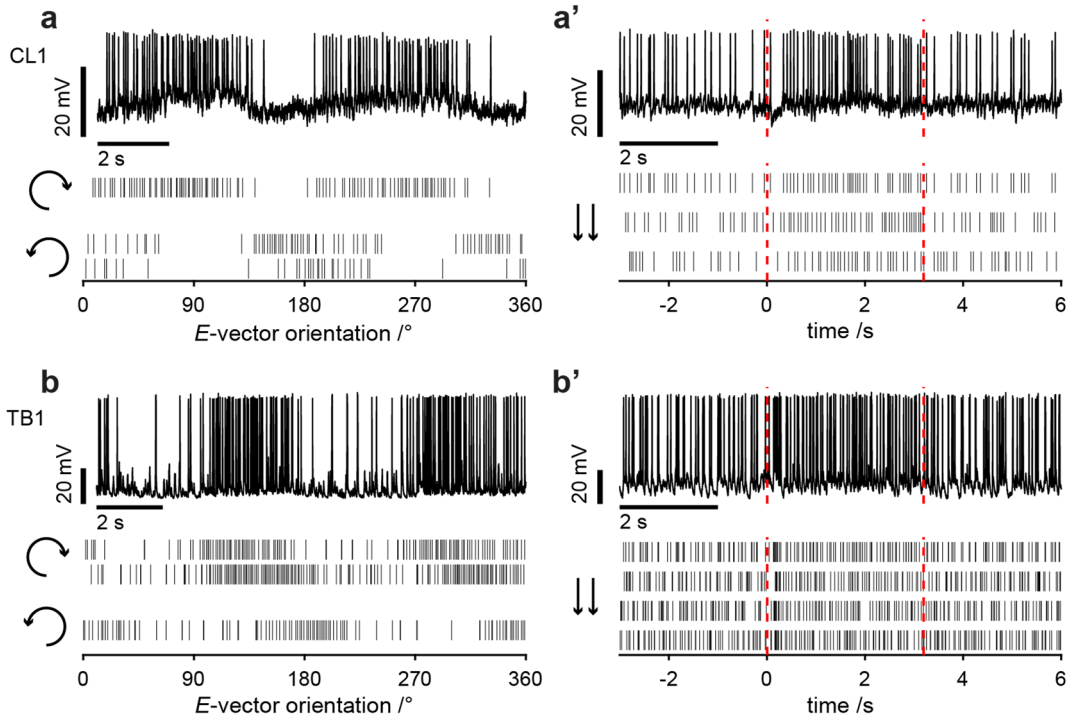

Figure 2. Responses to polarized light and progressive wide-field motion. (a) Response of a CL1 neuron to a 360° rotation of the polarizer. Upper panel shows the spike train of the first trial. Middle panel depicts rasterplot of response to clockwise (CW) rotation (curved arrow) of the polarizer. Bottom panel depicts rasterplots of responses to counterclockwise (CCW) rotation (curved arrow) of the polarizer. $\Phi_{max(CW)} = 73°$; $p_{(CW)} = 1\times10^{-6}$; $\Phi_{max(CCW)} = 0°$; $p_{(CCW)} = 2\times10^{-6}$. **(a')** Response of the CL1 neuron shown in **(a)** to progressive wide-field motion (p = 0.02). Arrows indicate the direction of motion on the screens (front to back). Onset and offset of motion are indicated by red dashed lines. **(b)** Response of a TB1 neuron to the rotating polarizer. Spike train (top trace) and rasterplots (bottom) as in **(a)**. $\Phi_{max(CW)} = 133°$; $p_{(CW)} = 6\times10^{-7}$; $\Phi_{max(CCW)} = 1°$; $p_{(CCW)} = 3\times10^{-6}$. **(b')** Response of the TB1 neuron shown in **(b)** to progressive wide-field motion (p = 0.1). Red dashed lines indicate on- and offset of motion. Arrows indicate the direction of motion (front to back).

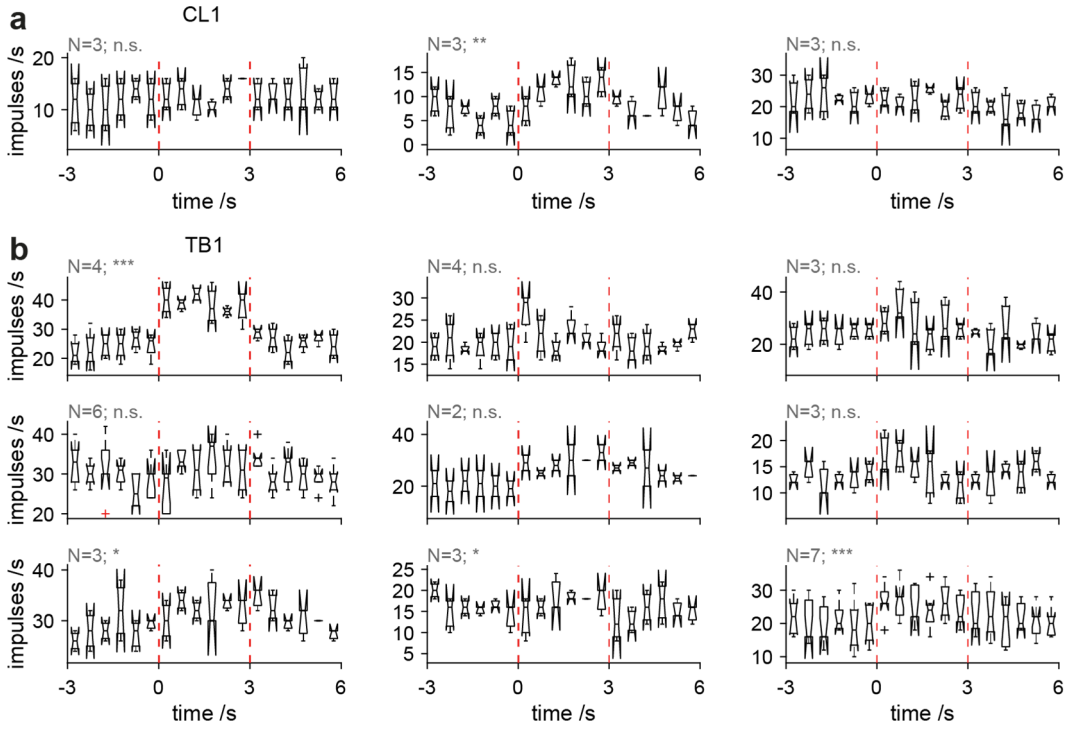

Figure 3. Responsiveness to progressive wide-field motion. Box plots show binned firing rates before, during and after stimulation with progressive motion. Motion onset is at 0 s, motion offset at 3.2 s. Firing rates in bins before the left red dashed line (i.e. during presentation of stationary grating) were compared with firing rates in bins between red dashed lines (i.e. during motion) using a paired t test. Significance is indicated by asterisks (***: $p < 0.001$; **: $p < 0.01$; *: $p < 0.05$). n.s., not significant. N, number of trials **(a)** Responses of three CL1 neurons. **(b)** Responses of nine TB1 neurons.

Interaction of progressive wide-field motion and polarized light signalling

In order to study the interaction between *E*-vector signalling and progressive motion signalling we presented both stimuli together. Throughout the recording the sinusoidal grating was stationary and visible to the animal. The influence of small moving objects on the compass response of locust CX neurons had been tested by Bockhorst and Homberg (29). We used a similar approach in experimental design and quantification of progressive motion responses at different *E*-vector angles. We tested one or two full 360° rotations of the polarizer to estimate the preferred and anti-preferred *E*-vector angle. Then we rotated the polarizer toward the preferred angle (Fig. 4). Neurons of the locust compass network typically adapt after several seconds (28). Therefore, we calculated the unadapted firing rate in a time-window of 2 s after the onset of stationary polarized light. After adaptation we started additional stimulation with progressive motion of gratings for several trials. After several trials we rotated the polarizer to the anti-preferred *E*-vector angle. Again adaptation and subsequent testing of wide-field motion sensitivity followed. The responses to the different stimulus conditions, progressive motion alone, progressive motion combined with stationary polarized light at Φ_{max}, and combined with polarized light at Φ_{min}, were highly individual. One CL1 neuron and two TB1 neurons responded to none of the conditions. One CL1 neuron and one TB1 neuron responded only to progressive motion presented alone. One CL1 neuron and three TB1 neurons did not respond to the progressive motion when presented alone, but

only when presented together with stationary polarized light. One of these recordings is shown in Fig. 5a-a''. The firing rate did not change when progressive motion was presented alone (Fig. 5a). The neuron was, however, excited by the moving grating when the *E*-vector was at the preferred angle, Φ_{max} (Fig. 5a'). In contrast, the neuron was slightly inhibited by progressive motion at the anti-preferred angle, Φ_{min} (Fig. 5a''). Three TB1 neurons were responsive to progressive motion presented alone and presented together with polarized light. Fig. 5b shows a neuron belonging to this group. It was strongly excited when progressive motion was presented alone (Fig. 5b). It was similarly excited as motion was presented together with polarized light at Φ_{max} (Fig. 5b') and at Φ_{min} (Fig. 5b'').

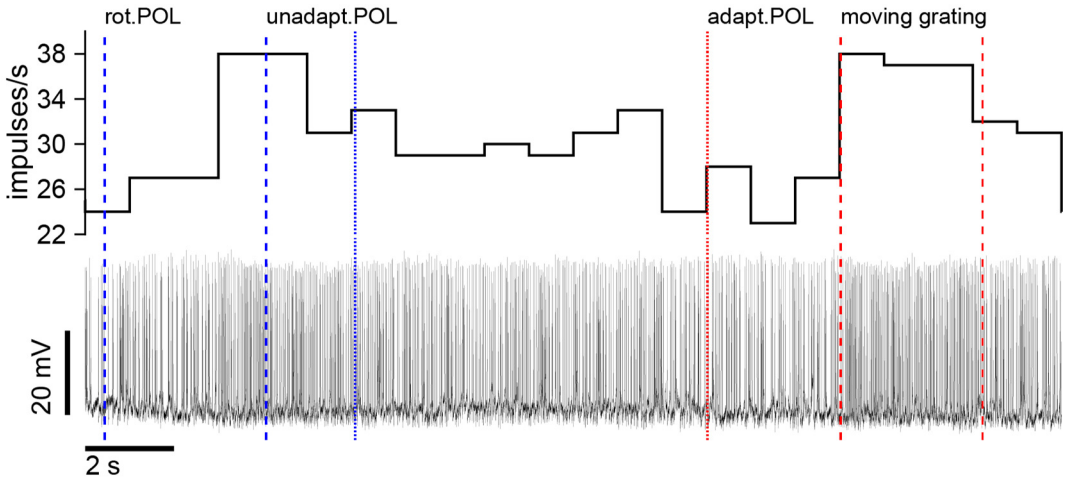

Figure 4. Response of a TB1 neuron to stationary polarized light and concurrent progressive motion. Spike train (lower trace) and stairs plot showing the mean firing rate (1 s bins; upper panel) of a TB1 neuron. Polarized light was presented during the whole time period. rot. POL, rotation of the polarizer toward preferred *E*-vector-orientation; on- and offset of rotation are indicated by the blue dashed lines. The blue dotted line shows the time-window of 2 s taken for calculating the unadapted response to the stationary preferred *E*-vector. The red dashed lines indicate the on- and offset of progressive motion of grating. The red dotted line shows the time-window of 3 s in which the adapted *E*-vector response was calculated.

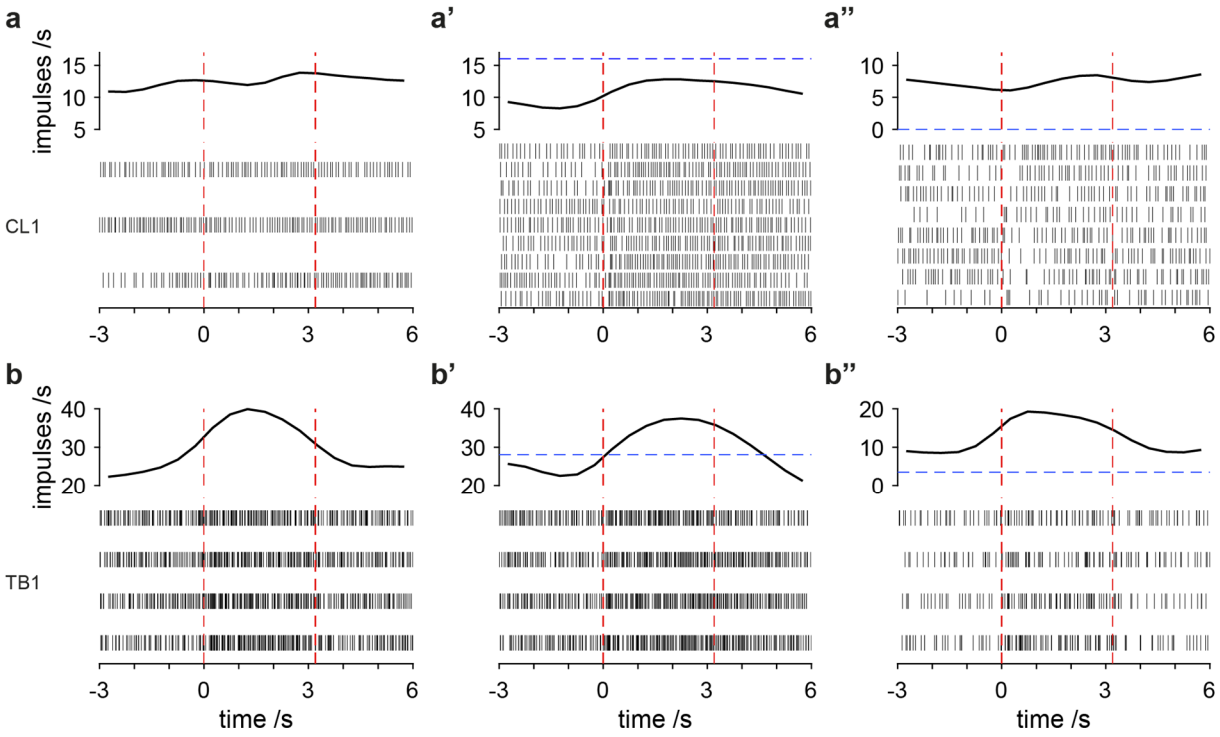

Figure 5. Responses to wide-field motion in the context of polarized light. In all plots the lower traces show trial-wise responses as raster plots with first stimulation in the uppermost row. Top traces show binned and smoothed spike rate averaged from all traces. Red dashed lines indicate on- and offset of grating motion. Responses of a CL1 neuron (**a, a', a''**) and a TB1 neuron (**b, b', b''**). **(a, b)** Responses to progressive motion stimulation presented alone. $p_{CL1} = 0.5$; $p_{TB1} = 0.006$. **(a', b')** Responses to progressive wide-field motion at stationary preferred *E*-vector angle. Blue dashed lines indicate the unadapted firing rate with stationary *E*-vector at preferred angle. $p_{CL1} = 0.001$; $p_{TB1} = 0.002$. **(a'', b'')** Responses to progressive wide-field motion presented together with stationary *E*-vector at anti-preferred angle. $p_{CL1} = 0.7$; $p_{TB1} = 0.007$. Blue dashed horizontal lines indicate the unadapted firing rate with stationary *E*-vector at anti-preferred angle.

To analyze the interaction between the processing of the two stimuli in more detail we normalized (1) the firing rates during progressive motion stimulation to the pre-stimulus activity (i.e. 3 s time window before start of grating motion), (2) the firing rates of the unadapted *E*-vector response to the firing rates of the adapted *E*-vector response (i.e. 3 s time window before start of grating motion), and (3) the firing rates during motion stimulation presented together with polarized light to the firing rates of the adapted *E*-vector response. The firing rate during moving grating plus polarized light stimulation of trials at Φ_{max} differed from that for trials at Φ_{min}, as indicated by non-overlapping notches of boxplots (Fig. 6a).

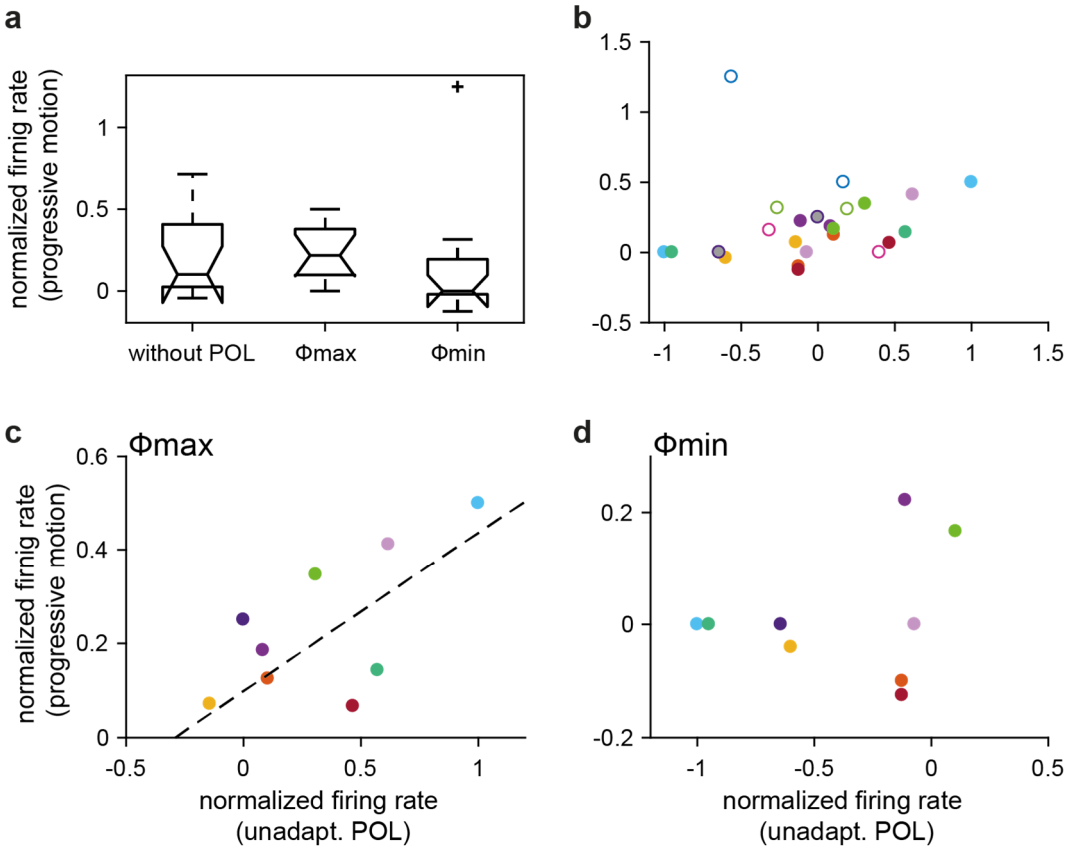

Figure 6. Interaction between *E*-vector and wide-field motion signalling. (a) Boxplots showing the mean firing rate during progressive grating motion, normalized to the mean pre-stimulation firing rate, when presented alone, together with a stationary *E*-vector at preferred angle (Φ_{max}), and at anti-preferred angle (Φ_{min}). N = 12; n = 12. **(b)** Firing rates at stationary polarized light stimulation (unadapt. POL) and during grating stimulation combined with stationary polarized light were normalized to the adapted polarized light response. Normalized firing rates of single trials were averaged (i.e. the median of all values) for presentation at Φ_{max} and for presentation at Φ_{min}, so that each neuron contributed two data points. Open circles indicate neurons showing a regression coefficient (slope) that equals zero or is negative. Grey filled circles indicate a neuron lacking correlation, but with a positive regression coefficient. Coloured filled circles show data from neurons showing correlation, with a positive regression coefficient. Correlation and regression coefficients were determined by analyzing mean firing rates of single trials. n = 12. The neuron from Fig. 5a is represented here as the light blue filled circle, and the neuron from Fig. 5b as the dark blue open circle. **(c)** Scatter plot showing data from **(b)** only for stimulation at Φ_{max} and of those neurons with positive regression coefficient. Colors indicate identical neurons presented in **(b)**. $\rho^2 = 0.5$; $p_{Correlation} = 7\times10^{-3}$; $p_{Regression} = 5^{-4}$; $y = 0.33x + 0.09$; N = 9; n = 9. **(d)** Scatter plot showing data from **(b)** only for stimulation at Φ_{min} and of those neurons showing a positive regression coefficient. Colors indicate identical neurons presented in **(b)**. $\rho^2 = 0.04$; $\beta = 0.05$; $p_{Correlation} = 0.27$; $p_{Regression} = 0.91$; N = 9; n = 9.

However, both firing rates did not differ from the firing rates during moving grating stimulation in the absence of polarized light (Fig. 6a). 8 out of 12 neurons showed correlation between the firing rates of the unadapted response to the *E*-vector and firing rates during progressive motion presented together with stationary polarized light (filled coloured circles in Fig. 6b). All of these 8 neurons had a positive regression coefficient (β; i.e. the slope as revealed by regression analysis) ranging from 0.23 to 0.67. This indicates a higher activity caused by progressive motion when the *E*-vector was at Φ_{max}, and a comparatively lower activity when the *E*-vector was at Φ_{min}. 7 of these 8 neurons had coefficients of determination (ρ^2) greater than 0.25 ($0.28 < \rho^2 < 0.88$), and one smaller than 0.25 ($\rho^2 = 0.18$). One of these neurons is the CL1 neuron shown in Fig. 5a-a''. One neuron showed a positive regression coefficient ($\beta = 0.3$; $\rho^2 = 0.28$), but lacked correlation (Fig. 6a, purple/filled grey). Three neurons lacked correlation as well ($0.01 < \rho^2 < 0.4$) and showed either a regression coefficient equal zero or a negative regression coefficient (open circles in Fig. 6b). One of those neurons is the TB1 neuron shown in Fig. 5b-b''. All neurons with a positive regression coefficient were included in correlation and regression analysis across neurons for motion stimulation at Φ_{max} and Φ_{min}. For stimulation at Φ_{max} firing rates unadapted to the stationary *E*-vector and firing rates at moving grating stimulation were correlated ($\beta = 0.3$; $\rho^2 = 0.5$; Fig. 6c). All neurons showed disadaptation at the preferred *E*-vector angle, as all values on the y-axis were positive. For stimulation at Φ_{min} firing rates were not correlated and the regression coefficient was not different from zero ($\beta = 0.05$; $\rho^2 = 0.04$; Fig. 6d). Only three neurons showed disadaptation of the response to the anti-preferred angle, as indicated by negative values on the y-axis.

Responses to rotational wide-field motion

Three neurons, two CL2 neurons and one TB1 neuron, were tested to wide-field motion simulating a right or left turn of the animal. Progressive motion of the grating on the left LCD screen and simultaneous regressive motion on the right LCD screen simulated a clockwise turn, whereas progressive motion on the right, and regressive motion on the left screen simulated a counterclockwise turn. The TB1 neuron was excited by grating motion simulating a clockwise turn (Fig. 7a), and inhibited by motion simulating a counterclockwise turn (Fig. 7a'). Here the excitatory response outlasted the actual stimulus. The neuron was excited as well by progressive grating motion (Fig. 7a''). The first CL2 neuron was excited in response to the simulated clockwise turn (Fig. 7b), but inhibited in response to the simulated counterclockwise turn (Fig. 7b'). It showed no change in firing rate caused by grating motion. The absolute firing rates between trials differed, because trials were tested several minutes apart from each other. The second CL2 neuron responded to motion simulating a clockwise turn with strong inhibition (Fig. 7c). In contrast it was excited to motion simulating a counterclockwise turn (Fig. 7c'). The neuron could not be tested to progressive wide-field motion.

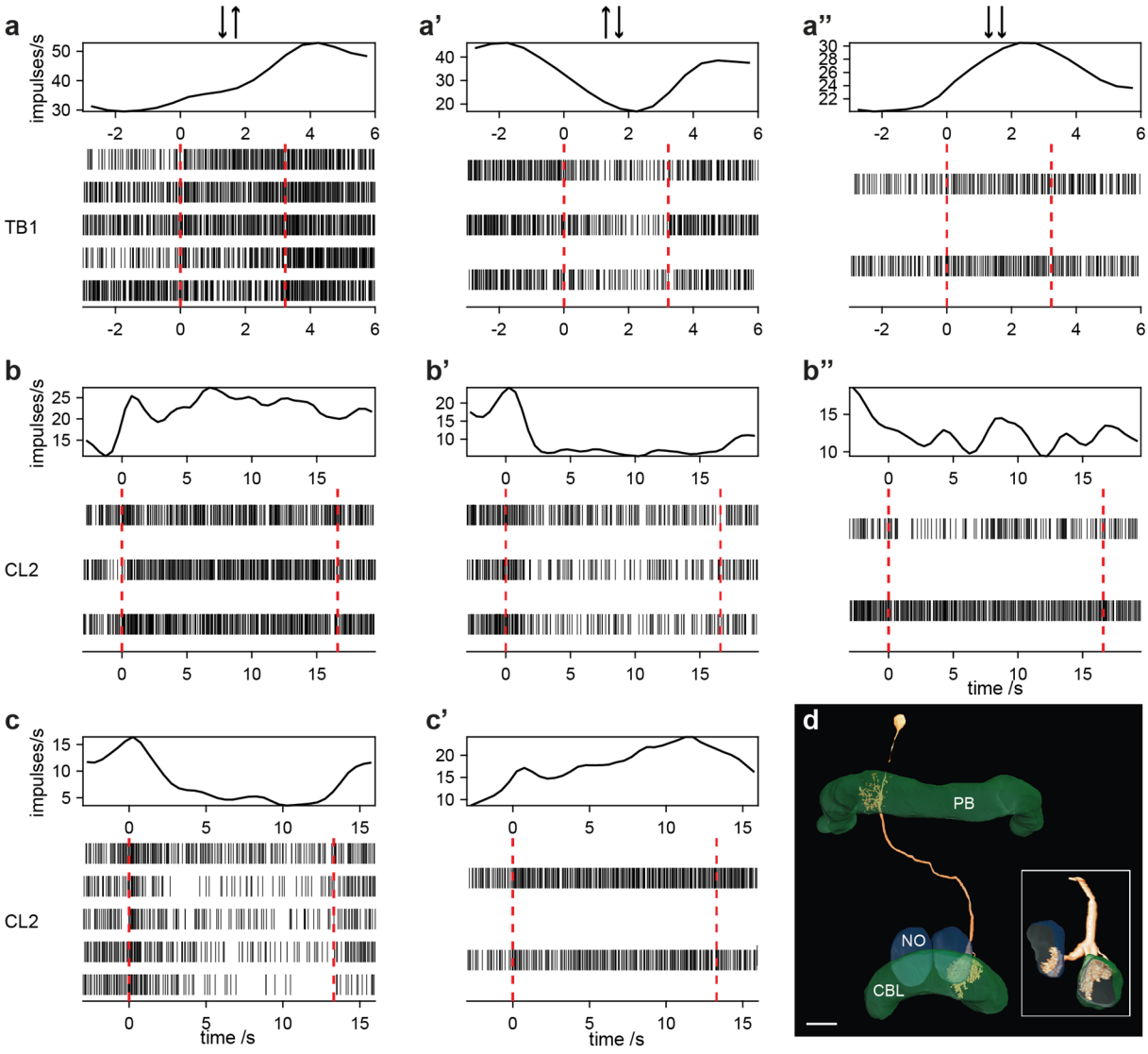

Figure 7. Signalling of rotational wide-field motion. Responses of a TB1 neuron **(a, a', a'')**, a CL2 neuron arborizing in the left nodulus **(b, b', b'')**, and a CL2 neuron arborizing in the right nodulus **(c, c')**. Lower traces show responses to single trials as rasterplots, with first stimulation in the uppermost row. Top traces show smoothed averaged firing rate across all trials. Red dashed lines indicate on- and offset of stimuli. Arrows indicate the direction of wide-field motion on the screens. **(a - c)** Responses to wide-field motion simulating a clockwise rotation. **(a' - c')** Responses to wide-field motion simulating a counterclockwise rotation. **(a'', b'')** Responses to progressive wide-field motion. The CL2 neurons from **c** was not tested to progressive wide-field motion. Stimulus duration in **(a - a'')** was considerably shorter than in **(b - c')**. **(d)** Three-dimensional visualization of the CL2 neuron shown in **b** and its location within the CX neuropils. Main panel shows the neuron from anterior together with surface reconstruction of innervated neuropils. Inset depicts a lateral view. CBL, central body lower division; NO, noduli; PB, protocerebral bridge. Scale bar, 40 µm (main panel and inset).

The soma of the TB1 neuron was located in the right brain hemisphere. Varicose arborizations were located in slices R5 and L4 of the PB. The position of the soma of the first CL2 neuron was also in the right brain hemisphere. The neuron additionally arborized in R4 of the PB, L2 of the CBL, and in the left nodulus (Fig. 7d). The lateral view revealed arborizations in dorsal layers 1-3 of the CBL (Fig. 7d inset). The second CL2 neuron had its soma in the left brain hemisphere. It arborized in L4 of the PB, R2 of the CBL and in the right nodulus.

Discussion

We tested 13 compass neurons of the locust CX to lateral progressive wide-field motion presented in combination with zenithal stationary polarized light. In most neurons we found a disadaptation of the adapted compass response elicited by the wide-field motion. Three CX neurons were tested to grating motion simulating a rotation of the animal around the yaw-axis. All three neurons encoded rotation direction.

Most of the recorded neurons showed correlation and positive regression between the unadapted firing rate of the stationary *E*-vector response and the firing rate caused by wide-field motion. While the response to the preferred *E*-vector was disadapted by wide-field motion, the response to the anti-preferred *E*-vector disadapted only in a minority of neurons and remained largely unaffected by progressive motion. This suggests unidirectional gain modulation of the compass response, rather than bidirectional disadaptation. The effects of wide-field motion observed here, therefore, differ from the comparatively short-term disadaptation of compass responses caused by small moving targets (29). Gain-modulation induced by wide-field motion was generally long lasting, indicating that progressive wide-field motion does not simply trigger the animal's arousal.

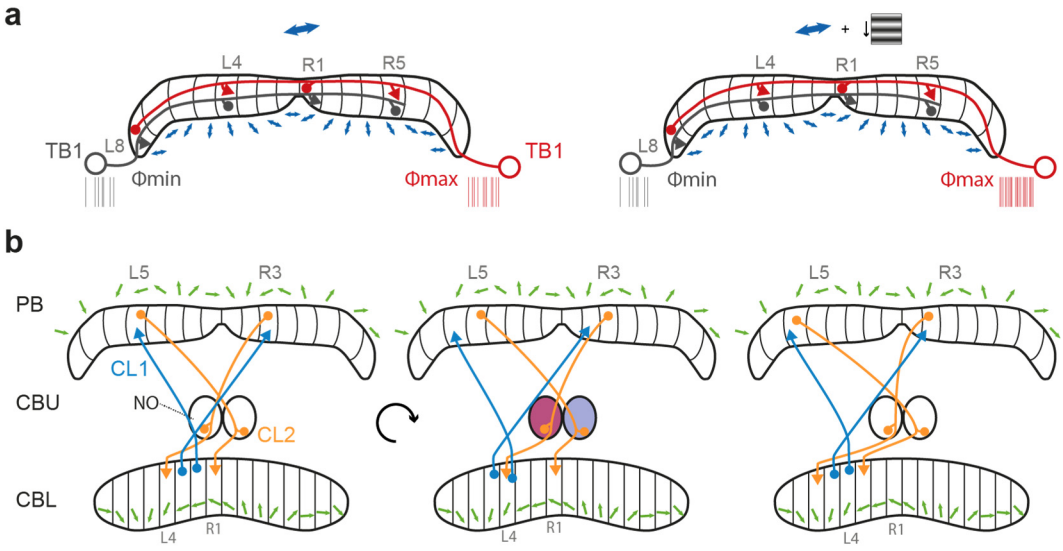

Figure 8. Sky compass signalling in the context of wide-field motion. (a) Illustration of the effect of wide-field motion on sky compass signalling in the locust CX. Two TB1 neurons are shown, one with soma position in the right hemisphere (open circle, red), one with soma position in the left hemisphere (open circle, grey). Arrowheads indicate varicose presynaptic arborizations that appear in two PB slices, separated by 7 slices. Dots indicate postsynaptic arborizations. Vertical lines indicate firing activity. Topographic representation of *E*-vectors across the PB in TB1 neurons is indicated by the blue double arrows. The large blue double arrow indicates a stationary *E*-vector. It is at Φ_{min} for the grey neuron and at Φ_{max} for the red neuron. Only the firing rate of the red neuron changes whenever wide-field motion is experienced in addition to the stationary *E*-vector (right panel). **(b)** Illustration of the possible role of CL2 neurons in the locust sky compass system. Green arrows indicate topographic representation of the azimuth of a light spot in the PB and the CBL. CL1 neurons (blue) coding for the same azimuth have varicose arborizations (arrowheads) in the PB separated by 6 slices and are postsynaptic (dots) in two neighbouring slices in the CBL. Arborizations of CL2 neurons (orange) are smooth in the PB and the noduli (dots) and varicose in the CBL (arrowheads). A clockwise turn (curved arrow, middle panel) of the animal will result in excitation of the CL2 neuron arborizing in the left nodulus (red) and in inhibition (light blue nodulus) of the CL2 neuron arborizing in the right nodulus (blue), activating the CL1 neuron arborizing to the left of the CL1 neuron that has been previously active (right panel). Excited CL1 neurons in turn can activate CL2 neurons arborizing in the same PB slices.

Celestial *E*-vectors are topographically represented in TB1 neurons (13). Recent experiments on TB1 neurons revealed an additional azimuth compass representing the position of the sun or a landmark (14). Modulation of compass responses caused by wide-field motion might lead to an enhanced representation of head direction in the slices of the PB. The compass neurons studied here adapt to stationary polarized light after several seconds (28). Our findings indicate that this adaptation is reduced by the presence of wide-field motion. In an animal experiencing a stationary *E*-vector signal, two gain modulated TB1 neurons in the PB with an *E*-vector preference separated by 90° will show, due to adaptation to near background activity, almost identical firing rate, if one of that preferred *E*-vector is present (Fig. 8a). If the animal experiences, in addition to the *E*-vector signal, progressive wide-field motion, the neuron preferring the current *E*-vector angle will increase its firing rate more strongly than the TB1 neuron not preferring the current angle. This suggests that, whenever the animal experiences progressive wide-field motion, compass neurons arborizing in the PB slice encoding the current *E*-vector will have an increased activity compared to those arborizing in other slices. This situation might happen whenever the animal is flying on a constant course. Gain modulation of locust compass neurons has been shown for small moving targets possibly simulating approaching predators or conspecifics passing by (29). However, as in the present study, some of the tested neurons did not show gain modulation. In *Drosophila* the gain modulation of responses to a variety of visual stimuli caused by an active motor state has been demonstrated for several types of CX neurons (15, 24,30). Therefore, it is possible that the interaction between compass and motion signals in the locust additionally depends on other inputs to the CX such as mechanosensory feedback associated with locomotion or flight.

Two CL2 and one TB1 neuron were tested for wide-field motion simulating rotation of the animal around the yaw axis. All neurons responded with excitation or inhibition dependent on simulated turning direction. The role of CL2 neurons (equivalent to PEN neurons in *Drosophila*) in head direction signalling has been studied in *Drosophila* and in the locust. In *Drosophila* PEN neurons encode the azimuth of a bright bar (30) and turning direction and turning speed of a tethered walking fly (30,31). They are directly connected to EPG neurons (the equivalent to locust CL1 neurons) that signal heading information with respect to the azimuth of a bright bar (30). Owing to the wiring of EPG and PEN neurons in the CBL and the PB, PEN neurons are suited to shift EPG activity across the slices of the CX (32). Locust CL2 and CL1 neurons are involved in *E*-vector signalling (34,35). CL1 neurons additionally encode head direction dependent on the azimuth of an unpolarized green light spot (35), and topographically represent this azimuth across PB and CBL slices, covering roughly 2×360° of circular space (14). The CL2 neurons shown here responded to rotational wide-field motion dependent on the direction of rotation and dependent on the innervated nodulus and PB hemisphere. Although based on only two recordings, our results suggest that CL2 neurons arborizing in the right hemisphere of the PB and the left nodulus are excited by rotation to the right, and inhibited by rotation to the left. The opposite may may be true for CL2 neurons of the left PB hemisphere and the right nodulus.

According to their wiring, CL1 neurons encoding identical heading direction in the PB arborize in two neighboring CBL slices (Fig. 8b). So far it is not known whether CL2 neurons also topographically represent heading directions. Assuming that they show

the same topographic representation of azimuth as CL1 neurons, CL2 neurons with highest activity at a certain head direction would arborize in the same PB slices as the CL1 neurons with highest activity. In the CBL these two CL2 neurons target the slices located directly next to the two neighbouring slices occupied by the CL1 neurons (Fig. 8b). Whenever the animal turns to the right or left, the activity peak of CL1 neurons needs to be shifted across the PB and CBL from right to left or left to right, respectively. During a right turn the CL2 neuron arborizing to the left of the two neighbouring slices, invaded by the CL1 neurons encoding the current heading direction, will be strongly excited (Fig. 8b). It is, therefore, well suited to support a shift of CL1 activity to the left by excitatory synaptic connection with the CL1 neuron arborizing in the same CBL slice. Similarly the CL2 neuron arborizing to the right of the two neighbouring slices, invaded by the excited CL1 neurons, will be inhibited by motion simulating a turn to the right, preventing a shift of CL1 activity to the right. In bees two types of tangential neuron (TN1, TN2) likely providing input to one of the noduli encoded the direction of translational optic flow (11). In the locust corresponding neurons invading the noduli have not been studied physiologically. An anatomical study, however, uncovered four bilateral pairs of neurons with smooth arborizations in the LAL and beaded or varicose terminals in the ipsilateral nodulus (36). These cells might be suited, as in the bee, to provide motion information to the CX. As locust CL2 neurons have fine and thus likely postsynaptic arborizations in the noduli, these ramifications are promising sites to receive motion signals from presynaptic partners. Turning information may additionally come from ascending information associated with motor activity in a walking or flying animal (37), but as our results show, the presence of a visual stimulus simulating a rotation is sufficient to strongly increase or decrease CL2 activity. The TB1 neuron responded to the rotational wide-field motion in a similar way as the CL2 neuron with soma in the same brain hemisphere. This finding might indicate that turning information encoded by CL2 neurons is transferred onto other compass neurons of the PB.

Some of our findings are similar to characteristics of the head direction system in the mammalian brain. Like the compass cells of insects head direction cells of rats encode the animals' heading relative to a landmark or salient visual cue (38). They exhibit a preferred angle of the cue relative to the animal's head or vice versa. The cell's firing rate changes according to head rotation when the animal is moving and the landmark is stationary (38). As in our experiments with the locust, the firing rate of rat head direction cells is likewise modulated when the cue changes position (39). In the rat the self-motion is important and sufficient for head direction coding (40,41), but the presence of visual cues enhances accuracy and updating of head direction coding (42,43). To these belong salient cues such as landmarks (42), which in the case of the locust would be substituted by celestial cues such as the solar azimuth or the polarization pattern. In addition rats can exploit optic flow to keep their internal heading representation updated (44,45), which is similar to the model we propose here for CL2 neurons in the locust.

In conclusion we showed here that wide-field progressive and rotational motion is integrated in the locust CX head-direction signalling network. Our findings suggest that wide-field motion is important for straight flight on a constant course as well as for maintaining the representation of the current heading direction during course changes.

Materials and methods

Animals and preparation

Desert locusts (*Schistocerca gregaria*) were reared under crowded conditions in a 12:12 h light:dark cycle. Only adult animals were used for experiments. Animals were mounted onto a metal holder using dental wax, with their anterior-posterior body axis oriented vertically (46). Wings and legs were cut off. The head capsule was opened from anterior, and fat tissue and tracheal air sacs were removed. In order to reduce body movements, muscles close to the brain were cut, and the gut was removed through an inscision in the abdomen. Mouthparts, leg stumps, and abdomen were immobilized by wax. A small twisted metal wire was positioned posterior to the brain for further stabilization. To allow penetration of the electrode the neural sheath covering the central brain was opened and partly removed. During preparation and intracellular recordings the brain was constantly immersed in locust saline (47) containing 0.09 mol l^{-1} saccharose.

Electrophysiology and visual stimulation

Sharp glass microelectrodes were drawn from borosilicate capillaries (Hilgenberg) using a Flaming/Brown horizontal electrode puller (P-97, Sutter Instrument). Electrode tips were filled with 1 mol l^{-1} KCl, containing 4% Neurobiotin (Vector Laboratories). Electrode shanks were filled with 1 mol l^{-1} KCl. Neuronal signals were amplified 10× (SEC5-LX amplifier; NPI), visualized by an oscilloscope (HM507 combiscope, Hameg Instruments), digitized by an analog-to-digital converter (CED1401 micro; Cambridge Electronic Design) at a rate of 20 kHz, and stored on a PC using the software Spike2 (Version 6.02, Cambridge Electronic Design). Linearly polarized light was generated by passing light of a blue LED (ELJ-465-617, 465 nm, EPIGAP Optoelektronik) through a polarizer (HN38S, Polaroid). The polarization stimulus device was positioned dorsally to the animal to stimulate the dorsal part of the eye (Fig. 1b). The polarized light stimulus covered a visual angle of 3.2° and had an intensity of 10^{14} photons cm^{-2} s^{-1}. The polarizer was rotated at angular velocities of 30°/s. Wide-field motion stimuli were generated by two LCD screens (8”TFT-LCDTouch, Faytech) one on each side of the animal (Fig. 1). They had a resolution of 800 × 600 pixels and a frame rate of 75 Hz. The Michelson contrast of monitor stimuli was 0.97, calculated with luminances of 70 cd/m^2 (bright monitor) and 1 cd/m^2 (dark monitor) measured with an OptiCAL photometer (Cambridge Research Systems). The light emitted by the LCD screens was depolarized by means of diffuser sheets mounted in front of the displays. Stimulus protocols were written in MATLAB (Version 2017a, The Math Works) using the Psychophysics Toolbox (48,49). Sinewave gratings were presented with a horizontal and vertical extent of 108° and with a spatial frequency of 39°/cycle. Throughout the duration of the recordings stationary gratings were always present except for the periods of motion. When moving they ran with a temporal frequency of 6 cycles per second. At the end of the recording Neurobiotin was injected into the neuron by applying a positive constant current of approximately 1 nA for several minutes.

Histology and image processing

After recording, brains were dissected in locust saline, immersed over night at 4°C in fixative containing 4% paraformaldehyde, 0.25% glutaraldehyde and 0.2% saturated picric acid diluted in 0.1 mol l^{-1} phosphate buffered saline (PBS). Brains were stored at 4°C in sodium phosphate buffer. They were incubated in PBS with 0.3% Triton X-100 and

Cy3 conjugated streptavidin (1:1000) for three days and dehydrated in an ascending ethanol series (30%, 50%, 70%, 90%, 95%, 100%), each step for 15 min. Brains were cleared in a mixture of 100% ethanol and methyl salicylate (1:1) for 20 min, and subsequently in 100% methyl salicylate for 1 h. Finally, brains were embedded between two cover slips using Permount mounting medium (Fisher Scientific). Neurons were visualized by scanning the preparations with a confocal laser scanning microscope (Leica). Cy3 was detected using a DPSS laser (561 nm). The software AMIRA (version 5.4.5, FEI Visualization Sciences Group) served to inspect the scans visually and to reconstruct neuropils. Visualization of the CL2 neuron in Fig. 7 was achieved by a threshold-based volume-rendering algorithm in AMIRA.

Experimental design and statistical analysis

Recording traces were visualized using Spike2. Action potentials were detected as events with a threshold based mechanism. The data were exported to a mat-file. All subsequent analysis was performed using custom functions written in MATLAB. For analyzing the responsiveness of a neuron to polarized light a stimulus response curve was obtained by calculating the mean spiking activity occurring during 360° rotation of the polarizer in 10° bins. A directed modulation of spike rate by the orientation of the *E*-vector was determined by an angular-linear correlation analysis (50). The responsiveness of the neuron to a stimulus was indicated by the significance (α=0.05) of the correlation coefficient (r_{al}). To calculate the preferred *E*-vector (Φ_{max}) spike times were transformed into angles by multiplying them with the stimulus rotation velocity. From these angles the mean vector Φ was calculated (51) and defined as the preferred angle (Φ_{max}). The anti-preferred angle (Φ_{min}) was defined as the angle 90° to Φ_{max}. Where necessary transformations from axial to circular scale were performed by doubling spike angles (51).

The moving grating stimulus lasted for 3.2 s for tests of CL1 and TB1 neurons and 16.6 s or 13.3 s for tests of CL2 neurons. For combined stimulation of polarized light and progressive motion, pre-stimulus activity (i.e. the adapted *E*-vector response) was calculated in a 3 s time window right before motion onset. CL1 and TB1 neurons were tested at least three times for each stimulus condition: progressive motion presented alone, together with the preferred *E*-vector angle, and together with the anti-preferred *E*-vector angle. Only in two neurons the trial number for one of the stimulus condition was two instead of three.

For better comparison between the unadapted firing rates in response to the stationary polarizer and the firing rates occurring during wide-field motion, both were normalized to the adapted firing rate in response to the stationary polarizer.The adapted firing rate was determined in a 3 s time window before onset of grating motion. The unadapted mean firing rate was calculated (only once for all subsequent trials of motion stimuli) within 2 s after offset of polarizer rotation (i.e. at the onset of stationary polarized light). The mean firing rate during grating presentation was calculated for each trial in 0.5 s bins within a 3 s time window starting with onset of the moving grating stimulus. Normalized firing rates were obtained by subtracting and dividing by the adapted firing rate.

Responsiveness to moving grating stimuli in general was determined by comparing the mean firing rate in the 3 s pre-stimulus time window with the mean firing rate during wide-field motion across trials, using a two-tailed paired-sample t test. Correlation between normalized firing rates during wide-field motion stimulation and normalized unadapted firing rates to polarized light was determined by simple linear

correlation (50). Data were tested for a correlation coefficient (ρ) equal or unequal zero on a significance level of $\alpha = 0.05$. For regression analysis the regression coefficient (β), which is the slope of the regression fit-line and the y-intercept were calculated. Data were tested for a regression coefficient equal or unequal zero (significance level $\alpha = 0.05$). The coefficient of determination (ρ^2) gives an estimate of the strength of straight-line relationship. A ρ^2 exceeding 0.25 indicates by convention a strong relationship.

The smoothed mean activity was determined by calculating the mean firing rate across trials within 0.5 s bins. A smoothing spline was fitted onto the resulting peristimulus time histogram (PSTH) using the MATLAB curve fitting toolbox. The smoothing parameter was set to 0.85 in Fig. 5 and Fig. 7 (18, 38 or 45 array elements).

In boxplots (Figs. 3,6a) the boxes range from the 25th (Q1) to 75th (Q3) percentile. Outliers were defined as data points less than $Q3-1.5\times(Q3-Q1)$ and greater than $Q3+1.5\times(Q3-Q1)$. Whiskers extend to the adjacent value that is the most extreme data point, which is not an outlier. Notches indicate the 95% confidence interval of the median. Two medians with non-overlapping confidence intervals were termed truly different at the 5% confidence level.

Acknowledgements

This work was supported by Deutsche Forschungsgemeinschaft grants HO 950/23-1 and HO 950/24-1. We thank Ronja Hensgen for assistance with AMIRA and Martina Kern for maintaining locust cultures.

Author contributions

U.P. and R.R. and U.H. planned and designed the study; R.R designed and built the setup for visual stimulation and programmed the visual stimuli; U.P. and R.R. performed the experiments; U.P. analyzed the data; U.P. and U.H. interpreted the data; U.P. provided the first draft of the manuscript; U.P. and U.H. edited the manuscript. All authors gave final approval for publication.

References

1. Brines, M. L. & Gould, J. L. Bees have rules. *Science* **206,** 571-573 (1979).

2. Rossel, S. & Wehner, R. Celestial orientation in bees: The use of spectral cues. *J. Comp. Physiol.* **155,** 605-613 (1984).

3. Wehner, R. The ant's celestial compass system: Spectral and polarization channels. In *Orientation and Communication in Arthropods* (ed. Lehrer, M.) 145-185. (Birkhäuser, 1997).

4. von Frisch, K. Die Polarisation des Himmelslichtes als orientierender Faktor bei den Tänzen der Bienen. *Experientia* **5,** 142-148 (1949).

5. Dacke, M., Baird, E., Byrne, M., Scholtz, C. H. & Warrant, E. J. Dung beetles use the milky-way for orientation. *Curr. Biol.* **23,** 298-300 (2013).

6. el Jundi, B., *et al.* Neural coding underlying the cue preference for celestial orientation. *Proc. Natl. Acad. Sci. U S A* **112,** 11395-11400 (2015).

7. Mappes, M. & Homberg, U. Behavioral analysis of polarization vision in tethered flying locusts. *J. Comp. Physiol. A* **190,** 61-68 (2004).

8. Vitzthum, H., Müller, M. & Homberg, U. Neurons of the central complex in the locust *Schistocerca gregaria* are sensitive to polarized light. *J. Neurosci.* **22,** 1114-1125 (2002).

9. Sakura, M., Lambrinos, D. & Labhart, T. Polarized sky light navigation in insects: model and electrophysiology of e-vector coding by neurons in the central complex. *J. Neurophysiol.* **99,** 667-682 (2008).

10. Heinze, S. & Reppert, S. M. Sun compass integration of skylight cues in migratory monarch butterflies. *Neuron* **69,** 345-358 (2011).

11. Stone, T. *et al*. An anatomically constrained model for path integration in the bee brain. *Curr. Biol.* **27,** 3069-3085 (2017).

12. Seelig, J. D. & Jayaraman, V. Neural dynamics for landmark orientation and angular path integration. *Nature* **521,** 168-191 (2015).

13. Heinze, S. & Homberg, U. Maplike representation of celestial *E*-vector orientations in the brain of an insect. *Science* **315,** 995-997 (2007).

14. Pegel, U., Pfeiffer, K., Scholtyssek, C. & Homberg, U. Two compasses in the central complex of the locust brain. *J Neurosci* under review (2018).

15. Rosner, R. & Homberg, U. Widespread sensitivity to looming stimuli and small moving objects in the central complex of an insect brain. *J. Neurosci.* **33,** 8122-8133 (2013).

16. Bockhorst, T. & Homberg, U. Compass cells in the brain of an insect are sensitive to novel events in the visual world. *PLoS One* 10**,** 10.1371/journal.pone.0144501 (2015).

17. Kathman, N. D., Kesavan, M., & Ritzmann, R. E. Encoding wide-field motion and direction in the central complex of the cockroach *Blaberus discoidalis*. *J. Exp. Biol.* **217,** 4079-4090 (2014).

18. Weir, P. T. & Dickinson, M. H. Functional divisions for visual processing in the central brain of flying *Drosophila*. *Proc. Natl. Acad. Sci. U.S.A.* **112,** E5523-5532 (2015).

19. Rowell, C. H. F. & Reichert, H. Three descending interneurons reporting deviation from course in the locust. II Physiology. *J. Comp. Physiol. A* **158,** 775-794 (1986).

20. Hensler, K. The pars intercerebralis neurone PI(2)5 of locusts: convergent processing of inputs reporting head movements and deviations from straight flight. *J. Exp. Biol.* **140,** 511-533 (1988).

21. Reichert, H. Sensory inputs and flight orientation in locusts. *Comp. Biochem. Physiol. A* **104,** 647-657 (1993).

22. Baader, A. Simulation of self-motion in tethered flying insects: an optical flow field for locusts. *J. Neurosci. Meth.* **38,** 193-199 (1991).

23. Sherman, A. & Dickinson, M. H. A comparison of visual and haltere-mediated equilibrium reflexes in

the fruit fly *Drosophila melanogaster*. *J. Exp. Biol.* **206,** 295-302 (2003).

24. Seelig, J. D. & Jayaraman, V. Feature detection and orientation tuning in the *Drosophila* central complex. *Nature* **503,** 262-266 (2013).

25. Weir, P. T., Schnell, B. & Dickinson, M. H. Central complex neurons exhibit behaviorally gated responses to visual motion in *Drosophila*. *J. Neurophysiol.* **111,** 62-71 (2014).

26. Rind, F. C., Santer, R. D. & Wright, G. A. Arousal facilitates collision avoidance mediated by a looming sensitive visual neuron in a flying locust. *J. Neurophysiol.***100,** 670-680 (2008).

27. Heinze, S. & Homberg, U. Neuroarchitecture of the central complex of the desert locust: intrinsic and columnar neurons. *J. Comp. Neurol.* **511,** 454-478 (2008).

28. Bockhorst, T. & Homberg, U. Amplitude and dynamics of polarization-plane signaling in the central complex of the locust brain. *J. Neurophysiol.* **113,** 3291-3311 (2015).

29. Bockhorst, T. & Homberg, U. Interaction of compass sensing and object-motion detection in the locust central complex. *J. Neurophysiol.* **118,** 496-506 (2017).

30. Turner-Evans, D. *et al.* Angular velocity integration in a fly heading circuit. *Elife* 6, 10.7554/eLife.23496 (2017).

31. Green, J. *et al.* Neural circuit architecture for angular integration in *Drosophila*. *Nature* **546,** 101-106 (2017).

32. Kakaria, K. S. & de Bivort, B. L. Ring attractor dynamics emerge from a spiking model of the entire protocerebral bridge. *Front. Behav. Neurosci.* 11, 10.3389/fnbeh.2017.00008 (2017).

33. Heinze, S., Gotthardt, S. & Homberg, U. Transformation of polarized light information in the central complex of the locust. *J. Neurosci.* **29,** 11783-11793 (2009).

34. Heinze, S. & Homberg, U. (2009) Linking the input to the output: New sets of neurons complement the polarization network in the locust central complex. *J. Neurosci.* **29,** 4911-4921 (2009).

35. Pegel, U., Pfeiffer, K. & Homberg, U. Integration of celestial compass cues in the central complex of the locust brain. *J. Exp. Biol.* **221,** 10.1242/jeb.171207 (2018).

36. Homberg, U., Seyfarth, J., Binkle, U., Monastirioti, M. & Alkema, M. Identification of distinct tyraminergic and octopaminergic neurons innervating the central complex of the desert locust, *Schistocerca gregaria*. *J. Comp. Neurol.* **521,** 2025-2041 (2013).

37. Homberg, U. Flight-correlated activity changes in neurons of the lateral accessory lobes in the brain of the locust Schistocerca gregaria. *J. Comp. Physiol.* **175,** 597-610 (1994).

38. Taube, J. S., Muller, R. U., Ranck, J. B. Head-direction cells recorded from the postsubiculum in freely moving rats. I. Description and quantitative analysis. *J. Neurosci.* **10,** 420-435 (1990).

39. Taube, J. S., Muller, R. U., Ranck, J. B. Head-direction cells recorded from the postsubiculum in freely moving rats. II. Effects of environmental manipulations. *J. Neurosci.* **10,** 436-447 (1990).

40. Shinder, M. E., Taube, J. S. Active and passive movement are encoded equally by head direction cells in the anterodorsal thalamus. *J. Neurophysiol.* **106,** 788-800 (2011).

41. Shinder, M. E., Taube, J. S. Self-motion improves head direction cell tuning. *J. Neurophysiol.* **111,** 2479-2492 (2014).

42. Goodridge, J. P., Taube, J. S. Preferential use of the landmark navigational system by head direction cells in rats. *Behav. Neurosci.* **109,** 49-61 (1995).

43. Goodridge, J. P, Dudchenko, P. A., Worboys, K. A., Golob, E. J., Taube, J. S. Cue control and head direction cells. *Behav. Neurosci.* **112,** 749-761 (1998).

44. Yoder, R. M. *et al.* Both visual and idiothetic cues contribute to head direction cell stability during navigation along complex routes. *J. Neurophysiol.* **105,** 2989-3001 (2011).

45. Arleo A. *et al.* Optic flow stimuli update anterodorsal thalamus head direction neuronal activity in rats. *J. Neurosci.* **33,** 16790-16795 (2013).

46. Pfeiffer, K., Kinoshita, M. & Homberg, U. Polarization-sensitive and light-sensitive neurons in two parallel pathways passing through the anterior optic tubercle in the locust brain. *J. Neurophysiol.* **94,** 3903-3915 (2005).

47. Clements, A. N. & May, T. E. Studies on locust neuromuscular physiology in relation to glutamic acid. *J. Exp. Biol.* **60,** 673–705 (1974).

48. Brainard, D. H. The psychophysics toolbox. *Spat. Vis.* **10,** 433-436 (1997).

49. Pelli, D. G. The VideoToolbox software for visual psychohysics: transforming numbers into movies. *Spat. Vis.* **10,** 437-442 (1997).

50. Zar, J. H. *Biostatistical Analysis* (4th ed.) (Prentice Hall, 1999).

51. Batschelet, E. *Circular Statistics in Biology*. (ed. Sibson, R. & Cohen, J. E.) (Academic Press, 1981).

Appendix

Processing polarized light from ventral direction in the locust brain

Many insect species use polarization caused by reflection of light on surfaces for the detection of water bodies. Especially aquatic insects have been studied in this respect. Many of them show a positive polarotaxis (meaning they are attracted) to polarization coming from ventral directions, like the backswimmer (Schwind, 1983a), the dragonfly (Wildermuth, 1998), the mayfly (Kriska et al., 2007), the yellow fever mosquito (Bernáth et al., 2012) and tabanid flies (Egri et al., 2012). In the fruit fly a polarotaxis was demonstrated as well (Wernet et al., 2011). These animals, however, showed alignment with the plane of polarized light presented from ventral direction. A ventral region of the compound eye with specialized photoreceptors has been shown in the backswimmer (Schwind et al., 1984; Schwind, 1983b) and the dragonfly (Armett-Kibel and Meinertzhagen, 1983), allowing the animals to detect polarized light coming from ventral directions. However, photoreceptors differ to those of the DRA (Heinloth et al., 2018). In the fruit fly such specialized photoreceptors organized in a clearly defined ventral region have not been shown so far. Nonetheless, individual photoreceptors of the ventral main retina are less twisted than sourrounding photoreceptros (Wernet et al., 2011). In untwisted photoreceptors microvilli are strictly aligned, which is a prerequisite for detecting polarized light (see *Introduction* for further explanation).

The locust *Schistocerca gregaria* is suggested to exhibit negative polarotaxis (meaning it is repelled) to reflections coming from the ground (Shashar et al., 2005). Animals could use this capabiltiy to avoid flying over the sea. These suggestions are based on the observation of a desert locust swarm flying around the gulf of Aqaba and on one field study, in which polarization was induced by a mirror (Shashar et al., 2005). A ventral polarization sensitive eye region region is therefore suggested for the locust, but remains to be shown (Horváth, 2014). Recordings from photoreceptors in the main retina of the locust showed that they are indeed polarizaton sensitve, especially in the green range of light, but polarization sensitvity is relatively weak compared to that of DRA photoreceptors (Schmeling et al., 2015). As the locust CX is known as a higher integration center likely producing a goal directed motor output, I wanted to study the responsiveness of CX neurons to polarized light coming from ventral direction. For intracellular recordings the animal was turned with its ventral side towards the polarizer, and the DRA was painted black to avoid perception of polrized light by DRA photoreceptors (Fig. 1).

I recorded from one TL2 neuron, one CL1 neuron, 4 CPU1 neurons, one CPU5 neuron, one CP1 neuron and one CP2 neuron. Except the CP1 and the CPU5 neuron none of the cell types was responsive. The response of the TL2 neuron is shown in Fig. 1*A*. So far almost no physiological data on CPU5 neurons exist. CPU5 neurons show fine arborizations in the upper division of the contralateral nodulus and an ipsilateral slice of the PB, and additionally varicose arborizations in the second layer of the CBU (Fig. 1*B*; Heinze and Homberg, 2008). The CPU5 neuron was responsive to two consecutive 360° rotations of the polarizer. However, the neuron was tested only three times. The CP1 neuron also responded to the ventral *E*-vector (Fig. 1*C*). The preferred angle was approximately at 90°, which is a hallmark of polarization on water surfaces close to the observer (Fig. 2*D*,*E*; Horváth, 1994; Horváth and Varju, 1997). The neuron likely arborized in slice L3 of the PB. According to the internal *E*-vector compass shown for CPU2, CP1 and CP2 neurons in Chapter 2, CP1 neurons arborizing in L3 are

assumed to have a preferred *E*-vector angle of approximately 90°. The recording of the CP1 neuron was the only one conducted without painting the DRA black, so that the detection of polarization caused by reflection of the polarized light on any surface behind the animalscannot be excluded with certainty.

Fig. 1. Locust head from dorsal view. Pictures illustrating the painting of the DRA (dorsal rim area). Left panel: Animal with DRA exposed. Right panel: Same animal with DRA painted black. Pictures taken by Vanessa Althaus.

Some additional recordings have been performed by a master student I supervised, Vanessa Althaus. She recorded from two CL1 neurons, 6 TB1 neurons, three CPU1 neurons and four pontine neurons. None of the recorded neurons showed a consistent polarization sensitivity. Pontine neurons connect distinct ipsilateral slices of the CBU with distinct contralateral slices of the CBU (Heinze and Homberg, 2008), and are reported to be sensitive to looming stimuli (Rosner and Homberg, 2013). One pontine neuron responded to the stimulus, however in only one out of 5 tests (data not shown). In conclusion the results indicate that most neurons of the CX involved in processing polarization perceived from dorsal directions do not process polarization originating from ventral directions. In contrast, the CPU5 neuron was responsive. CPU5 neurons may not be involved in processing polarized light from dorsal directions via the DRA (Pegel, 2014). Instead they might be involved in processing signals perceived by the main retina, like the azimuth of an unpolarized light spot (Pegel, 2014). However, these suggestions have been made based on only one recording. Owing to the low sample size for responsive CX neurons any suggestions about the involvement of the CX in ventral polarization vision are highly speculative. If the ventral polarization signal is fed into the CX network (e.g. via the noduli and CPU5 neurons), it is most likely not integrated with the polarization signal from dorsal direction.

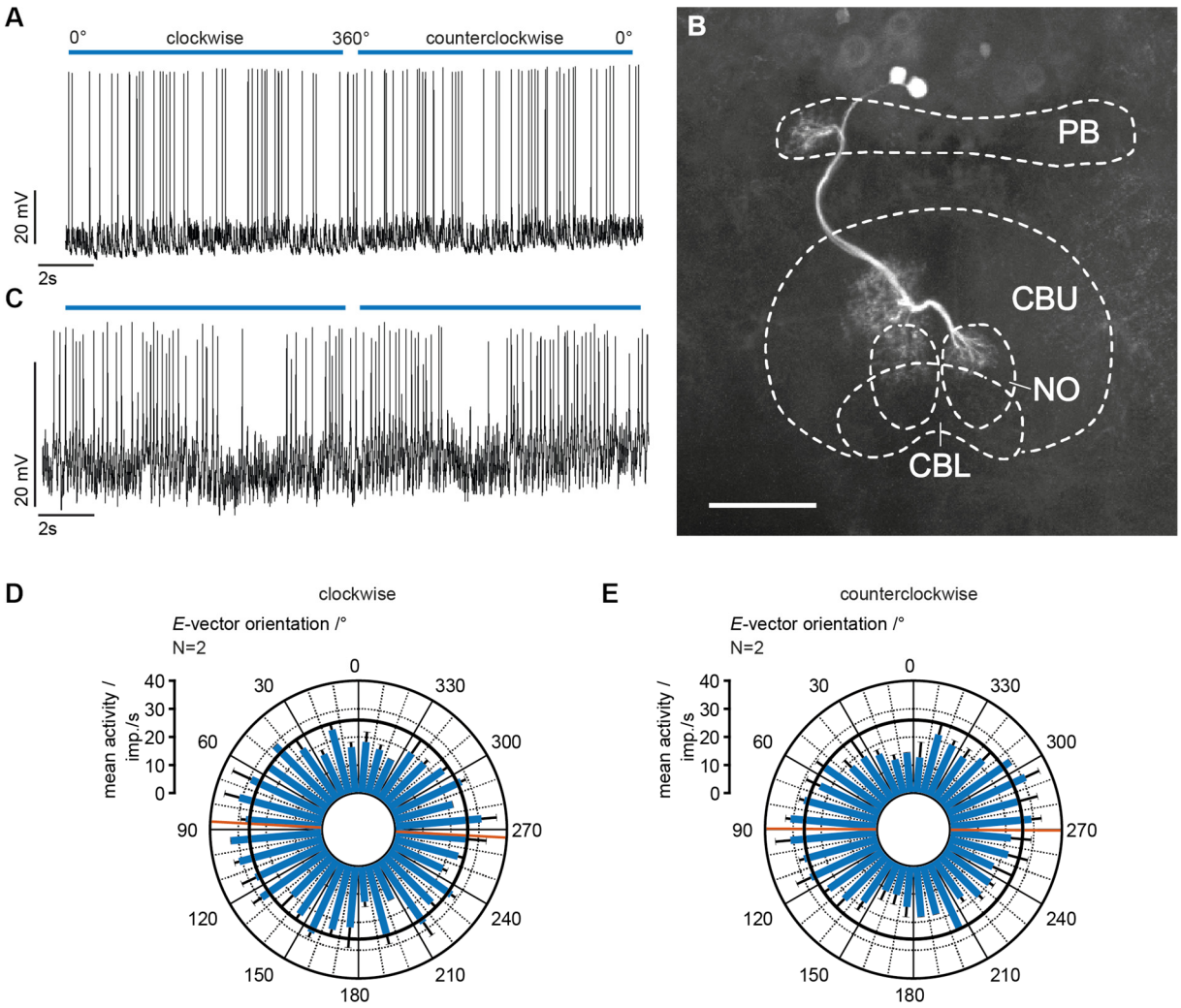

Fig. 1. Morphology and responses of CX neurons to polarized light from ventral direction. ***A,*** Spike train showing the response of a TL2 neuron to a clockwise rotation of the polarizer and a counterclockwise rotation. Polarizer and blue LED were positioned at the ventral side of the animal. The neuron was not responsive in both tests. It was similarly not responsive in all other tests. ***B,*** Projection view of confocal image stacks of a CPU5 neuron. Two neurons were stained, but both invaded the same slices in the PB and the CBU. Scale bar = 100 µm. ***C,*** Spike train showing the response of the CPU5 neuron from B to a clockwise and a counterclockwise rotation of the polarizer. ***D, E,*** Circular histograms showing the responses of a CP1 neuron to clockwise (***D***) and counterclockwise (***E***) rotation of the polarizer. The neuron was inhibited at Φ_{min} and only little excited at Φ_{max}. Blue bars indicate mean spiking activity. Black bars indicate standard deviations. Black circles indicate background activity. N, number of tests. Red line indicates the preferred E-vector (Φ_{max}). ***D,*** $p = 3\times10^{-4}$; $\rho^2 = 0.4$; $\Phi_{max} = 87°$. ***E,*** $p = 10^{-5}$; $\rho^2 = 0.6$; $\Phi_{max} = 90°$.

Besides CX neurons Vanessa recorded from 5 neurons of the lobula and three descending neurons. Two of the lobula neurons have not been described yet, and did not respond to the stimulus. However, three neurons of the lobula belonged to the LPM1 type (Gewecke and Hou, 1993). They connect the two lobulae. In the ipsilateral brain hemisphere neurons invaded the inner lobula and the outer lobula with smooth arborizations (Fig. 2*A*). In the contralateral hemisphere they invaded as well the inner lobula and parts of the outer lobula. Some single branches extended into the medulla (Fig. 2*A*) and the dorsal lobula (not visible in Fig. 2). So far, these cells were described to respond to motion sitmuli and looming stimuli (Gewecke and Hou, 1993). One neuron showed a preferred *E*-vector orientation for both rotation directions (clockwise and counterclockwise) of 93° (data not shown). Another neuron responded only to counterclockwise stimulation (Φ_{max} = 143°).

The LPM1 neuron shown in Fig. 2*A* was tuned to an *E*-vector of 43°, but only during clockwise rotations (Fig. 2*B*). Neurons connecting the ipsilateral outer lobula with the contralateral outer and inner lobula (termed IL neurons) have already been shown to process polarized light presented at an elevation of 90°, possibly mimicking the reflection of light on water located on the horizon (Beetz et al., 2016). Responses were not affected by painting the DRA, thus IL neurons most likely process polarized light perceived by the main retina. As LPM1 and IL neurons arborize in the same compartments of the lobula, the recordings shown here confirm the possible role of the outer and inner lobula in processing polarized light coming from ventral directions. Likewise preferred *E*-vector orientations of IL neurons varied between recordings and were not fixed at 90° (Beetz et al., 2016). The morphology of one of the descending neurons has not been described, yet. It was not responsive to the stimulus (data not shown). However two of the descending neurons were responsive. Of these one belonged to the PI(2):6 type (Fig. 2*C*) and one to the PI(2):5 type (Fig. 2*F*) described by Williams (1975). The PI(2):6 neuron was not responsive to counterclockwise rotation of the polarizer (Fig. 2*D*), but showed a preferred *E*-vector during clockwise rotations (Fig. 2*E*). The PI(2):5 responded with phasic inhibition in the first two rotations of the polarizer. Here the neuron showed a preferred *E*-vector of 32° (not shown) and of 81° (Fig. 2*G*). In all consecutive rotations it was tonically inhibited and did not respond to the *E*-vector anymore (Fig. 2*F*). Rapidly vanishing responses to polarized light have been shown in a recording of one IL neuron (Beetz et al., 2016). The neuron was tested for polarized light at different elevations. It showed phasic responses only during the very first rotation of the polarizer at each elevation, whereas all consecutive stimulations evoked tonic excitation. This phenomenon might reflect some kind of novelty detection, which might be required on a behavioral level for a water aviodance response.

When the locust approaches a water surface it might detect the horizontal (90°) *E*-vector directly below. Dependent on how large the surface is, *E*-vectors further away (i.e. at less negative elevations) can have different orientations as the polarization pattern is partly mirrored on water surfaces (Zhou et al., 2013; Horvath, 1994). Consequently, if the locust turns in front of a water surface, the *E*-vector to its very ventral side will remain constant (90°), independent of the turning direction. In contrast *E*-vectors closer to the horizon (i.e. at less negative elevations) will change their orientation relative to the animal depending on its turning direction.

If the activity of PI(2):5 and PI(2):6 neurons is simply added up in the thoracic ganglia, the response to the 90° *E*-vector might result in excitation in the first place (no inhibition of PI(2):5 and excitation of PI(2):6). Later the excitation of PI(2):6 might be suppressed by the ongoing inhibition of PI(2):5. This could result in a nonrecurring aviodance respone (i.e. turn to the right or left). In the context of behavior it might be necessary that the animal does not turn away as long as the water is still in sight. The locust swarm that was flying around the gulf of Aqaba (Shashar, 2005) flew along the coast line where the water still might be visible to the animals. For this maneuver the avoidance response should be supressed after some time, otherwise the animal might turn towards the direction it originally came from.

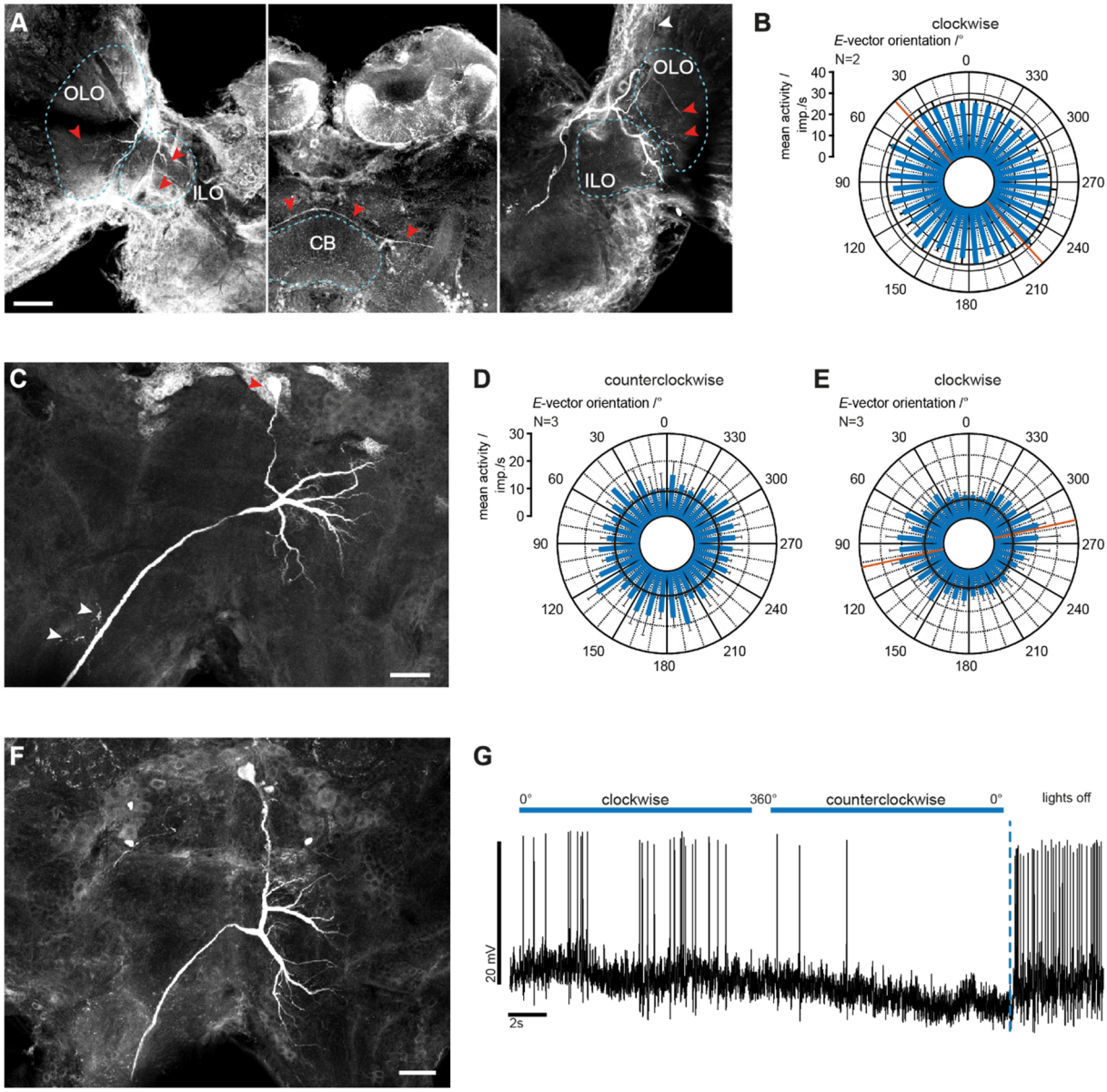

Fig. 2. Morphology and responses of optic lobe and descending neurons. ***A,*** Projection view of confocal image stacks of a LPM1 neuron. Neuropil boundaries are indicated by cyan dashed lines. Arborizations in the left outer (OLO) and inner lobula (ILO) were smooth (left panel, red arrowheads). The primary neurite passed the protocerebrum antero-dorsally to the CB (central body; middle panel; red arrowheads). Arborizations in the right OLO and ILO were varicose (right panel; red arrowheads). One additional branch extended into the medulla (white arrowhead). The position of the soma could not be determined. ***B,*** Circular histogram showing the response of the neuron from ***A*** to the polarizer rotating in clockwise direction. Blue bars indicate mean spiking activity. Black bars indicate standard deviations. Black circles indicate background activity. N, number of tests. Red line indicates the preferred E-vector (Φ_{max}).The neuron was inhibited at Φ_{min}. $p = 5\times10^{-3}$; $\rho^2 = 0.3$; $\Phi_{max} = 43°$. ***C,*** Projection view of confocal image stacks of a PI(2):6 neuron. The soma was located in the pars intercerebralis (red arrowhead). Arborizations in the ipsilateral protocerebrum were smooth, arborizations close to the antennal mechanosensory and motor center (AMMC) were varicose (red arrowheads). Scale bar = 100 µm. ***D, E,*** Circular histograms showing the responses of the PI(2):6 neuron to counterclockwise rotation (***D***) and clockwise (***E***) of the polarizer. The neuron was tonically excited during counterclockwise stimulation ($p = 0.2$), and showed a preferred E-vector when the polarizer rotated in clockwise direction with excitation only at Φ_{max} ($p = 3\times10^{-5}$; $\rho^2 = 0.6$; $\Phi_{max} = 113°$). ***F,*** Projection view of confocal image stacks of a PI(2):5 neuron. The neuron's morphology showed only minor differences compared to that of the PI(2):6 neuron. Processes in the ipsilateral protocerebrum extended toward more ventral regions and arborizations in the AMMC were lacking. Scale bar = 100 µm. ***G,*** Spike train showing the response of the PI(2):5 neuron to the second rotation of the polarizer (counterclockwise) and the third rotation (clockwise). Blue dashed line indicates switch-off of polarized light. The neuron was responsive to the clockwise rotation ($p = 0.01$; $\rho^2 = 0.2$; $\Phi_{max} = 81°$), but tonically inhibited by the consecutive counterclockwise rotation ($p = 0.8$).

One of the descending neurons, PI(2):6, also responds to polarizer orientation presented from dorsal direction (Träger and Homberg, 2011). In the experiments by Träger and Homberg, however, the requirement of polarized light perception by the DRA has not been studied. It is likely that in these types of descending neurons the polarization signals coming from dorsal directions are processed together with polarization signals coming from ventral directions, both contributing to behavioral output. However, these neurons remain to be tested for their receptive fields for plane polarized light that might cover the complete visual field of the compound eye, ranging from the zenith to the ground.

References

Armett-Kibel C, Meinertzhagen IA (1983) Structural organization of the ommatidium in the ventral compound eye of the dragonfly *Sympetrum*. J Comp Physiol A 151:285-295.

Beetz MJ, Pfeiffer K, Homberg U (2016). Neurons in the brain of the desert locust *Schistocerca gregaria* sensitive to polarized light at low stimulus elevations. J Comp Physiol A 202:759-781.

Bernáth B, Horváth G, Meyer-Rochow VB (2012) Polarotaxis in egg-laying yellow fever mosquitoes *Aedes (Stegomyia) aegypti* is masked due to infochemicals. J Insect Physiol 58:1000-1006.

Egri Á, Blahó M, Sándor A, Kriska G, Gyurkovszky M, Farkas R, Horváth G (2012) New kind of polarotaxis governed by degree of polarization: attraction of tabanid flies to differently polarizing host animals and water surfaces. Naturwissenschaften 99:407-416.

Gewecke M, Hou T (1993) Visual brain neurons in *Locusta migratoria*. In: Gribakin FG, Popov AV, Renninger G (eds) Sensory systems of arthropods. Birkhäuser, Basel, pp119-144.

Heinloth T, Uhlhorn J, Wernet MF (2018) Insect responses to linearly polarized reflections: Orphan behaviors without neural circuits Front Cell Neurosci 12: 10.3389/fncel.2018.00050.

Heinze S, Homberg U (2008) Neuroarchitecture of the central complex of the desert locust: intrinsic and columnar neurons. J Comp Neurol 511:454-478.

Horváth G (1994) Reflection-polarization patterns at flat water surfaces and their relevance for insect polarization vision. J Theor Biol 175:27-37.

Horváth G, Varjú D (1997) Polarization pattern of freshwater habitats recorded by video polarimetry in red, green and blue spectral ranges and its relevance for water detection by aquatic insects. J Exp Biol 200:1155-1163.

Horváth, G (2014) Polarized light in animal vision. Springer Berlin.

Kriska G, Bernáth B, Horváth G (2007) Positive polarotaxis in a mayfly that never leaves the water surface: polarotactic water detection in *Palingenia longicauda* (Ephemeroptera). Naturwissenschaften 94:148-154.

Pegel (2014) Integration von Himmelskompass-Signalen im Zentralhirn der Wüstenheuschrecke *Schistocerca gregaria*. Masterthesis, Philipps-University of Marburg.

Rosner R, Homberg U (2013) Widespread sensitivity to looming stimuli and small moving objects in the central complex of an insect brain. J Neurosci 33:8122-8133.

Schmeling F, Wakakuwa M, Tegtmeier J, Kinoshita M, Bockhorst T, Arikawa K, Homberg U (2015) Opsin expression, physiological characterization and identification of photoreceptor cells in the dorsal rim area and main retina of the desert locust, *Schistocerca gregaria*. J Exp Biol 217:3557-3568.

Schwind R (1983a) A polarization-sensitive response of the flying water bug *Notonecta glauca* to UV light. J Comp Physiol 150:87-01.

Schwind R (1983) Zonation of the optical environment and zonation in the rhabdom structure within the eye of the backswimmer, *Notonecta glauca*. Cell Tissue Res 232:53-63.

Schwind R, Schlecht P, Langer H (1984) Microspectrophotometric characterization and localization of three viual pigments in the compound eye of *Notonecta glauca* L. (Heteroptera). J Comp Physiol A 154:341-346.

Shashar N, Sabbah S, Aharoni N (2005) Migrating locusts can detect polarized reflections to avoid flying over the sea. Biol Lett 1:472-475.

Träger U, Homberg U (2011) Polarization-sensitive descending neurons in the locust: connecting the brain to thoracic ganglia. J Neurosci 31:2238-2247.

Wernet MF, Velez MM, Clark DA, Baumann-Klausener F, Brown JR, Klovstad M, Labhart T, Clandinin TR (2011) Genetic dissection reveals two separate retinal substrates for polarization vision in *Drosophila*. Curr Biol 22:12-20.

Wildermuth H (1998) Dragonflies recognize the water of rendezvous and oviposition sites by horizontally polarized light: A behavioural field test. Naturwissenschaften 85:297-302.

Williams JLD (1975) Anatomical studies of the insect central nervous system: A ground-plan of the midbrain and an introduction to the central complex in the locust, *Schistocerca gregaria* (Orthoptera). J Zool Lond 176:67-86.

Zhou G, Xu W, Niu C, Zhao H (2013) The polarization patterns of skylight reflected off wave water surface. Opt Express 21:32549-32565.

Die folgenden zwei Seiten enthalten persönliche Daten (Lebenslauf). Sie sind daher kein Bestandteil der Online-Veröffentlichung.

Danksagung

Zunächst möchte ich mich bei meinem Zweitkorrektor Joachim Schachtner, sowie den Dritt und Viertgutachtern Annette Borchers und Michael Bölker bedanken, die sich so selbstverständlich als Mitglieder der Prüfungskommission zur Verfügung gestellt haben.

Allen aktuellen und ehemaligen Mitgliedern der AG Neurobiologie möchte ich danken, die während meiner Zeit hier zum angenehmen Arbeitsklima beigetragen haben.

Insbesondere gilt mein Dank Martina Kern für die Rettung meiner Präparate und sonstige Unterstützung im Labor, sowie für die Pflege meiner Versuchstiere. Ebenso möchte ich Jutta Seyfarth für jegliche Hilfe im Labor danken.

Außerdem möchte ich danken: Kim Le und Dajana Müller für die lustige Zeit im Labor, meinen Masterstudenten Vanessa Althaus und Marius Beck, die mir Ableitungen liefern bzw. lieferten, Anne Wosnitza für die ausführliche Einweisung in extrazelluläre Ableitungen, Ronja Hensgen, Joss von Hadeln und Björn Trebels für Hilfe mit Amira und anderen Angelegenheiten, Frederick Zittrell für hilfreiche Ideen zur Durchführung meiner Analysen, Stefanie Jahn für die Einweisung in die Immunfärbungen, sowie Keram Pfeiffer für jegliche technische Hilfe und viele richtungsweisende Gespräche.

Ein ganz herzlicher Dank geht auch an Basil el Jundi, Eva Fischer, Stanley Heinze und Roy Ritzmann für das Korrekturlesen dieser Arbeit.

Meinen Eltern und Geschwistern möchte ich danken für jedwede Unterstützung im Studium, Hilfe bei Umzügen und spontane Besuche.

Mein größter Dank gilt Uwe Homberg, der nicht nur diese Arbeit sondern auch meine beruflichen Perspektiven entscheidend mitgestaltet hat. Dies impliziert die Möglichkeit elektrophysiologische Techniken bereits im Masterstudium kennen zu lernen und anzuwenden, eine Vielzahl anderer Methoden zu lernen, die in diesem Labor etabliert sind, die Möglichkeit an Konferenzen und am ‚Neural Systems and Behavior'-Kurs in Woods Hole teilzunehmen, das Schreiben von Gutachten für verschiedenste Bewerbungen, das Korrekturlesen meiner Texte, die ständige Erreichbarkeit und Möglichkeit zur Diskussion, und all die Gespräche durch die ich so viel gelernt habe.

Erklärung

Hiermit versichere ich, dass ich meine Dissertation

“Processing of sky compass cues and wide-field motion in the central complex of the desert locust (*Schistocerca gregaria*)”

[Verarbeitung von Himmelskompasssignalen und Großfeldbewegung im Zentralkomplex der Wüstenheuschrecke (*Schistocerca gregaria*)]

selbstständig, ohne unerlaubte Hilfe angefertigt und mich keiner anderen als der von mir ausdrücklich bezeichneten Quellen und Hilfen bedient habe.

Die Dissertation wurde in der jetzigen oder in einer ähnlichen Form noch bei keiner anderen Hochschule eingereicht und hat noch keinen sonstigen Prüfungszwecken gedient.

Marburg, den 05.06.2018

_____

(Uta Pegel)